Robust digital image watermarking algorithms for copyright protection

Von der Fakultät für Ingenieurwissenschaften

der Universität Duisburg-Essen

zur Erlangung des akademischen Grades einer

Doktorin der Ingenieurwissenschaften

genehmigte Disertation

von

Nataša Terzija

aus Belgrad

Referent: Prof. Dr. Walter Geisselhardt

Korreferent: Prof. Dr. Josef Pauli

Tag der mündlichen Prüfung: 18.10.2006

Acknowledgement:

I would like to express my thanks to Prof. Walter Geisselhardt, who supervised my academic activities at the University Duisburg-Essen and gave me freedom and optimal conditions necessary for my research. I especially thank Prof. Josef Pauli, who read the manuscript and provided corrections and useful comments.

Thanks are also due to Prof. Hans-Dieter Kochs, who has also supported my research, and to all those outstanding individuals with whom I have worked in the past, who helped me understanding watermarking and its applications better, including Prof. Gerlind Plonka-Hoch and Prof. Zoran Bojkovic (Univ. of Belgrade, Serbia).

I would also like to thank my whole family for encouragement and love. Without it, my thesis could never have been completed.

Keywords

Digital image watermarking, Scale invariant feature point detectors, Image registration, Synchronization technique for watermark detection, Discrete Wavelet Transform, Complex Wavelet Transform, Error Correction Codes.

ABSTRACT

Digital watermarking has been proposed as a solution to the problem of resolving copyright ownership of multimedia data (image, audio, video). The work presented in this thesis is concerned with the design of robust digital image watermarking algorithms for copyright protection.

Firstly, an overview of the watermarking system, applications of watermarks as well as the survey of current watermarking algorithms and attacks, are given. Further, the implementation of feature point detectors in the field of watermarking is introduced. A new class of scale invariant feature point detectors is investigated and it is shown that they have excellent performances required for watermarking.

The robustness of the watermark on geometrical distortions is very important issue in watermarking. In order to detect the parameters of undergone affine transformation, we propose an image registration technique which is based on use of the scale invariant feature point detector. Another proposed technique for watermark synchronization is also based on use of scale invariant feature point detector. This technique does not use the original image to determine the parameters of affine transformation which include rotation and scaling. It is experimentally confirmed that this technique gives excellent results under tested geometrical distortions.

In the thesis, two different watermarking algorithms are proposed in the wavelet domain. The first algorithm belongs to the class of additive watermarking algorithms which requires the presence of original image for watermark detection. Using this algorithm the influence of different error correction codes on the watermark robustness is investigated. The second algorithm does not require the original image for watermark detection. The robustness of this algorithm is tested on various filtering and compression attacks. This algorithm is successfully combined with the aforementioned synchronization technique in order to achieve the robustness on geometrical attacks.

The latter watermarking algorithm presented in the thesis is developed in complex wavelet domain. The complex wavelet transform is described and its advantages over the conventional discrete wavelet transform are highlighted. The robustness of the proposed algorithm was tested on different class of attacks. Finally, in the thesis the conclusion is given and the main future research directions are suggested.

Content:

ACRONYMS

ACF	autocorrelation function
AWGN	additive Gaussian white noise
bpp	bit per pixel
BCH	Bose-Chaudhuri-Hocquenghem error correction code
CWT	Complex Wavelet Transform
DCT	Discrete Cosine Transform
DFT	Discrete Fourier Transform
DT-CWT	Dual-Tree Complex Wavelet Transform
DWT	Discrete Wavelet Transform
ECC	Error Correction Code
FMT	Fourier-Mellin Transform
HVS	Human Visual System
ICWT	Inverse CWT
IDWT	Inverse DWT
JND	just noticeable difference
JPEG	Joint Photographic Expert Group
LoG	Laplacian of Gaussian
LPM	Log Polar mapping
LSB	Least Significant Bit
MSE	Mean Square Error
PR	Perfect Reconstruction
PSNR	Peak Signal to Noise Ratio
RS	Read-Solomon error correction code
QIM	Quantisation Index Modulation
SIFT	Scale Invariant Feature Transform
SS	Spread Spectrum

List of Figures

List of Tables

Chapter 1

Introduction

With the widespread distribution of digital information over the World Wide Web (WWW), the protection of intellectual property rights has become increasingly important. These information, which include still images, video, audio, or text are stored and transmitted in a digital format. Information stored in digital format can be easily copied without loss of quality and efficiently distributed. Because of easy reproduction, retransmission and even manipulation, it allows a pirate (a person or organization) to violate the copyright of real owner. The design of techniques for preserving the ownership of digital information is in the basic of the development of future multimedia services.

1.1 Importance of Digital Watermarking and Watermarking Applications

There are few approaches designed for protecting data and securing systems. One of them is data encryption (cryptography). Based on conventional cryptographic system, parts of the data may be protected from an unauthorized person by applying any of existing cryptographic algorithms [1]. Only a person who possesses appropriate key (or keys) can decrypt the encrypted data. The drawback of this data protection strategy is that once such a data is decrypted by a pirate, there is no way to protect the data and track the illegal distribution. Also it is impossible legally to prove the ownership. The next approach to protect the intellectual property rights is watermarking. Watermarking is a technique for embedding hidden data that attaches copyright protection information to digital information. This provides an indication of ownership of the digital data.

Watermarking is closely related to steganography in that they are both concerned with covert communication and belong to a broader subject known as information hiding. Steganography, derived from Greek, literally means "covered writing" is the art of hiding information inside other data in ways that prevent the detection of hidden message. A steganographic system is typically not required to be robust against intentional removal of the hidden message. On the other hand, the watermarking requires that the hidden message should be robust to attempts aimed at removing it. In the case of copyright protection the copyright information should resist any modifications by pirates intending to remove it. This is a significant step forward compared to a common steganography.

Watermarking is either "*visible*" or "*invisible*". Perceptible mark ("*visible watermark*") of ownership or authenticity has been around for centuries in the form of stamps, seals, signatures or classical watermarks. Nevertheless, for known data manipulation technologies the imperceptible digital watermarks are mandatory in most of applications. The up to date known watermarking applications considered in the open literature are as follows [2]:

- *Copyright Protection:* for the protection of the intellectual property, the data owner can embed a watermark representing copyright information in the data. The embedded watermark can be used as a proof, e.g. in a court if someone intentionally infringed the copyrights.
- *Fingerprinting:* to trace the source of illegal copies, the owner can use the fingerprinting technique. In this case, the owner can embed different watermarks in the copies of the data that are supplied to different customers. Fingerprinting can be compared to embedding a serial number that is related to the customer's identity in the data. It enables the intellectual property owner to identify customers who have broken their license agreement by supplying the data to third parties.
- *Copy protection:* the information stored in watermark can directly control digital recording devices for copy protection purposes. In this case the watermark represents a copy-prohibit bit and watermark detectors in the recorder determine whether the data offered to the recorder may be stored or not.

- *Broadcast monitoring:* by embedding a watermark in commercial advertisements, an automated monitoring system can verify whether the advertisements are broadcasted as contracted. Broadcast monitoring can protect not only the commercials but also the valuable TV products.
- *Data authentication:* the so called fragile watermarks can be used to check the authenticity of data. A fragile watermark indicates whether the data has been altered. Further it offers the information in which part the data are being altered.
- *Indexing:* indexing of video mail, where comments can be embedded in the video content; indexing of movies and news items, where markers and comments can be inserted in order to be used by search engines.
- *Medical safety:* embedding the date and the patient's name in medical images could be a useful safety measure.
- *Data Hiding:* watermark techniques can be used for the transmission of secret messages. Since various governments restrict the use of encryption services, people can hide their messages in other data.

1.2 Motivation

Digital media (image, video, audio, etc.) are now widely distributed on the Internet. Because of easy reproduction and manipulation of digital media, the protection of intellectual property rights has become an important issue. Digital watermarking is expected to be a perfect tool for protecting the intellectual property rights.

The main advantages of the watermarks over other techniques are:

- They are imperceptible.
- They are not removed when the data are converted to other file formats.
- They undergo the same transformations as the data in which they are embedded.

The ideal properties of a digital watermark include the imperceptibility and robustness. The watermarked data should retain the quality of the original one as closely as possible.

Robustness refers to the ability to detect the watermark after various types of intentional or unintentional alterations (so called *attacks*). Various watermarking schemes have been proposed in the present. Unfortunately, up to now there is no algorithm that perfectly fulfils the aforementioned fundamental watermarking requirements: the imperceptibility to the human visual perception and the robustness to any kind of watermarking attacks. Particularly this fact was a challenge to investigate the opportunities of designing watermarking techniques being capable to achieve the imperceptibility and robustness criteria.

Part of the watermarking research is focused on the *watermark embedding process*. A watermark can be embedded in a spatial domain [3-8], Discrete Fourier Transform (DFT) domain [9-11], Discrete Cosine Transform (DCT) domain [12-16], Discrete Wavelet Transform domain (DWT) [17-21], Complex Wavelet Transform [22, 23] etc. Watermarking algorithms performed in the spatial domain show very good results regarding the watermark imperceptivity and capacity. At the same time they show the lack of robustness on compression and general signal processing attacks. On the other hand, the algorithms in the transform domain showed excellent robustness properties. Various image transforms have been considered, among them the DCT, used in the JPEG [24] coding standard, and the DWT, which becomes more and more attractive with its use in the JPEG2000 [25] coding standard. The CWT has not been widely used in the field of watermarking. Only few algorithms using the CWT have been introduced in the past. Te CWT [26] was developed as an extension of the commonly known DWT. Although the CWT has several important improvements with regard to the DWT (approximately shift invariance and improved directional selectivity), there is still a need to study deeply the watermark embedding techniques in the CWT domain.

The robustness of the watermark on geometrical attacks is the next open problem in the field of watermarking. Even the minor geometrical manipulation to the watermarked image can dramatically reduce the ability of the watermark detector to detect the watermark. Commonly used approaches to protect the watermark against geometrical distortions are based on invariant transformations [27-29], embedding synchronization marks [30-34], robust image content characteristics [35-37], etc. The image content-based methods also referred to as a *second generation watermarking schemes* [35], use significant data features in watermarking process (here the *data* is referred to be an image). One example of significant data features are *feature points*, which can be used as the reference locations for

the both the watermark embedding and detection process. Here the feature point detectors are used to extract the feature points.

In the open literature a wide variety of feature point detectors can be found. Among them the Harris corner detector [38] and the Mexican scale interaction method [39] are widely used in designing the watermarking schemes. The group of *scale invariant feature point detectors* [40], which are robust on transformations such as rotation, scale, translation, illumination changes or even projective transformation [41], are promising techniques to be considered in the field of watermarking.

1.3 Thesis contribution

In this thesis the *robust digital image watermarking algorithms* for copyright protection are studied. The objectives of this work were to develop novel image watermarking algorithms providing a performance enhancement over the other existing algorithms presented in the open literature and to validate their performance in the presence of the standard watermarking attacks.

The key points addressed in this research include the following:

1. Performance comparison of a relatively new class of scale-invariant feature points detectors. The robustness of two different scale-invariant feature point detectors to the standard image processing operations is tested and compared. The potential application of this new class of feature point detectors in watermarking field is outlined.
2. Demonstration of an image registration technique [42, 43], based on establishing point-by-point correspondence between the original image and image possibly altered by unknown geometrical transformation (received image). When the correspondence between two images is determined, the parameters of the undergone geometrical transformation are estimated and an inverse geometrical transformation is calculated and applied to the received image. This technique effectively estimates the parameters of undergone affine transformation.

3. Development of a new synchronization technique [44], which can be used in a process of watermark detection. The technique is based on the application of scale-invariant feature point detectors and it enables the calculation of the affine transformation parameters. The parameters of affine transformation are limited to scale and rotation. This technique does not require the original image and can be also applied if the affine transformed original image is cropped.
4. A classical non-blind additive watermarking algorithm in wavelet domain has been used to investigate the impact of different error correction codes on the watermark robustness [45, 46].
5. The proposal of a wavelet based watermarking algorithm, which does not require the original image for watermark extraction. In order to increase the robustness on geometrical distortions, the proposed watermarking algorithm can be successfully combined with the aforementioned synchronization technique.
6. The proposal of a complex wavelet based watermarking algorithm [47], which improves the existing watermarking algorithms based on the complex wavelet transform. The complex wavelets have not been widely used in the watermarking, although they have several desirable features, which can be applied for watermarking. The proposed algorithm requires the original image for watermark extraction and it can be combined with the image registration technique for increasing the robustness on geometrical attacks.

1.4 Thesis organization

In Chapter 2 the introduction to watermarking technology is given. The basic terms in the field of watermarking are explained. Chapter 3 gives firstly an overview of watermarking techniques based on use of feature point detectors. Then a new class of scale invariant feature point detectors is introduced and it will be later implemented for the design of the watermark synchronization technique. A comparison between two different scale-invariant feature point detectors is performed in order to show which scale invariant feature point detector has the best performances for image watermarking. The synchronization issue in watermarking schemes is considered in Chapter 4. Firstly, an image registration

technique is described and experimentally tested. Then, an overview of the existing watermarking techniques, which consider the problem of desynchronisation without access to the original image content is given. After that a new synchronization technique based on use of scale invariant feature point detectors is described and tested. The watermarking algorithms in discrete wavelet domain are considered in Chapter 5. The brief description of discrete wavelet transform with its properties related to the watermarking is given as well as the classification and literature survey of the existing watermarking algorithms based on DWT. After that, the two different watermarking algorithms based on discrete wavelet transform are proposed and tested. Chapter 6 introduces the watermarking in the complex wavelet transform. The Complex wavelet transform with its properties is firstly, briefly described. Then the existing watermarking algorithms based on complex wavelet transform are overviewed. The new watermarking algorithm based on complex wavelet transform is proposed and tested. Finally, summary of this thesis and further research directions are presented in Chapter 7.

The thesis organization is summarized in the Figure 1.1.

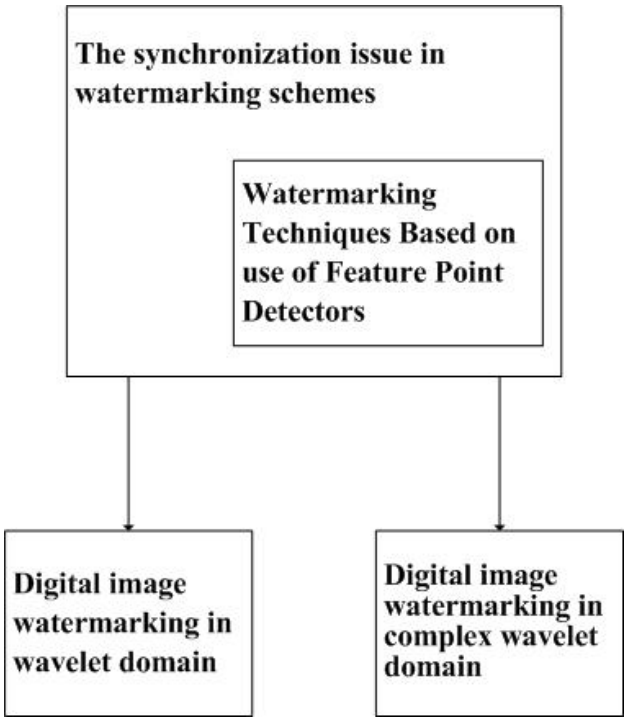

Figure 1.1: Thesis organization.

Chapter 2

Introduction to Watermarking Technology

This Chapter gives a brief introduction to watermarking technology. Section 2.1 introduces the basic terms of digital watermarking. The watermarking requirements and the structure of the typical watermarking system are given in Sections 2.2 and 2.3. In Section 2.4 the watermarking problem is formulated as a communication problem. Section 2.5 considers the most important properties of the watermarking system. A literature survey of the watermarking algorithms is presented in Section 2.6. In Section 2.7 the evaluation parameters of the watermarking algorithms, as well as the current benchmarking software are considered. The watermarking protocol for copyright protection is discussed in Section 2.8.

2.1 Types of digital watermarks

Digital watermarking is the process that embeds data called a *watermark* into a multimedia object in such a way that the watermark can be later on detected or extracted for object assertion purposes. The multimedia objects, in which the watermark is embedded, are usually called: the original, cover signal, host signal or simply the work.

A *digital watermark* is a distinguishing piece of information that is assigned to the data to be protected. One important requirement by this is that the watermark cannot be easily extracted or removed from the watermarked object.

Watermarks and watermarking techniques can be classified into several categories taking into account by this various criteria (see Figure 2.1 in which the types of watermarks are presented) [2]. As it can be noted, one of the criteria is *embedding domain* in which the

watermarking is implemented. For example, watermarking can be done in the spatial domain. An alternative possibility is the watermarking in the frequency domain.
In Figure 2.1 different types of watermarks are overviewed presented.

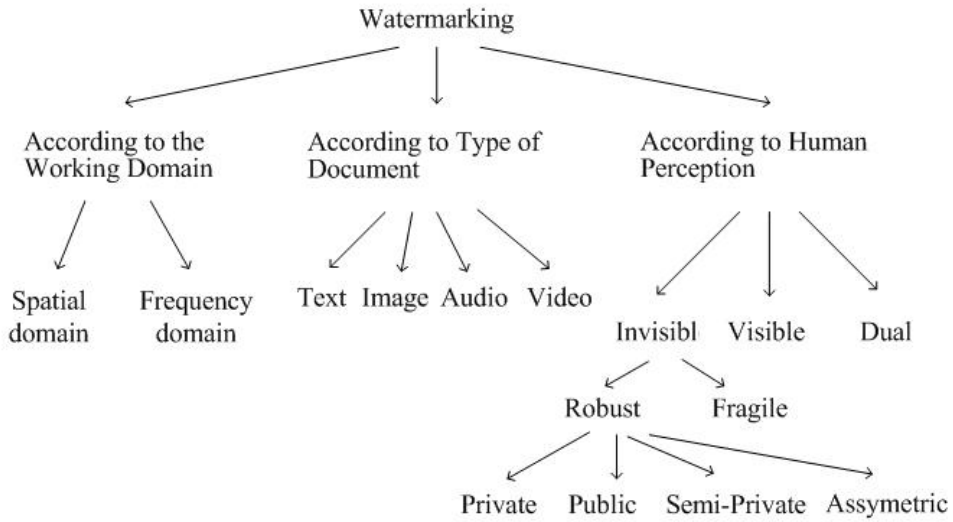

Figure 2.1: Types of watermarking techniques.

Watermarking techniques can be classified into the following four categories according to the type of the multimedia document to be watermarked:

- Image Watermarking
- Video Watermarking
- Audio Watermarking
- Text Watermarking.

According to the human perception, digital watermarks can be classified into three different categories, as follows:

- Visible watermark
- Invisible-Robust watermark
- Invisible-Fragile watermark
- Dual watermark.

The **visible** watermark appears visible to a casual viewer on a careful inspection. The **invisible-robust** watermark is so embedded that alterations made to the pixel cannot be perceptually noticed. Also the watermark should withstand the standard signaling operations (so called “attacks”, see Section 2.5) and it can be recovered with appropriate decoding mechanism only. The **invisible-fragile** watermark is embedded in such a way that any manipulation or modification of the image causes the watermark destruction, or alteration. The **dual** watermark is a combination of the visible and the invisible watermarks. In this type of watermarks an invisible watermark is used as a back up for the visible watermark.

The robust watermarking schemes can be classified in the following categories:

- **private** watermarking scheme, which requires the original image for watermark detection. There are two types of private watermarking schemes:
    - Type I systems, which extract the watermark from the tested, possibly distorted image and use the original image to find the location of the watermark in distorted image.
    - Type II systems, which requires an additional copy of the embedded watermark for watermark detection and they are only able to tell whether a given watermark is present or not in the tested image.

  In both systems knowledge about the private/embedded key is required. Here the private key is a secret data used to embed the watermark.
- **semi-private** watermarking, which does not use the original image for detection. It gives the information if the watermark is present or not.
- **public** watermarking (also referred to as *blind* watermarking), which requires neither the secret original image nor the embedded watermark in watermark extraction procedure.
- **asymmetric** watermarking (also referred to as *public-key* watermarking), in which the detection process and particularly the detection key are fully known to anyone, as opposed to blind watermarking approaches where a secret key is required for detection of watermark. The knowledge of the public key either does not help to compute the private key, or does not allow the watermark removal.

2.2 Watermark requirements for still images

In the open literature various watermarking techniques have been proposed in the past. In order to be effective, a watermark should have the main features, as outlined below [2]:

- *Fidelity:* the embedding algorithm must embed the watermark in such a way that this does not affect the quality of the host image. If the humans cannot distinguish the original data from the data with the inserted watermark, the watermark-embedding procedure is considered to be truly imperceptible. Even the smallest modification in the host image may become apparent when the original data is compared with watermarked data. Usually the users of the watermarked data do not have access to the original data. Thus, the aforementioned comparison cannot be performed. It may be sufficient that the modifications in the watermarked data stay unnoticed, as long as the data are not compared with the original image.
- *Payload of the Watermark:* the amount of information that can be stored in a watermark.
- *Robustness:* The watermark must be difficult to be removed from the object. The watermark should be immune to standard unintentional and intentional manipulations. It should be robust against various common signal processing techniques (e.g. compression, quantization, etc.) and common geometric distortions (e.g. cropping, rotation, etc.). Furthermore, it should be statistically unremovable. That means that a statistical analysis should not produce any advantage from the attacking point of view.
- *Unambiguousness*: the retrieval of the watermark should unambiguously identify the owner.

2.3 Structure of a typical watermarking system

Every watermarking system consists of at least two different units:

- the watermark embedding unit and
- the watermark detection/extraction unit.

Both units can be considered as separate processes, described in the next Subsections.

2.3.1 Embedding process:

In Figure 2.2 the embedding process for still images is presented and used for the explanation purposes. Let us denote an original image by $\mathbf{I}$, a watermark by $\mathbf{W}$, the watermarked image by $\mathbf{I}_{\mathrm{W}}$ and K is the embedded key (see Figure 2.2). The embedding function E_{mb} takes on its input the image $\mathbf{I}$, watermark $\mathbf{W}$ and key K and generates a new watermarked image, denoted with $\mathbf{I}_{\mathrm{W}}$. Introduction of the embedded key K is necessary for enhancing the security aspect of the watermarking system. Before the embedding process, the original image can be either transformed in the frequency domain or the embedding can be performed in spatial domain. The domain selection depends on the selected watermarking technique. If the embedding is performed in frequency domain, the inverse transform must be applied in order to obtain the watermarked image. Mathematically expressed, the embedding function for the spatial domain techniques can be represented as follows:

$$\mathrm{E}_{mb}(\mathbf{I}, \mathbf{W}, K) = \mathbf{I}_W \tag{2.1}$$

for the frequency domain technique, the following expression is valid.

$$\mathrm{E}_{mb}(\mathbf{f}, \mathbf{W}, K) = \mathbf{I}_W \tag{2.2}$$

where **f** represents the vector of coefficients of the transformation applied.

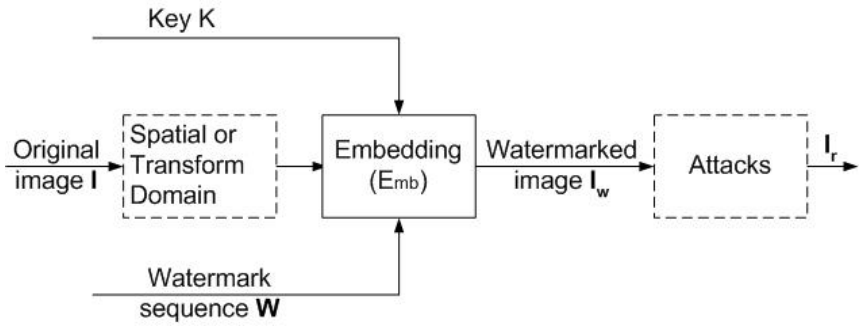

Figure 2.2: Embedding unit, as a part of a watermarking system.

When the watermarked image is obtained and placed on Internet or transmitted over the communication channel possibly, the attacks occur (image $\mathbf{I}_r$ is generated).

2.3.2 Extraction/detection process:

In Figure 2.3 the extraction/detection process for still images is presented and used for the further explanation purposes. A detector function D_{tc} (see Figure 2.3) takes an image $\mathbf{I}_r$ whose ownership is to be determined. The image $\mathbf{I}_r$ can be a watermarked or an un-watermarked image. In a general case, it can be also an altered image. The detector function either recovers a watermark $\mathbf{W}_e$ from the image, or checks the presence of the watermark $\mathbf{W}$ in a given watermarked image $\mathbf{I}_r$. In this procedure the same key K is used. In this process the original image $\mathbf{I}$ can also be included, what depend on the selected watermarking scheme.

Mathematically expressed, the extraction procedure for blind extraction (extraction without using the original image $\mathbf{I}$) can be expressed as follows:

$$D_{tc}(\mathbf{I}_r, K) = \mathbf{W}_e \tag{2.3}$$

for non-blind extraction (extraction using the original image) the following holds:

$$D_{\mathrm{tc}}(\mathbf{I}_{\mathrm{r}}, \mathbf{I}, K) = \mathbf{W}_{\mathrm{e}} \tag{2.4}$$

The blind watermark detection generates at its output a binary value indicating the presence or absence of the watermark $\mathbf{W}$. By this, the following can be assumed:

$$D_{\mathrm{dtc}}(\mathbf{I}_{\mathrm{r}}, \mathbf{W}, K) = \begin{cases} 1, \text{watermark is present} \\ 0, \text{watermark is not present} \end{cases} \tag{2.5}$$

A watermark must be extractable or detectable. In the watermarking extracting schemes the watermark is being extracted in its exact, original form. On the other hand, if detecting only whether a specific given watermarking signal is present in an image, or not, the scheme is called the watermark detection scheme. Note that the watermark extraction can prove the ownership, whereas the watermark detection can only verify it.

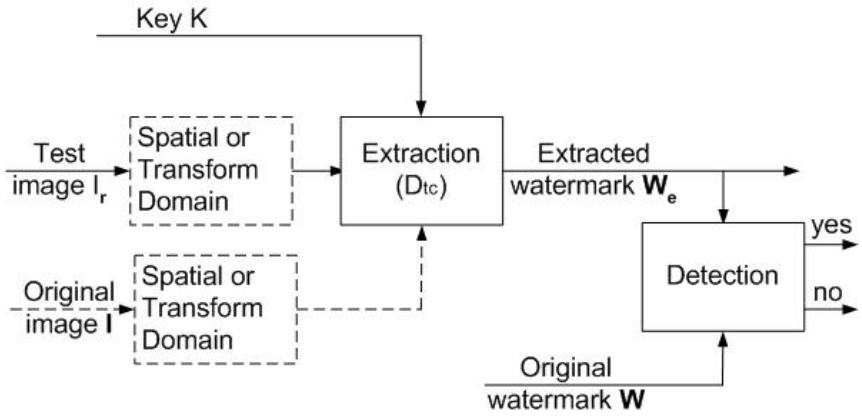

Figure 2.3: The extraction/detection process.

2.4 Watermarking as a communication problem

The watermarking process is usually described as a *communication over distorting channel* [2]. To understand the similarities between watermarking and conventional communication, we will briefly review the traditional model of communication system.

Then some components of a communication system that will be relevant to the extension to watermarking will be highlighted.

In Figure 2.4 the main elements of the traditional data communications model are depicted.

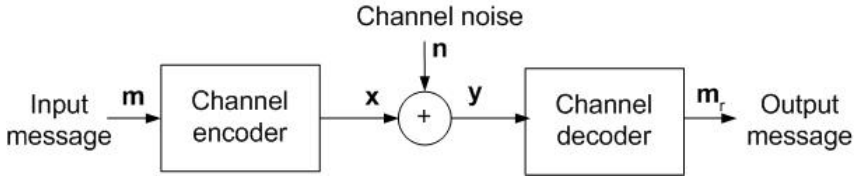

Figure 2.4: Standard model of communication system.

Here the main objective is to transmit a message **m** across a communications channel. In order to prepare it for transmission over the channel, the channel encoder usually encodes this message. The channel encoder is a function, mapping each possible message into a code word, in Figure 2.4 denoted as **x**, drawn from a set of signal that can be transmitted over the communications channel. Commonly, the encoder consist of a source coder and a modulator. The source coder removes the redundancy from the input message and maps a message into a sequence of symbols drawn from some alphabet. The role of the modulator is to convert a sequence of symbols from the source coder into a signal suitable for the transmission through a physical communications channel. By this, different modulation techniques, such as amplitude, phase, or frequency modulation, can be implemented.

The signal **x** is subsequently sent over the communications channel, which is assumed to be noisy. The consequence of the presence of noise is that the *received signal*, conventionally denoted as **y**, is generally different from **x**. The intensity of this difference depends of the level of the noise present in the channel. Here it is assumed that the noise is considered as an additive noise. In other words, the transmission channel is modeled by adding a random noise **n** to the encoder's output **x**. At the receiver part of the system, the received signal, **y**, is forwarded, as the input signal, to the channel decoder which inverts the encoding process and attempts to correct the errors caused by the presence of noise. This is a function that maps transmitted signals into messages $\mathbf{m}_r$. If the channel code is well matched to a given channel model, the probability that the decoded message contains an error is negligibly small.

The noise signal $\mathbf{n}$ is usually modeled independently of the signal $\mathbf{x}$. The simplest and most important channel for analysis is a Gaussian channel where each element of the noise signal is drawn independently from a normal distribution with zero mean and a variance σ_n^2. By this, the variance models the level of distortion of the signal introduced by the channel noise. The zero mean distribution means that the channel noise does not have an impact on the DC component of the transmitted signal. This model is the most frequently used one in the watermark literature.

The fundamental process in each watermarking system can be modeled as a form of communication in which a message is transmitted from the watermark embedder to the watermark receiver [2]. In the watermarking-communications model, the process of the watermarking is seen as a transmission channel through which the watermark message is being sent, with the host image being a part of this channel. Firstly, the message $\mathbf{m}$, which has to be transmitted, is encoded typically by the error correction codes to produce the coded message. This coded message is mapped into a watermark pattern $\mathbf{w}$ using a secret key K. After that, the watermark is added to the host image $\mathbf{I}$, constructing by this the watermarked image $\mathbf{I}_w$. If the watermark embedding process does not use information about the host image, it is called the blind watermark embedding, otherwise the process is referred to as an informed watermark embedding. After the added pattern is embedded, it is assumed that the watermarked image is distorted by watermark attacks. As in the data communications model, the distortions of the watermarked signal are modeled as additive noise. The next step in this model is watermark extraction and message decoding.

The original image plays an important role if it is available to the embedder. This watermarking is referred as a communication problem with side information at the transmitter [48]. The idea is that instead of treating the cover image as a noise, it could be treated as side information and used to improve the fidelity and detectability characteristics of the watermark. The side information at the embedder (*informed embedding*) can be used to determine how the watermark signal power can be maximized while ensuring the imperceptibility. The visual masking models show that the interaction between the original image and the watermark must be taken into account in order to achieve the desired invisibility. Another possibility to benefit from the availability of the original image is to adapt the message coding process to the cover signal characteristics (*informed coding*). This supposes that the same message can be represented by several different codes (a *dirty-paper codes*). The code, which is the closest to the cover signal, should be selected as a

watermark. The dirty-paper coding theory [49] gives a way to build codes able to achieve the watermarking capacity (the maximum data payload), which is independent from the characteristics of the cover signal. It is assumed that the cover signal and attacks are additive, Gaussian and independent. A scheme that was derived in [49] performs well as if the original data (the side information at the encoder) were perfectly known to the decoder.

2.5 Properties of the watermark

There are a number of papers that have discussed the characteristic of watermark [2, 3, 90]. Some of the properties discussed are: payload encoding, payload capacity, complexity, visual quality, detection reliability, robustness, key capacity, security. In practice, it is impossible to design a watermarking system that excels all of these. Hence, it is necessary to make tradeoffs between them and those tradeoffs must be chosen with careful analysis of the application. In this Subsection the properties listed above will be defined and discussed:

- ***Payload encoding*.** Before starting the watermark embedding procedure a message intended to be used as a watermark can be encoded into a robust form. Using the error correction coding, modulation or both can accomplish the encoding. The error correction coding is a conversion of the original bit sequence into a longer sequence where the additional bits can be used for error detection and correction. The modulation is the process of converting each bit into a waveform, which is sent across the channel. Here the following encoding techniques will be presented:

  - **Spread-Spectrum** Since watermarking systems can be modeled as communication systems, where the watermark represents a message and the image represents communications channel, a spread spectrum technique can be applied in the watermarking [5, 12, 13, 27, 50, 51]. Spread spectrum technique is based on spreading the message energy over a bandwidth much larger than the minimum bandwidth required. This technique has a few major advantages:

- *Low power spectral density* relates to the fact that the transmitted energy is spread over a wide band, and consequently the amount of energy for any specific frequency band is low. The effect is that such a signal will not interfere with other signals sharing the same frequency band. Assuming that a watermark represents a message, the low power density means that the watermark will introduce negligible changes to the image and therefore the embedded watermark should be imperceptible.
- *Redundancy* relates to the fact that the message is present at different frequency bands, so that if there is an error in one band, the message could still be recovered from other bands. Redundancy maps to robustness, and means that a watermark will be recoverable even if it suffered certain level of intentional or unintentional distortion/attack.

One example of a watermarking system based on the Direct-Sequence Spread Spectrum (**DSSS**) communications techniques is proposed in [50]. A watermark, representing an individual message bit $b_j \in \{-1,1\}$, is created in two steps. Firstly, the bit is spread by a large spreading factor *cr,* in an analogy to spread spectrum communications equivalent called the chip-rate. The purpose of spreading is to distribute one bit of information across many pixels of an image. The spread bit is then modulated with a pseudo-noise sequence, yielding one watermark. This procedure is repeated for each information bit of a message, and the created watermarks are added together yielding a final watermark which represents the whole watermarked message.

The recovery of the multi-bit message is accomplished by correlating the watermarked image with the same pseudo-noise sequence being used on the message encoding side. If the peak of the correlation is positive, the current information bit is $+1$. Contrary, if the peak of the correlation is negative, the current information bit is -1. After decoding of one bit, the next cr pixels are processed in the same way to recover the next bit. This scheme works only if both the message encoder and the message decoder use the same key (the same pseudo-noise sequence).

- **Error-correcting codes** If a watermarking algorithm is not sufficiently robust, a small signal distortion could cause that watermark cannot be correctly retrieved. Using the error correcting codes could solve this problem. The objective of the error-correcting code is to encode the data by adding a certain amount of redundancy to

the message, so that the original message can be recovered if not too many errors have occurred. The simplest error correcting codes can correct single-bit errors (single error correction) and detect double-bit errors (double error detection). Other codes can detect, or correct the multi-bit errors. The following error correction codes are available for the purpose of improving the watermarking robustness: Hamming, BCH, Reed-Solomon, Trellis codes, etc. The class of turbo codes [52] is known for its good performance, and it is also used to encode watermark messages [53].

Payload capacity is the bit length of the embedded watermark, without the potential redundancy introduced by error correcting codes for channel coding.

Visual Quality. As a measure of distortions introduced by the watermarking process, the *visual quality metrics* are used. It can be distinguished between the visual quality of the data due to the embedding of the watermark and the visual quality of the watermarked data due to attacks performed on it. The visual quality of the watermarked data is required to be as high as possible meaning that the degradation of the data due to the watermarking operation is imperceptible. The mostly used visual quality metrics in the existing watermarking algorithms are as follows:

- Peak Signal to Noise Ratio (PSNR), defined as:

$$\mathrm{PSNR}(dB) = 10\log_{10}\left(N_1 N_2 \frac{\max\limits_{x_1,x_2} \mathbf{I}^2{}_{x_1,x_2}}{\sum\limits_{x_1,x_2} (\mathbf{I}_{x_1,x_2} - \mathbf{I}_{\mathrm{W}x_1,x_2})^2}\right) \tag{2.6}$$

where N_1 and N_2 are dimensions of the original image $\mathbf{I}$ and watermarked image $\mathbf{I}_{\mathrm{W}}$, and $x_1 = 1,\ldots,N_1$, $x_2 = 1,\ldots,N_2$. The PSNR is measured in decibels (dB).

- Mean Square Error (MSE) criteria defined as:

$$\mathrm{MSE} = \frac{1}{N_1 N_2} \sum_{x_1,x_2} (\mathbf{I}_{x_1,x_2} - \mathbf{I}_{\mathrm{W}x_1,x_2})^2) \tag{2.7}$$

A more detailed list of distortion measures is given in [54].

An accepted measure for evaluation of the level of distortion is a *Just Noticeable Difference* (JND). It represents a minimum distortion that is generally perceptible. The watermark perceptibility can be measured by using different experiments developed as a result of various psychophysics studies. One approach, which develops an automated technique for quality measure, is proposed in [55]. It tries to estimate the number of JNDs between images.

Detection reliability: Detection is the process trying to decide the presence or absence of a watermark in the watermarked data. In order to determine if a test signal $\mathbf{I}_t$ contains the watermark embedded by using the key K, the following hypothesis can be used:

$$\begin{aligned} H_0 &: \text{The signal } \mathbf{I}_t \text{ does not contain a watermark} \\ H_1 &: \text{The signal } \mathbf{I}_t \text{ contains a watermark} \end{aligned} \tag{2.8}$$

Given a decision $\mathrm{D}_{cs} = \{H_0, H_1\}$, its performance can be measured by using:

- *Detection probability* (P_D) – the probability P_r of deciding H_1 when the signal $\mathbf{I}_t$ contains a watermark, calculated as:

$$P_D = \mathrm{P}_r\{\mathrm{D}_{cs} = H_1 / H_1\} \tag{2.9}$$

- *False alarm probability* (P_{FA}) - the probability of deciding H_1 when the signal $\mathbf{I}_t$ does not contain the watermark. It means that in the detection test the positive result is obtained. The false alarm probability is calculated as follows:

$$P_{FA} = \mathrm{P}_r\{\mathrm{D}_{cs} = H_1 / H_0\} \tag{2.10}$$

Robustness and watermarking attacks. Most watermarking algorithms are based on the concept of the spread spectrum communication by embedding a pseudorandom watermark into the image content and detect it by using the correlation method. To archive the high reliability of watermark detection, the watermark detection process has to be robust to the alterations in the host image caused from both unintentional and intentional distortions

(attacks). The aim of attacks is not always to completely remove or destroy the watermark but usually to disable its detection. Distortions are limited to those not producing excessive degradations. Otherwise, the transformed watermarked object would be unusable. These distortions could also introduce degradation to the performance of the system.

In practice, a watermarked object may be altered either intentionally, or accidentally. In both cases the watermarking system should be able to detect and extract the watermark after attacks. The best-known watermarking attacks, which may be intentional or unintentional, depending on the application, are:

- ***Additive Noise***. A random signal with a given distribution (e.g. Gaussian, uniform, Poisson, Bernoulli) is added to the image unintentionally. In certain applications the additive noise may originate from D/A and A/D converters, or as a consequence of transmission errors. However, an attacker may introduce perceptually shaped noise (image-dependent mask) with the maximum unnoticeable power. This will typically force to increase the threshold at which the correlation detector operates.
- ***Filtering.*** Filtering attacks are linear filtering: high pass, low pass filtering, Gaussian and sharpening filtering, etc. Low-pass filtering, for instance does not introduce considerable degradation in watermarked images, but can dramatically affect the performance, since spread-spectrum-like watermarks have non negligible high-frequency spectral contents. To design a watermark robust to a known group of filters that might be applied to the watermarked image, the watermark message should be designed in such a way to have most of its energy in the frequencies which filters change the least.
- ***Denoising attacks.*** Image denoising (filtering) attacks [56] explores the idea that a watermark is an additive noise (which can be modeled statistically) relative to the original image. These attacks include: local median, midpoint, trimmed mean filtering, wiener filtering, as well as hard and soft thresholding.
- ***Watermark removal and interference attacks.*** The aim of these attacks is to predict, or to estimate the watermark and further to use the estimated watermark either to remove watermark or to impair its unique extraction at the detector side. Some known efficient removal attacks are: the median watermark prediction followed by subtraction [57], the Wiener prediction and subtraction [58] and perceptual remodulation [56], which combines both removal and interference attacks.

- ***Compressions.*** This is generally an unintentional attack, which appears very often in multimedia applications. Practically all the audio, video and images currently being distributed via Internet have been compressed. If the watermark is required to resist different levels of compression, it is usually advisable to perform the watermark embedding in the same domain where the compression takes places. For instance, the DCT-domain image watermarking is more robust to JPEG compression than the spatial-domain watermarking. Also the DWT-domain watermarking is robust to JPEG2000 compression.
- ***Statistical Averaging.*** The aim of these attacks is retrieving the host image and/or watermark by statistical analysis of multiple marked data sets. An attacker may try to estimate the watermark and then to "unwatermark" the object by subtracting the estimate. This is dangerous if the watermark does not depend substantially on data. This is a good reason for using perceptual masks to create a watermark. In this group of attacks belong the averaging and collusion attacks. *Averaging attack* consists of averaging many instances of a given data set (e.g. *N*) each time marked with a different watermark. In this way an estimate of the host data is computed and each of the watermarks is weakened by a factor *N*. *Collusion attack* consists of averaging *N* different host data containing the same watermark. The resulting signal may serve as a good estimate of the watermark, which can be used to remove it from the watermarked data.
- ***Multiple Watermarking.*** An attacker may watermark an already watermarked object and later make claims of ownership. The easiest solution in this case is to timestamp the hidden information by a certification authority.
- ***Geometrical Attacks.*** Geometrical attacks do not pretend to remove the watermark by itself, but to distort it through spatial alterations of the watermarked image. With such attacks watermarking detector loses the synchronization with the embedded information. These attacks can be subdivided into attacks applying general affine transformations and attacks based on projective transformation. Common geometrical attacks are rotation, scaling, change of aspect ratio, translation and shearing, etc.
- ***Cropping.*** This is a very common attack since in many cases the attacker is interested in a small portion of the watermarked object, such as parts of a certain

picture or frames of video sequence. With this in mind, in order to survive, the watermark needs to be spread over the dimensions where this attack takes place.

- ***Random Geometric Distortions.*** The Stirmark attack [59, 60] has shown remarkable success in removing data embedded by commercially available programs. Stirmark attack introduces first a minor unnoticeable geometric distortion and then the image is slightly stretched, sheared, shifted, bent and rotated by an unnoticeable random amount. Further, a slight deviation is applied to each pixel, which is greatest at the centre of the picture and almost null at the border (see Figure 2.5).

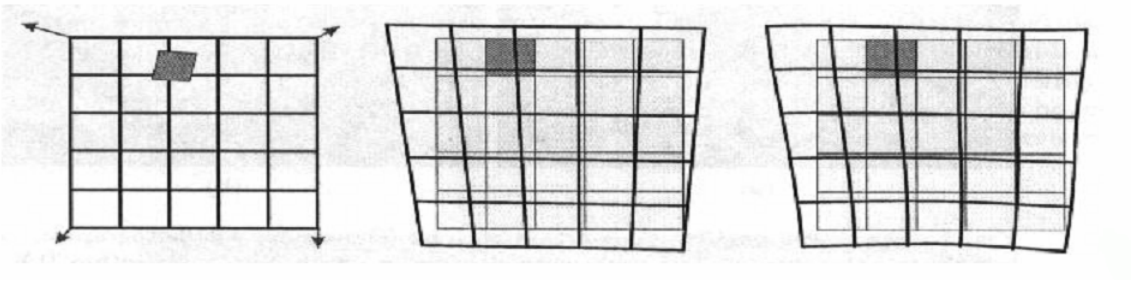

Figure 2.5: Random geometric distortion model (a) Original image (b) Geometric distortion applied without randomization (c) Geometric distortion applied with randomization.

The aim of this attack is that the detector loses the synchronization with the embedded watermark. In Figure 2.5 the Stirmark attack is illustrated. Figure 2.5.a presents the original image. The geometrical distortion is applied on original image and presented on Figure 2.5.b. In Figure 2.5.c the same geometrical distortion is applied as well as the slightly randomization which can be observed in the centre of the grid.

- ***Cryptographic Attacks.*** There are two categories of cryptographic attacks: the brute force attack, aiming to find the secret information trough an exhaustive search and the Oracle attack, being used to create a non-watermarked image when watermark detector device is available.
- ***Protocol Attacks.*** The aim of protocol attack is to attack the concept of the watermarking application. The *copy attack* [61] belongs to this group. Its aim is to predict the watermark from the watermarked image and to copy the predicted watermark to the target data. To satisfy the imperceptibility requirements, the estimated watermark is further adapted to the local features of the host data.

- ***Printing-Scanning.*** For applications like document authentication and integrity, it is relevant to test the robustness against document printing and scanning. This implies a digital-to-analogue conversion when printing, followed by an analogue-to-digital conversion when the printed document is scanned. This process introduces geometrical as well as noise-like distortions within these two processes (scaling, dithering, averaging, etc.).

Key capacity is the total number of secret keys that could be potentially used for embedding a watermark. Watermarking keys can be designed to use secret keys in a manner similar to that in spared spectrum communications. By this, in spread spectrum communication a narrow band signal is spread over a much larger bandwidth. The exact form of spreading is a secret known only by transmitter and receiver. Without knowledge of a spreading function it is almost impossible to detect the transmitted signal. In watermarking algorithms usually a watermark pattern is added to the original image. In order to detect the watermark correctly the embedder and detector must use the same watermark pattern. Thus, a watermark pattern can be considered as a secret key. Typically a secret key (embedded key) is the integer number/vector used for embedding the watermark data in cover image. At the receiver side usually the same key controls the process of extraction or detection of the watermark. Also we have to distinguish this key from the encryption key which could be potentially used to encrypt the message. That means that the message can be firstly encrypted using one encryption key and then embedded using a different embedded key.

Security According to the Kerckhoffs's principle, the security of watermarking algorithm should not rely on the secrecy of its algorithm but on the knowledge of the key. One way to break the system is the illegal generation of the key by performing the brute force attacks. The brute force attacks consist of an exhaustive search of all possible keys. In order to prevent these attacks it is necessary that the key capacity is sufficiently large, so that the exhaustive search becomes computationally unfeasible. Another way to break the system is performing the collusion attacks where different watermarks are embedded to the watermarked data using different keys than the original one. The attackers are also able to estimate the original watermark and to remove it. Non-invertibility of a watermarking system is also one of the important security issues [62].

Complexity is defined as the number of operations (additions, divisions, multiplications, etc.) needed to embed and extract the watermark.

In the next Session the classification of the watermarking algorithms according to the watermarking domains will be briefly overviewed.

2.6 Watermarking Algorithms

The watermarking algorithms (techniques) can be performed either in spatial domain or in the transform domain. The spatial-domain techniques [3-8] directly modify the intensities or color values of some selected pixels. One commonly used spatial domain technique is the Least Significant Bits (LSB) technique [3, 4]. In this technique the watermark is embedded in the least significant bits of some randomly selected pixels. This technique is very easy and fast for implementation. One disadvantage of spatial domain watermarks is that picture cropping (a common operation of image editors) can be used to eliminate the watermark. In a similar manner to spatial domain watermarking, the transform domain techniques modify the values of selected transformed coefficients. Since high frequencies will be lost by compression or scaling, the watermark signal is applied to middle frequencies, or better yet, applied adaptively to frequencies that contain important information of the original image. After that the inverse transform should be applied to obtain the watermarked image. Since watermarks applied to the transform domain will be dispersed over the entirety of the spatial image upon inverse transformation, this technique is more robust to cropping then the spatial technique. The transform techniques commonly used for watermarking purposes are respectively: the Discrete Cosine Transform (DCT) [12-16], the Discrete Fourier Transform (DFT) [9-11] and the Discrete Wavelet Transform [17-21]. These are also less known approaches implementing the Complex Wavelet Transform (CWT) [22, 23] and the Fourier-Mellin Transform (FMT) [27, 28]. With the standardization process of JPEG2000 and the shift from DCT- to wavelet-based image compression methods, watermarking schemes operating in the wavelet transform domain have become even more interesting. In the next Chapters the advantages and disadvantages of all transformations listed above will be highlighted.

2.7 Benchmarking and performance evaluation of watermarking schemes.

In order to investigate the watermark robustness against various attacks selected alterations have to be made to the watermarked image. For this purpose the benchmarking software packages are used. The usually applied benchmarking software are listed bellow:

- **Stirmark** [63] is a benchmarking tool designed to test the robustness of the digital watermarking schemes. For a given watermarked input image, Stirmark generates a number of modified images, which can then be used to verify if the embedded watermark can still be detected. The following image alterations have been implemented in Stirmark: Cropping, Flip, Rotation, Rotation-Scale, sharpening, Gaussian filtering, Random bending, linear transformations, Aspect ratio, Scale changes, Line removal, Color reduction and JPEG compression.

- **Checkmark** [64] is a benchmarking suite for digital watermarking developed on Matlab under UNIX and Windows. It has been recognized as an effective tool for evaluation and rating of watermarking systems. Checkmark offers some additional attacks not present in Stirmark. The following image alterations are here offered: Wavelet compression (JPEG 2000), Projective transformations, Warping, Copy, Template removal, Denoising (midpoint, trimmed mean, soft and hard thresholding, wiener filtering), Denoising followed by perceptual remodulation, Non- linear line removal and Collage attack.

- **Certimark** [65] is a benchmarking suite developed for watermarking of visual content and a certification process for watermarking algorithms.

In this Thesis the Checkmark benchmarking software is used for generating the watermark attacks and for investigating the watermarking schemes.

In general there is a trade-off between watermark robustness and watermark fidelity. The parameters directly influencing the robustness of watermarks are as follows:

- **Amount of payload information**- If more information is embedded into the image, then the robustness is lower.

- **Watermark embedding strength**- This parameter presents the trade-off between the watermark strength (and the robustness) and watermark perceptibility. Increased robustness requires a stronger embedding which increases perceptibility of the watermark.

- **Image size**- The image size and its nature are influencing the robustness. The watermark detector should be able to detect the watermark either from small images or from the part of larger images.

- **Secret information (key).** This parameter plays an important role in watermarking system security. The key space should be large enough to make the exhaustive search practically impossible.

2.8 Watermarking for copyright protection

The use of watermarking techniques for protection of owners' rights (copyright protection) requires efficient *watermarking protocols*. Watermarking protocol is a series of steps, involving one or more persons who claim the ownership of an image, designed to achieve the reliable judgment of possession. The general concept of the watermarking protocol for proving ownership can be explained in the following steps:

1. Alice creates the image (called original image).
2. Alice watermarks the original image and gets the watermarked image. She keeps privately the "evidence's" which can be used to claim the ownership.
3. Alice makes her watermark image available to the public.

4. Alice discovers that her image is used by an unauthorized person (e.g. Bob, Chris, etc).
5. To claim the ownership of such an image, Alice must reveal substantial evidence to the trusted arbitrator (i.e. court of law).
6. Using the admitted evidence and appropriate watermark detection technique the trusted arbitrator makes an official decision as to whom the watermark image belongs.

The declaration made by the trusted arbitrator, based on the watermarking protocol, must indicate that Alice is the only owner of the image. However, several difficulties on the protocol to resolve the ownership have been addressed, especially when the piracy exists. The ownership problem can be classified like in [66]:

- Ownership deadlock: The ownership can not be established while the pirate is able to provide an ownership proof that is as conclusive as the actual owner's proof.
- Counterfeit ownership: The pirate provides an ownership proof which is more convincing than that of the actual owner.
- Theft of ownership: The pirate obtains an embedded object and embeds a new watermark in it, pretending that it is a cover-object. He claims ownership on the variant of the cover object of the right owner.

A solution to ownership problem requires that when two or more persons are involved in a dispute, where all persons claim ownership the true owner is identified reliably. More difficult problem arises when the true owner is not involved in the ownership dispute. The ownership problem is introduced due to the malicious class of attack called protocol attacks. The copy attack belongs to this group of attacks. The aim of the copy attack is to predict the watermark from the watermarked image and to copy the predicted watermark to the target data. Another protocol attack is the inversion attack [67] (ambiguity attack). An attacker, which possesses a watermarked object, finds such watermark performing brute-force search. This watermark $\mathbf{W}'$ (generated by the pirate) can be detected in the watermarked object as well as the watermark $\mathbf{W}$ embedded by the owner. The attacker generates a fake original by de-embedding (subtracting) the watermark $\mathbf{W}'$ from the watermarked object. In such a way the attacker can cause the ownership deadlock

problem. In order to overcome this problem, several approaches are proposed [68, 69]. They are based on the invariability requirement of the embedding/detection scheme, as presented [67]. By this, the invertibility requirement ensures that the watermark embedding cannot be reversed so that a watermark cannot be subtracted from an object to produce a fake original.

Other approaches [70-72] involve a trusted third party centre where owners should register their watermarked products. In return it generates a variant of the product and an ownership certificate including e.g. owner's identity, time of creation, etc. The trusted third party is responsible for performing detection of the owner content provided the information that owner has already registered its watermarked products to the trusted third party.

The general watermark requirements for proofing the ownership are listed below:

- Invisibility at high quality.

- A payload size, which could range from one bit to a length of 48-64 bits for a complete identification of the right owner. Part of this information may be carried out by the watermark embedding key. This key can be private, or shared with a group of right owners.

- Extremely low probability of the false alarm, since it is supposed to be used in juridical processes. A high reliability of the successful detection process.

- Robustness to non-intentional attacks like standard digital compression, format conversions, etc. Robustness or capability to multiple watermarking (typically up to 3 other embedded watermarks).

- Robustness to malicious removing attacks, attacks on the synchronization of the watermark, non-invertibility, as well as robustness on against attacks that attempt to replace the watermark by another.

- Robustness to cryptographic attacks, secure to collusion attacks.

- Involvement of a trusted party.

2.9 Chapter Summary

In this Chapter a brief introduction to watermarking technology is given. The main points are covered in following:

- Basic definitions and classifications of watermarking system.
- The most important watermarking requirements for still images: fidelity, payload of watermark, robustness and unambiguousness.
- Description of basic structure of typical watermarking system.
- Description of watermarking system over communication model.
- The suitability of a given watermarking system for a given application may be judged in the terms of the following properties of that system:
  - Payload encoding;
  - Payload capacity;
  - Complexity;
  - Visual quality;
  - Detection Reliability;
  - Robustness on watermarking attacks;
  - Key capacity;
  - Security.

  The required properties of watermarking system strongly depend on the application. Thus, the appropriate evaluation criteria are application dependent.
- Benchmarking is a reasonable means of comparing the watermarking system.
- The watermarking protocol and the most important requirements for copyright protection.

In the next Chapter the watermarking techniques that use the feature point detectors will be introduced. Scale invariant feature point detectors will be compared and it will be shown how they can be further implemented for watermarking.

Chapter 3

Watermarking Techniques Based on use of Feature Point Detectors

In this Chapter firstly the literature survey of watermarking techniques which are based on use of feature point detectors will be given. It is outlined which feature point detectors are used in the watermarking field till the present. Then a new class of scale invariant feature point detectors, which are robust to transformations like rotation, scale and translation, is introduced. A comparison between two scale-invariant feature point detectors:

- Harris-Affine feature point detector [40] and
- Scale Invariant Feature Transform (SIFT) [41],

will be performed. It will be shown that the SIFT feature point detector is more suitable feature point detector for the development of the technique for recovering the watermark synchronization. This will be considered in the next Chapter. Before the comparison of the scale invariant feature point detectors starts, the SIFT feature point detector will be described in detail.

3.1 Introduction

Salient features are landmarks in an image, which are often intuitively obvious to a human. For example, these include corners of a building, the eyes on a human face, the edges of an object, etc. Traditionally, the salient features such as contour segment and corners are applied in many applications, e.g. tracking. Recently there has been an increased

interest in finding new types of salient features providing properties, which are robust to transformations like rotation, scale and translation. Typical applications in which the aforementioned salient features are successfully applied are *image registration* and *object recognition*.

The feature point detectors are being used for finding the salient features in natural images. A wide variety of feature point detectors exist in the open literature. In this thesis the focus will be given to those feature point detectors, which are commonly used for watermarking purposes. In the field of watermarking, the feature points can be used as the reference points for the both the watermark embedding and detection processes. The following significant results in the field of application of feature points detectors are listed:

- In [35] a feature based synchronization scheme is proposed. The feature points are extracted using the *scale interaction method based on two dimensional Mexican Hat wavelet* [73]. The features are used to compute the Voronoi partition [74] on the image. In each segment of the image the watermark is independently embedded using the spread spectrum watermarking. In the watermark detection procedure the same features are extracted and used to partition the received image. The watermark is extracted from each segment separately.
- In [36] the Harris corner detector [38] is applied to extract the features. Furthermore, in order to decompose the image into a set of disjoint triangles, the *Delaunay tessellation* of the feature points is performed. These triangles are used as the location for watermark insertion and extraction.
- In [37] the *scale interaction method based on two dimensional Mexican Hat wavelet* [73] is also used for the feature points extraction. Here the nonoverlapped discs of a fixed radius around the feature points are extracted from the image. By this, the image normalization approach [75] is used. Because the objects in the normalized image are invariant to geometrical image distortions, the image normalization is applied on every disc. The watermark is embedded in the DFT domain of 32x32 image blocks selected from every normalized image disc.
- In [76] the Harris-Affine detector is applied. Harris-Affine detector extracts the feature points and the elliptical regions around the feature points, which represent the affine-invariant regions of the image. The watermark is embedded in these regions using DFT transform.

In the Figures 3.1-3.3 the feature points extracted with Harris corner detector (Figure 3.1), Harris-Affine (Figure 3.2) and SIFT feature point detector (Figure 3.3) are presented. It can be observed from the Figures that the numbers and locations of the extracted feature points are different for every feature point detector. Depending on the applied watermarking approach, it is more desirable that the feature points are uniformly distributed on the image, like in the Figure 3.1. The next watermarking requirement is that the extracted feature point should be robust on different non-malicious attacks (compressions, filtering, geometrical distortions). Among the listed non-malicious attack, the most challenging requirement is that the feature points are robust on affine geometrical distortions. The feature points extracted with Harris corner detector are only robust on rotation transformation. In the Section 3.3 the suitability of scale invariant feature point detectors for image watermarking will be investigated. Further, two scale invariant feature points detectors will be compared in terms of the robustness of the feature points on compressions, different filtering and geometrical transformations.

In the table 3.1 the properties of the aforementioned feature point detectors will be summarized. By this, these properties are related to the invariance of the feature points to the geometrical transformations and the affine invariance is only approximately achieved.

Figure 3.1: Feature points of the Lena image extracted with the Harris corner detector.

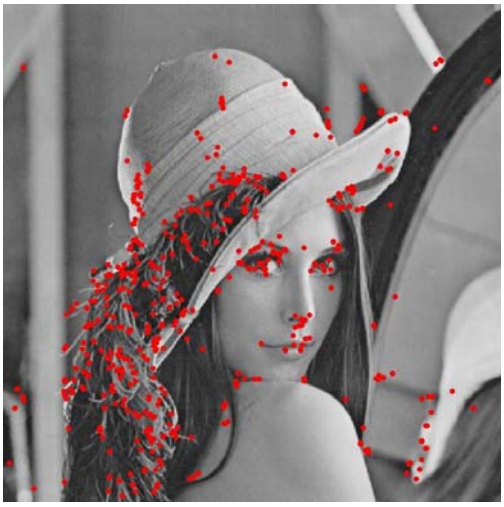

Figure 3.2: Feature point on Lena image detected with Harris-Affine detector.

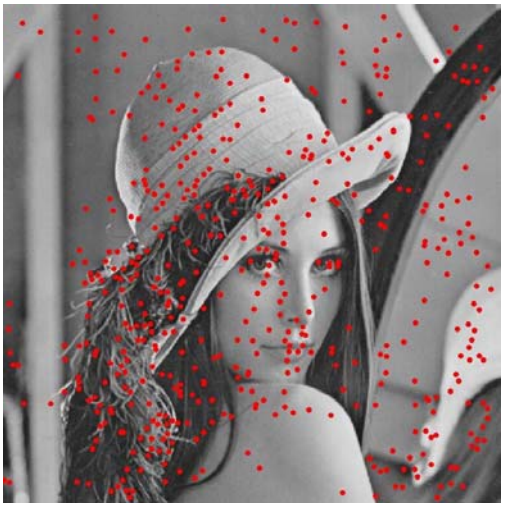

Figure 3.3: Feature point on Lena image detected with SIFT detector.

Table 3.1: The properties of the feature point detectors

	rotation invariance	scale invariance	affine invariance
Harris	yes	no	no
Harris-Affine	yes	yes	yes
SIFT	yes	yes	yes

3.2 Scale Invariant Feature Transform

For describing the SIFT feature point detector, the concept of *scale-space* and *characteristic scale* are required to be introduced.

Scale-space. The scale-space representation is a set of images represented at different levels of resolution. Different levels of resolution are created by the convolution of the Gaussian kernel $G(\sigma)$ with the image $\mathbf{I}(x_1, x_2)$:

$$\mathbf{I}_S(x_1, x_2, \sigma) = G(\sigma) * \mathbf{I}(x_1, x_2) \tag{3.1}$$

where $*$ is a the convolution operation in x_1 and x_2.
The variance σ of the Gaussian kernel is referred to as *scale parameter*.

Characteristic scale. The properties of characteristic scale are studied in [77]. The characteristic scale is a feature relatively independent of the image scale. The characteristic scale can be defined as that at which the result of a differential operator is maximized. Different differential operators are comparatively evaluated in [78]. Laplacian obtains the highest percentage of correct scale detection. The ratio of the scales, at which the extreme were found for corresponding points in two rescaled images, is equal to the scale factor between the images.
The characteristic scale of a local image structure is the scale parameter at which the Laplacian function attains a local maximum over scale factors [78].

Generally, the Laplacian of Gaussian filter centered on zero with Gaussian standard deviation σ has the following form:

$$LoG(x_1, x_2) = -\frac{1}{\pi\sigma^4}\left[1 - \frac{{x_1}^2 + {x_2}^2}{2\sigma^2}\right] e^{-\frac{{x_1}^2 + {x_2}^2}{2\sigma^2}} \tag{3.2}$$

SIFT detector proposed by [41] considers local image characteristic and retrieves feature points that are invariant to image rotation, scaling, translation, partly illumination changes and projective transform. The scale-invariant feature extractor detects feature points through a staged filtering approach that identifies stable points in the scale-space. The Gaussian kernel function is used to build a scale-space. The scale-space of an image is defined as a function $\mathbf{I}_S(x_1, x_2, \sigma)$ that is produced from the convolution of a variable scale Gaussian $G(x_1, x_2, \sigma)$ with an input image $\mathbf{I}(x_1, x_2)$:

$$\mathbf{I}_S(x_1, x_2, \sigma) = G(x_1, x_2, \sigma) * \mathbf{I}(x_1, x_2) \tag{3.3}$$

$$G(x_1, x_2, \sigma) = \frac{1}{2\pi\sigma^2} e^{-(x_1^2 + x_2^2)/2\sigma^2} \tag{3.4}$$

To detect efficiently the stable keypoint locations in scale space, the scale-space extreme in the difference-of Gaussian function convolved with an image is used. This function denoted as $D_{DG}(x_1, x_2, \sigma)$ can be computed from the difference of two nearby scales separated by a constant multiplicative factor k_c:

$$\begin{aligned} D_{DG}(x_1, x_2, \sigma) &= (G(x_1, x_2, k_c\sigma) - G(x_1, x_2, \sigma)) * \mathbf{I}(x_1, x_2) = \\ &= \mathbf{I}_S(x_1, x_2, k_c\sigma) - \mathbf{I}_S(x_1, x_2, , \sigma) \end{aligned} \tag{3.5}$$

In Figure 3.4 an efficient approach for construction of $D_{DG}(x_1, x_2, \sigma)$ is presented. The original image $\mathbf{I}(x_1, x_2)$ is incrementally convolved with a Gaussian function to produce images separated by a constant factor k_c in scale space. Each octave of scale space is divided into an integer number, s_p, of intervals, so $k_c = 2^{1/s_p}$ (In Figure 3.4 $s_p = 4$). The difference between the adjacent convolved images is computed. After that, the image is subsampled and the Gaussian convolution is repeated to obtain the other levels of the difference of Gaussian pyramid.

To detect the local maxima and minima of $D_{DG}(x_1, x_2, \sigma)$ each point is compared with its 8 neighbors at the same scale, and its 9 neighbors from the upper and lower scale (see Figure 3.5). If this value is the minimum or maximum of all these points then this point is an extreme.

When the candidate points are found the points with a low contrast or poorly localized points are removed by measuring the stability of each feature point at its location and scale. The stability of each feature point is calculated from the $2x2$ Hessian matrix $\mathbf{H}_{SS}$.

$$\mathbf{H}_{SS} = \begin{bmatrix} D_{DG x_1 x_1} & D_{DG x_1 x_2} \\ D_{DG x_1 x_2} & D_{DG x_2 x_2} \end{bmatrix} \tag{3.6}$$

where $D_{DG x_1 x_1}$, $D_{DG x_1 x_2}$, $D_{DG x_2 x_2}$ are derivatives of difference of Gaussian function.

Using the same approach for Harris corner detector, the computing of eigenvalues of Hessian matrix can be avoided by concerning only the ratio of eigenvalues. If λ_1 and λ_2 are eigenvalues of Hessian matrix $\mathbf{H}_{SS}$ with ratio $\lambda_1 = r\,\lambda_2$ then

$$\frac{Tr(\mathbf{H}_{SS})^2}{Det(\mathbf{H}_{SS})} = \frac{(D_{DG x_1 x_1} + D_{DG x_2 x_2})^2}{D_{DG x_1 x_1} D_{DG x_2 x_2} - D_{DG x_1 x_2}} = \frac{(\lambda_1 + \lambda_2)^2}{\lambda_1 \lambda_2} = \frac{(r\lambda_2 + 1)^2}{r\lambda_2} = \frac{(r+1)^2}{r} \tag{3.7}$$

$$Stability = \frac{Tr(\mathbf{H}_{SS})^2}{Det(\mathbf{H}_{SS})} < \frac{(r+1)^2}{r} \tag{3.8}$$

The keypoint is considered as stable if r is below some threshold.

If the feature point is considered as stable the scale at the point was found will be used as characteristic scale.

Keypoint neighborhood orientation. Orientation of each feature point is assigned by considering the local image properties. The keypoint descriptor can then be represented relative to this orientation, achieving invariance to rotation. The scale of the keypoint is used to select the Gaussian smoothed image $\mathbf{I}_S$. For each image sample $\mathbf{I}_S(x_1, x_2)$ at this scale the gradient magnitude $m_{ag}(x_1, x_2)$ and orientation $\theta_{Gor}(x_1, x_2)$ is computed using the pixel differences:

$$m_{ag}(x_1, x_2) = \sqrt{(\mathbf{I}_S(x_1 + 1, x_2) - \mathbf{I}_S(x_1 - 1, x_2))^2 + (\mathbf{I}_S(x_1, x_2 + 1) - \mathbf{I}_S(x_1, x_2 - 1))^2} \tag{3.9}$$

$$\theta_{Gor}(x_1, x_2) = \tan^{-1}((\mathbf{I}_S(x_1 + 1, x_2) - \mathbf{I}_S(x_1 - 1, x_2))/((\mathbf{I}_S(x_1, x_2 + 1) - \mathbf{I}_S(x_1, x_2 - 1))) \tag{3.10}$$

An orientation histogram is formed from the gradient orientation of sample points within a region (a circular window) around the keypoint. Each sample added to the histogram is weighted by its gradient magnitude and by Gaussian-weighted circular window. Peaks in the orientation histogram correspond to dominant orientation of local gradients. Using this peak and any other local peak within 80% of the height of this peak, a keypoint with that orientation is created. Some points will be assigned with multiple orientations.

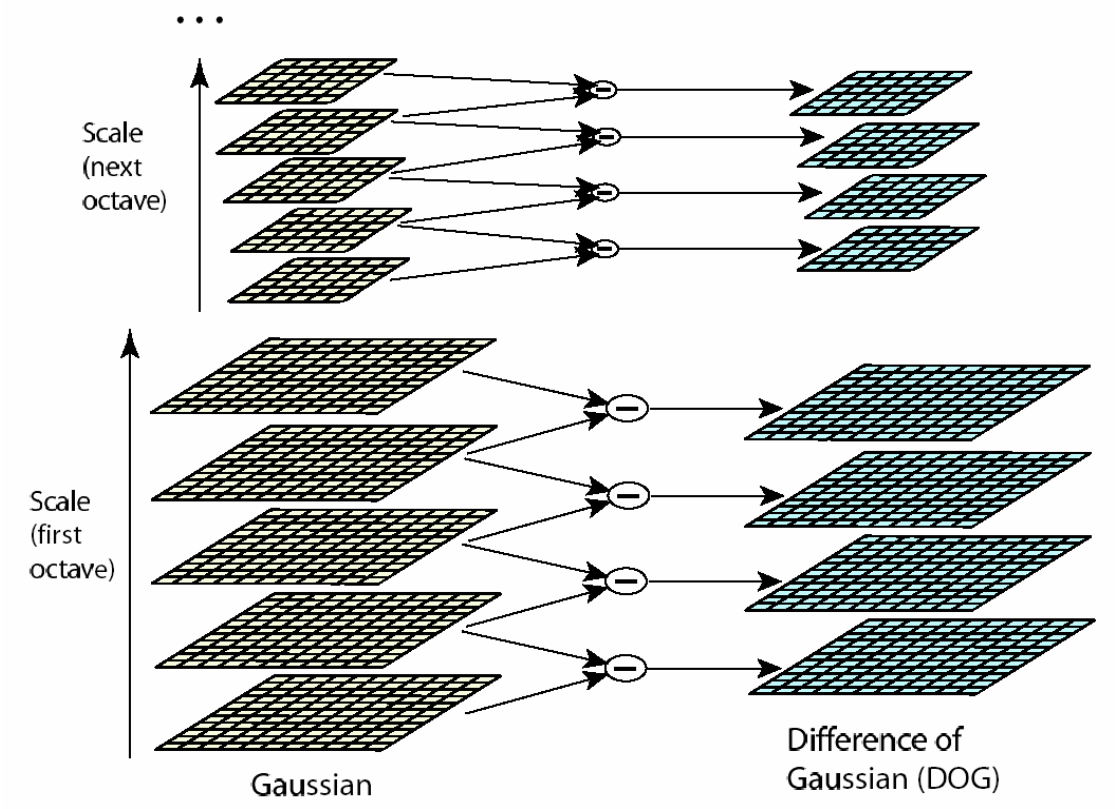

Figure 3.4: The pyramid of difference of Gaussian [40]

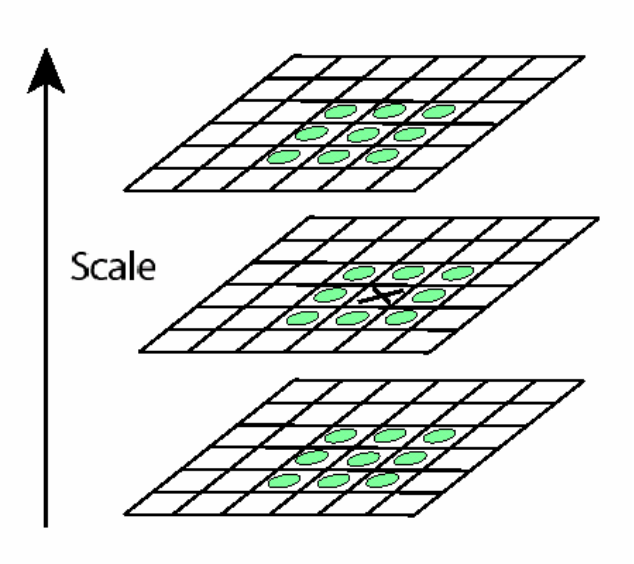

Figure 3.5: Maximum and minimum of SIFT images are detected by comparing the pixel **X** to its 8 neighbors at the same scale and its 9 neighbors from upper and lower scale [41].

Local image descriptors

Many different techniques for describing local image regions have been developed. The local image descriptors are mainly used for finding correspondences between the images. The simplest descriptor is a vector of image pixels. To compute a similarity score between two descriptors the cross-correlation can be used. In [79] the performance of different local descriptors is evaluated. It was concluded that Scale Invariant Feature Transform (SIFT) [41] based descriptors perform best.
In the further part of the work the SIFT descriptor will be used for matching between the corresponding points of two different images.

SIFT descriptor

The previous operations have assigned an image location, scale and orientation to each keypoint. The next step is to compute the descriptor. The local gradient data, used above, is also used to create keypoint descriptors. In order to achieve the rotation invariance the

coordinates of the descriptor and the gradient information is rotated to line up with the orientation of the keypoint. The gradient magnitude is weighted by a Gaussian function with variance, which is dependent on keypoint scale. This data is then used to create a set of histograms over a window centered on the keypoint. Figure 3.6 illustrates the computation of keypoint descriptor. The Figure shows 2x2 array of orientation histograms.

Keypoint descriptors typically use a set of 16 histograms, aligned in a 4x4 grid, each with 8 orientation bins. This results in a feature vector containing 4x4 x8=128 elements.

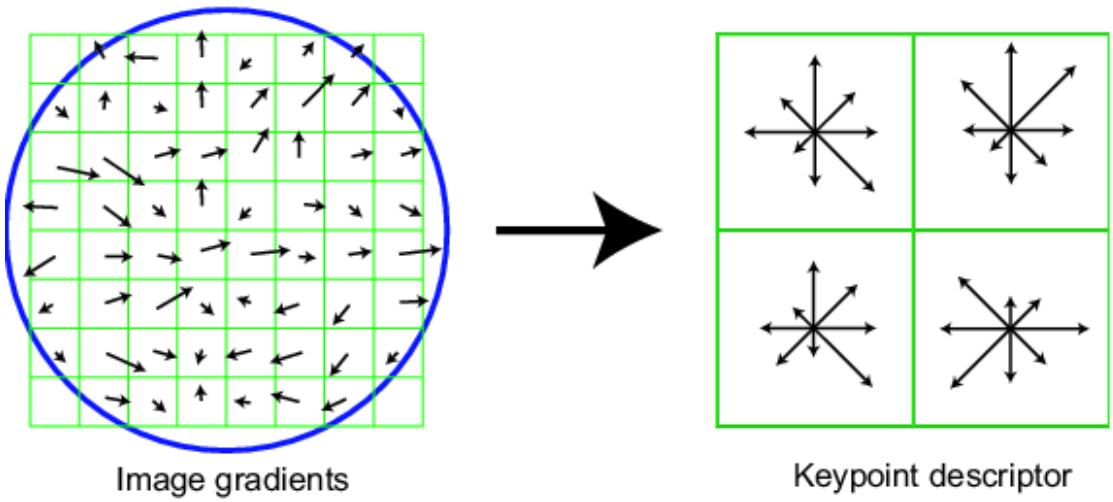

Figure 3.6: This figure shows a $2x2$ descriptor array computed from a $8x8$ set of samples. On the left image the gradient magnitude and orientation is computed at each image sample point in a region around the keypoint location. They are weighted by a Gaussian window (indicated by the circle). These samples are then accumulated into orientation histograms summarizing the contents over $4x4$ subregions, as shown on the right. The length of each arrow corresponds to the sum of the gradient magnitudes near that direction within the region.

3.3 Comparison of feature point detectors

There are several ways how the feature point detectors can be compared. In [80] the *repeatability score* is used as a criterion for comparison of detectors. By this, the repeatability score for a given pair of images is computed as a ratio between the number of point-to-point correspondences and the minimum number of points detected in the images. In [81] Lee made an evaluation of feature extraction techniques for robust watermarking. They perform Bas' approach [36] using tree different feature point detectors: Harris detector used in original Bas' approach, Mexican hat wavelet scale interaction method and SIFT feature point detector. After feature extraction, the set of triangles is generated by Delaunay tessellation. For all tree detectors, they compute the numbers of extracted triangles on original image and compare it with the number of extracted triangles on distorted image. The distorted image was obtained after applying the geometrical distortions, as well as different filtering and JPEG compressions. It is shown that SIFT detector has a good potential to be used in watermarking.

In this part the comparative evaluation of the scale-invariant feature point detectors: SIFT and Harris-Affine, will be done. The aim of this comparison is to show which feature point detector gives more robust feature points under different distortions. These points will be used later for image watermarking. The software implementation of these feature point detectors is used from [82]. Our evaluation will be performed for 10 images with the size of 512 x 512: *barbara*, *boats*, *cameraman*, *couple*, *einstein*, *elaine*, *f16*, *goldhill*, *house* and *lena* (see Appendix D) image which are commonly used images in image processing applications. On every test image, the different signal processing operations will be applied. Among them are non-geometrical operations like: compressions (JPEG, JPEG2000), filtering operation (Gaussian, median, wiener, trim mead mean), noise addition (salt' n pepper or Poisson) or geometrical distortion like: rotation, scaling, cropping or combination of them. These images will be referred as distorted images. The feature points will be extracted on the test image and on its distorted version using both feature extraction methods. It will be measured how many corresponding feature points can be found on original and distorted image.

However, in our experiments we will not observe the total number of extracted feature points. We will reduce it to the set of feature points with the largest characteristic scale. In the next Chapter the watermark synchronization technique will be developed based on use of feature points with the largest characteristic scale. The synchronization information will be embedded into the circular neighborhood of the feature point, with radius proportional to the characteristic scale. From this point of view it was more reasonable to observe in our experiments only the feature point with the largest characteristic scale.

The whole procedure is performed in the following steps:

1. The feature points will be extracted on original and on distorted image using SIFT and Harris-Affine feature point detectors;
2. For every feature point extracted with this two detectors its characteristic scale will be computed;
3. The points from the same image will be sorted in descending order by the characteristic scale and first i ($i \in \{10, 20, 30\}$) points from this set will be selected. Actually these points are points with the largest characteristic scale;
4. In order to compare the corresponding points on original and distorted image, the SIFT descriptors for the selected points will be computed ($SIFT_t$ for the test image and $SIFT_d$ for the distorted image, where $t = 1 \ldots i, d = 1 \ldots i$);
5. The i SIFT descriptors of test image will be compared with i SIFT descriptors of distorted image. Matching will be performed applying the correlation. The correlation coefficient between the SIFT descriptors will be computed:

$$corr(SIFT_t, SIFT_d) > thr \tag{3.11}$$

6. If the correlation coefficient is grater then a threshold thr the matching points are found. thr value is set to 0.9.

Figure 3.7shows the feature points with the largest characteristic scale extracted on Lena image: (a), (c), (e) shows the first i points ($i \in \{10, 20, 30\}$, respectively) with the largest characteristic scale extracted with SIFT detector while (b), (d), (f) presents the first i points ($i \in \{10, 20, 30\}$, respectively) with the largest characteristic scale extracted with Harris-Affine detector.

(a)

(b)

(c)

(d)

(e)

(f)

Figure 3.7 Feature points extracted on Lena image: first 10 points with the largest characteristic scale extracted with SIFT detector (a) and Harris-Affine detector (b); first 20 points with the largest characteristic scale extracted with SIFT detector (c) and Harris-Affine detector (d); first 30 points with the largest characteristic scale extracted with SIFT detector (e) and Harris-Affine detector (f).

The results of the comparison of SIFT and Harris-Affine feature point detectors are presented in the Tables A.1-A.3 (see Appendix A). Columns denoted with SF presents the corresponding points found with SIFT detector and HA- the corresponding points found with Harris-Affine detector.

In the Table A.1 the results for the following non-geometrical operations are presented: jpg40- JPEG compression with quality factor 40; jpg50- JPEG compression with quality factor 50; wc40- JPEG2000 compression with 0.4 bpp; wc50- JPEG2000 compression with 0.5 bpp; med- median filtering with 3x3 window size; gaus- Gaussian filtering with 5x5 window size; wien- wiener filtering with 5x5 window size; trim- trimmead mean filtering with 7x7 window size; salt- salt' n pepper noise added to the image, pois- possion noise added to the image.

In Table A.2 the results for the following operation are given: rot1- rotation for 5 degrees, rot2- rotation for 10 degrees, rot3- rotation for 15 degrees, rot4- rotation for 30 degrees, sc1- image scaling with new image size of 0.8 x image size, sc2- image scaling with new image size of 0.9 x image size, sc3- image scaling with new image size of 1.2 x image size, sc4- image scaling with new image size of 1.5 x image size.

In the Table A.3 the results of image cropping and combination of rotation, scaling and cropping is presented. cr1- 5 % image cropping, cr2- 10 % image cropping, cr3- 15 % image cropping, cr4- 20 % image cropping, cr5- 25 % image cropping, rs1- rotation of 5 degrees and scaling with new image size of 1.2 x image size; rs2- rotation of 15 degrees and scaling with new image size of 0.9 x image size; rs3- rotation of 10 degrees and scaling with new image size of 1.5 x image size; rs4- rotation of 30 degrees and scaling with new image size of 0.8 x image size.

For every distortion separately the average number of all corresponding points for all test images is computed. The computation is done separately for the first i points with the largest characteristic scale ($i = 10, 20, 30$) and presented on the Figures 3.8-3.10. Distortions are placed on *x-axis* and on *y*-axis are the average numbers of corresponding points in percentage (computed as the total number of corresponding points for all images divided with i and multiplied with 100%).

In the case of non-geometrical distortions in can be observed from the Figure 3.8 that more corresponding points are found with Harris-Affine detector. However, the difference between SF and HA is not very big and it can be concluded that both detectors give very good results. Comparing the number of corresponding points for different sets of selected

points with the largest characteristic scale, better results are obtained using only the $i = 10$ points then $i = 20$ and $i = 30$ points.

The performance of the detectors is not as good for geometrical distortions as with the non-geometrical distortion (Figure 3.8, 3.9). For the most of the geometrical distortions which consist of rotation, scaling or combinations of them, feature extraction method based on SIFT detector gives more corresponding points then Harris-Affine. However, most of the corresponding points which are found with Harris-Affine detector (without reducing the observation point set on set of points with the largest characteristic scale) have actually small characteristic scale. Comparing the number of corresponding points by i parameter more points are obtained for $i = 20$, although the percentages of corresponding points for $i = 10$ and $i = 20$ are similar.

For the image cropping distortion the results for both detectors are very good (Figure 3.10). It can be observed that at least 50% of corresponding points can be found. The results strongly depend of the points distribution over the image.

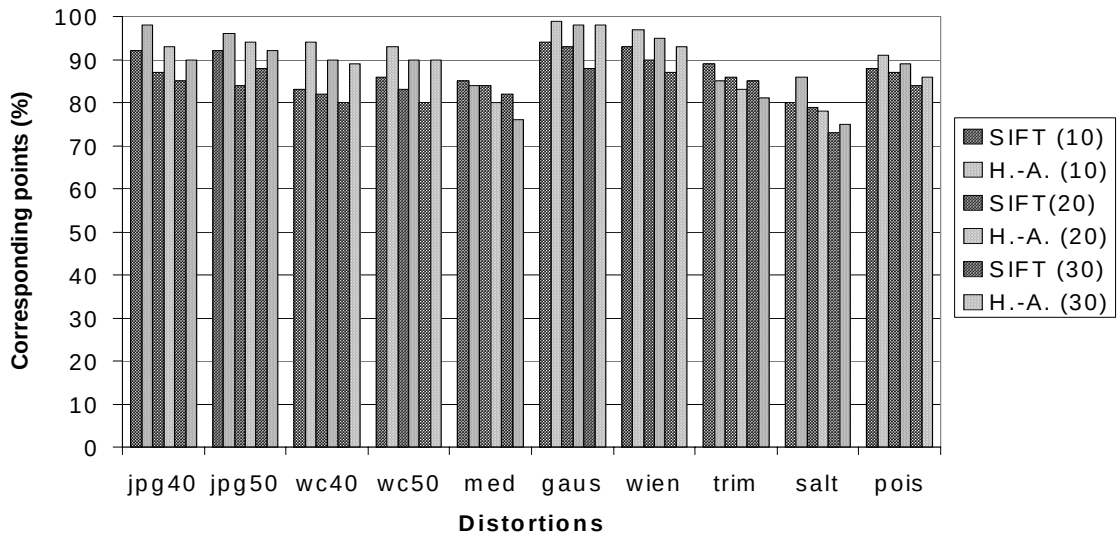

Figure 3.8: The average number of the corresponding points for all test images in the case of non-geometrical distortions.

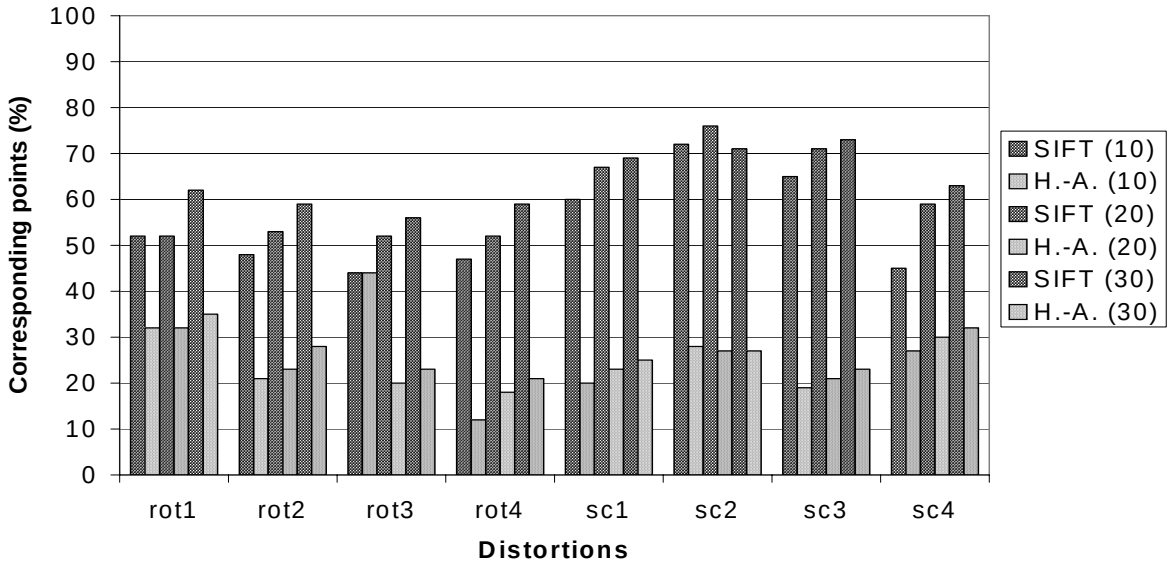

Figure 3.9: The average number of the corresponding points for all test images in the case of rotation and image scaling distortions.

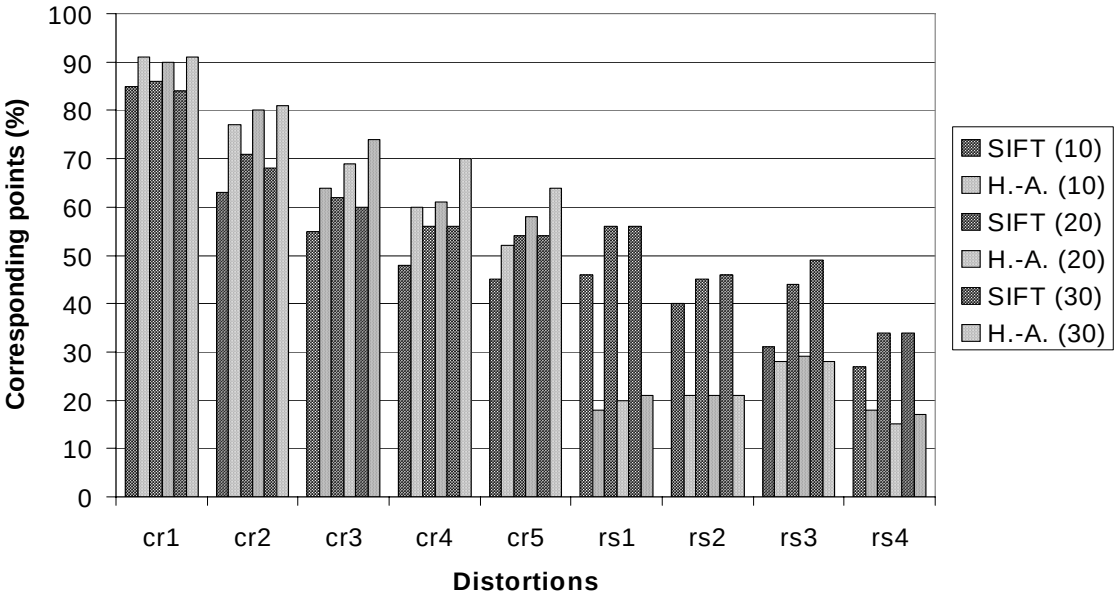

Figure 3.10: The average number of the corresponding points for all test images in the case of image cropping and combination of rotation and image scaling distortions.

3.4 Chapter Summary

In this Chapter we introduce the implementation of feature point detectors in watermarking. The brief overview of existing watermarking techniques, which are based on the use of feature point detectors, is given. It is outlined which feature point detectors are used in the watermarking field till the present. Then a new class of scale invariant feature point detectors is introduced and particular SIFT feature point detector is described. After that a comparison between two scale-invariant feature point detectors: SIFT and Harris-Affine is performed. The aim of this comparison is to show which feature point detector gives more robust feature points under different distortions. However, in the experiments only the feature points will the largest characteristic scale were observed. It is shown that the SIFT feature point detector gives more robust feature points and it is more suitable for the development of the technique for recovering the watermark synchronization.

In the next Chapter the synchronization issue in watermarking will be introduced. Firstly, and image registration technique will be described. Then the literature survey of existing watermarking techniques, which consider the problem of synchronization without access to the original image content, will be overview. A new synchronization technique which is based on use of the feature points detected with SIFT detector will be developed and tested in the next Chapter.

Chapter 4

The synchronization issue in watermarking schemes

The resistance of watermarking schemes against geometrical distortions has been the subject of quite research in the last ten years. Even the minor geometrical manipulation to the watermarked image can dramatically reduce the ability of the receiver to detect the watermark. The effect of geometrical distortions can be better understood by making the analogy between the watermark and any communication system. In communication system the synchronization between the encoder and decoder is related to the time-synchronization. In watermarking system the synchronization principle can be applied and it is related to the geometric synchronization. In order to detect watermark correctly, the watermark decoder should use the same coordinates as on original image. If the received image is geometrically manipulated the coordinates of the received image will be different from the original one. As a consequence, the watermark detector will loose the synchronization. Hence, it is required to implement a synchronization recovery technique as a pre-processing step at the decoder side.

Roughly, the watermarking schemes dealing with the problem of synchronization can be divided into two groups:

1. techniques that use the original image content (image registration techniques);
2. techniques without the access to the original image content.

In Section 4.1 an image registration technique is described and experimentally tested. Section 4.2 gives an overview of the existing watermarking techniques, which

consider the problem of synchronization without access to the original image content. In Section 4.3 the proposed synchronization technique is described and tested.

4.1 Image registration techniques

If the original image is available to the watermark detector, firstly, an image registration technique can be used to establish point-by-point correspondence between the original image and image possibly altered by unknown geometrical transformation (received image). When the correspondence between the two images is found the parameters of the undergone geometrical transformation can be estimated. From these parameters an inverse geometrical transformation can be calculated and applied to the received image. After that, the watermark detection procedure is performed.

In this part a registration method applied on original image and image possibly altered by unknown geometrical transformation (received image), used in our work [42, 43] will be briefly described:

1. On the original and distorted image the feature points are detected using the SIFT feature point detector, described in the Chapter 3.
2. For every feature point, the corresponding SIFT descriptor is calculated. Array of SIFT descriptors calculated for original image is denoted by $SIFT_0$ and $SIFT_d$ for the received image, where $o = 1 \ldots n_1, d = 1 \ldots n_2$. n_1 and n_2 are the total numbers of feature points detected on original image and received image, respectively.
3. The comparison between each element of $SIFT_0$ and $SIFT_d$ is performed applying the correlation. The correlation coefficient between the $SIFT_0$ and $SIFT_d$, $o = 1 \ldots n_1, d = 1 \ldots n_2$ is computed:

$$corr(SIFT_0, SIFT_d) = \frac{\sum_{i=1}^{128} (SIFT_{0i} - \overline{SIFT_0})(SIFT_{di} - \overline{SIFT_d})}{\sqrt{\sum_{i=1}^{128} (SIFT_{0i} - \overline{SIFT_0})^2 \sum_{i=1}^{128} (SIFT_{di} - \overline{SIFT_d})^2}} \quad (4.1)$$

where $\overline{SIFT_0}$ and $\overline{SIFT_d}$ are the mean values of $SIFT_0$ and $SIFT_d$. By this SIFT descriptor of every feature point is vector of 128 elements.

4. If the correlation coefficient is grater then a threshold thr the corresponding points are found. thr value is set to 0.9.

$$corr(SIFT_0, SIFT_d) > thr \tag{4.2}$$

Now a few experiments will be performed in order to show ability of our method to register the image after geometric distortion. In our experiments it is assumed that the original image is transformed by an affine transformation.

An affine transformation can be expressed as:

$$\begin{bmatrix} x_{1d} \\ x_{2d} \\ 1 \end{bmatrix} = \mathbf{A}_{\text{ff}} \begin{bmatrix} x_1 \\ x_2 \\ 1 \end{bmatrix} \tag{4.3}$$

$$\mathbf{A}_{\text{ff}} = \begin{bmatrix} a_{11} & a_{12} & t_{x_1} \\ a_{21} & a_{22} & t_{x_2} \\ 0 & 0 & 1 \end{bmatrix} \tag{4.4}$$

where x_1, x_2 are the image coordinates which are transformed to the coordinates x_{1d}, x_{2d} using an affine matrix $\mathbf{A}_{\text{ff}}$. The coefficients a_{11}, a_{12}, a_{21}, a_{22} present the linear part of transformation ($\mathbf{A}_{\text{ffL}}$); t_{x_1} and t_{x_2} are parameters of translation. The linear part $\mathbf{A}_{\text{ffL}}$ of affine matrix $\mathbf{A}_{\text{ff}}$ can be expressed as combination of rotation, scaling and shearing transformation with the corresponding parameters:

$$\mathbf{A}_{\text{ffL}} = \begin{bmatrix} a_{11} & a_{12} \\ a_{21} & a_{22} \end{bmatrix} = \begin{bmatrix} cos(\theta) & sin(\theta) \\ -sin(\theta) & cos(\theta) \end{bmatrix} \begin{bmatrix} S_{x_1} & 0 \\ 0 & S_{x_2} \end{bmatrix} \begin{bmatrix} 1 & Sh \\ 0 & 1 \end{bmatrix} \tag{4.5}$$

Each of the parameters of the transformation can be computed:

$$tan(\theta) = -\frac{a_{21}}{a_{11}} \quad \text{for rotation} \tag{4.6}$$

$$S_{x_1} = \sqrt{a_{11}{}^2 + a_{21}{}^2}\,,\ S_{x_2} = \frac{\det(\mathbf{A}_{\text{ffL}})}{S_{x_1}} \quad \text{for image scaling} \tag{4.7}$$

$$Sh = \frac{a_{11}a_{12} + a_{21}a_{22}}{\det(\mathbf{A}_{\text{ffL}})} \quad \text{for shearing} \tag{4.8}$$

In order to determine the parameters of affine transformations it is enough to detect 3 corresponding points on original and received image.

Six combined affine geometrical attacks are performed. These attacks consist of rotation, scaling, shearing, or combination of them with the image cropping. These attacks are denoted as G1-G6 and the parameters of the affine transformations are given in the Table 1. G1 is the shearing attack with $Sh = 0.5$; G2 is the rotation attack with $\theta = 30^\circ$; G3 is the scaling attack with $S_{x_1} = S_{x_2} = 0.8$; G4 is the combination of rotation attack with $\theta = 20^\circ$, scaling with $S_{x_1} = S_{x_2} = 1.2$ and cropping; G5 is combination of rotation with $\theta = 45^\circ$, scaling with $S_{x_1} = 1.3$, $S_{x_2} = 0.9$; G6 is combination of rotation $\theta = 8^\circ$ and scaling $S_{x_1} = S_{x_2} = 0.5$.

In Figures 4.1-4.6 the six geometrical attacks are presented: (a) is the original Lena image, (b) is geometrically transformed Lena image and (c) is the reconstructed image after applying the inverse affine transform. The corresponding feature points are presented on Figures (a) and (b). From the Figures it can be seen that for different distortion the different corresponding feature points are found.

In Table 4.1 the following parameters are presented: the total number of feature points extracted on original image ("fpo"); the total number of feature points extracted on transformed image ("fpt"); the size of the transformed image; the total number of corresponding points ("cp"); the parameters of applied affine transformation (a_{O11}, a_{O12},

a_{O21}, a_{O22}) and parameters of computed affine transformation $\mathbf{A}_{\text{ffC}}$ (a_{C11}, a_{C12}, a_{C21}, a_{C22}). The size of the original Lena image was $512\,x\,512$. In order to express the quality of the computed parameters the Mean Square Error (MSE) was calculated. MSE value was 8.610^{-7} which shows that the difference between the originally applied parameters of affine transformation and computed parameters using this image registration technique is negligible.

(a) (b) (c)

Figure 4.1: (a) Original Lena image. (b) Lena image after G1 attack. The corresponding feature points are presented on the both images. (c) Reconstructed image.

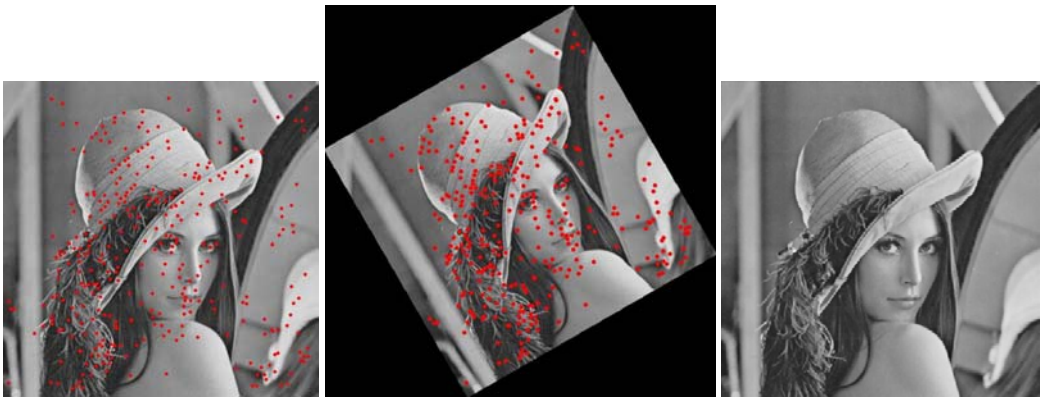

(a) (b) (c)

Figure 4.2: (a) Original Lena image. (b) Lena image after G2 attack. The corresponding feature points are presented on the both images. (c) Reconstructed image.

(a) (b) (c)

Figure 4.3: (a) Original Lena image. (b) Lena image after G3 attack. The corresponding feature points are presented on the both images (c) Reconstructed image.

(a) (b) (c)

Figure 4.4: (a) Original Lena image. (b) Lena image after G4 attack. The corresponding feature points are presented on the both images. (c) Reconstructed image.

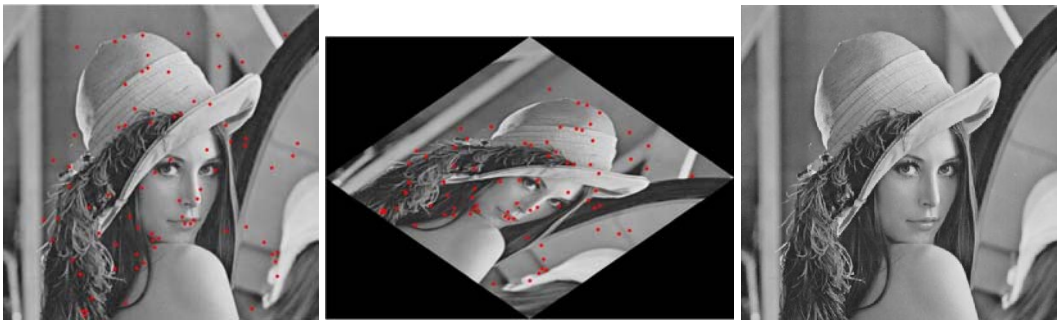

(a) (b) (c)

Figure 4.5: (a) Original Lena image. (b) Lena image after G5 attack. The corresponding feature points are presented on the both images (c) Reconstructed image.

(a) (b) (c)

Figure 4.6: (a) Original Lena image. (b) Lena image after G6 attack. The corresponding feature points are presented on the both images (c) Reconstructed image.

Table 4.1: The affine computation

	fpo	fpt	size	cp	a_{O11}	a_{O12}	a_{O21}	a_{O22}	a_{C11}	a_{C12}	a_{C21}	a_{C22}
G1	515	550	512x768	37	1	0	0.5	1	1.0023	0.0011	0.5002	1.0010
G2	515	582	701x701	340	0.8666	-0.5	0.5	0.8666	0.8661	-0.5004	0.5000	0.8655
G3	515	363	409x409	152	0.8	0	0	0.8	0.7987	-0.0003	0.0001	0.7986
G4	515	778	614x614	187	1.1276	0.41	-0.41	1.1276	1.1268	-0.4097	0.4101	1.1272
G5	515	646	652x941	79	0.9192	0.6364	-0.9192	0.6354	0.9180	0.6354	-0.9207	0.6368
G6	515	166	293x293	49	0.4951	0.0696	-0.0696	0.4951	0.4955	0.0695	-0.0695	0.4945

It is shown from our experiments that this image registration technique can successfully calculate the parameters of affine transformation. Using the correlation threshold above 0.9 to measure the similarity between the SIFT descriptors, only the corresponding and some nearly corresponding points will be extracted on original and transformed image. The percentage of nearly corresponding points is very low and it does not have influence of the computation of the affine parameters because the larger set of points is included in the computation of the affine parameters, then it is necessary. In the Next Chapters it will be shown how this technique can increase the robustness of the proposed watermarking algorithms on geometrical distortions.

4.2 Watermarking techniques dealing with the problem of synchronization without access to the original image content

In the following Section a survey of the watermarking techniques claiming resistance to geometrical distortions will be presented. These techniques do not use the original image content. The classification will be organized according to the common approaches. Some techniques can be classified in more then one class because they combine several different approaches.

4.2.1 Exhaustive search

This approach considers all possible geometrical distortions that could take place. The inverse transformation is applied to the received image and the watermark detection, too. The embedded watermark is extracted choosing the best detection confidence value (e.g. correlation coefficient), which is beyond the appropriate threshold. The main drawbacks of these approaches are increased computational costs and possibility of false detection. The possibility of false watermark detection under exhaustive search is deeply studied in [83, 84, 85].

Usually in these approaches the transformation sets are limited to translation, scaling and rotation. In order to decrease the computational costs and to observe more complex transformations, detection procedure can be performed on smaller image regions [86].

4.2.2 Periodical sequences

One strategy to solve the synchronisation problem introduced by geometrical distortions is to add redundancy during the embedding process. This redundancy can be used to localize the position of the watermark and to improve the detection stage [87, 88,

89]. In these approaches the search for synchronization is limited to one repetition period. In [90] the periodical watermark insertion is used to perform the synchronization. This scheme is designed against StirMark attack, which introduce small local geometrical distortions. The correlation technique with sliding windows (commonly used in communication in order to recover synchronization) is implemented. The image is divided in blocks and marks are embedded in these blocks. The technique of sliding window is implemented on image blocks and the correlation between the image block of received image, possibly containing the watermark and the block with the watermark is measured. If the mark is detected in the block the location of the mark in the neighbor block is initialized by the previous location.

4.2.3 Invariant domains

The main idea of watermarking in the transform invariant domain is to perform the watermark embedding or detection in the domain invariant to geometrical transformations. One of the examples is to apply a Fourier-Mellin transform (see Appendix C) to the DFT magnitude of the original image spectrum [27, 28]. In Fourier domain magnitude spectrum is insensitive to translation, image scaling produces inverse scaling in frequency domain and image rotation causes the spectrum rotation for the same angle. Transforming the Cartesian coordinates of the Fourier domain in log-polar, image scaling and rotation become the translation. Applying again the Fourier transformation to the log-polar representation of the magnitude spectra, the Fourier-Mellin domain is obtained (see Figure 4.7). Fourier-Mellin domain is rotation, scale and translation invariant. The main problem with the implementation of discrete Fourier-Mellin transformation is that the forward and inverse transformations are not straightforward. The logarithmic sampling of the log-polar mapping must be carefully implemented in order to avoid the interpolation errors (see Figure 4.10).

Another possibility to obtain an invariant domain was the implementation of the log-log mapping of the Fourier spectra [29]. Such a representation was insensitive to image cropping, scaling, modification of aspect ratio, but not invariant to rotation.

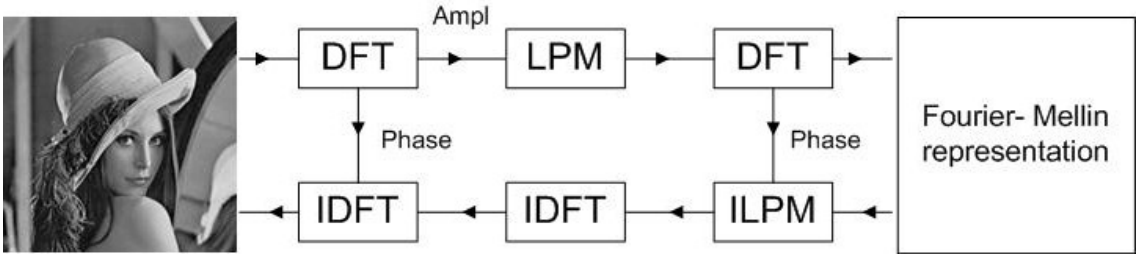

Figure 4.7: Rotation, scale, translation invariant Fourier Mellin domain.

4.2.4 Synchronization marks

These approaches use the training signal, also called pilot signals, which have known and easily detectable features. They do not convey the payload information. To estimate the distortion at the detector side it is necessary to register correctly the received signal with the original pilot signal. The detection of pilot signals must be robust to the addressed distortions. In [30, 31] the pilot registration is performed in spatial domain. Here we will focus more on the pilot signal, also called *template* which is embedded in the frequency domain [32, 33, 34]. The template itself does not contain payload information and it is only used to recover the geometrical transformation. A few examples of the templates are presented in the Figure 4.8.

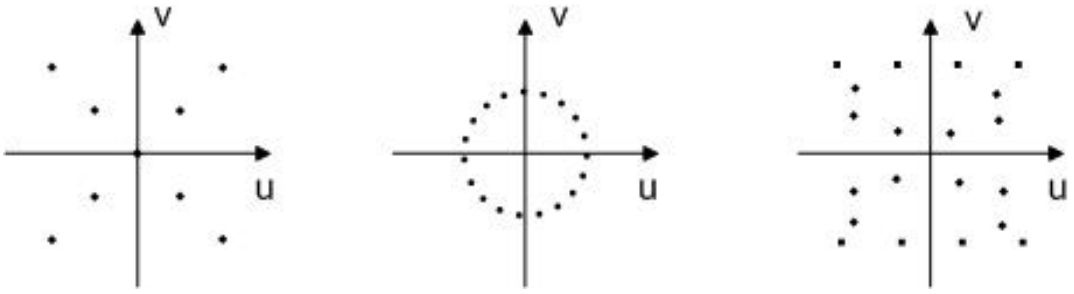

(a) (b) (c)

Figure 4.8: The examples of different templates used in the DFT domain (a) diagonal, (b) circular, (c) key dependent (random).

In the template based approaches it is important to resolve the following problems:

- Where to embed such a template to satisfy the trade-off between the visibility and robustness. Template points should be embedded as local peaks in its neighborhood.
- How to detect peaks after geometrical attacks possibly followed by lossy compression.
- Design an efficient and fast template matching algorithm for estimation of the parameters of affine transformation [91].

In [92] template registration was performed using log-polar and log-log mapping. For improving the efficiency of the template registration, in our work [93] we propose the implementation of Radon transform (see Appendix B). The Radon transform is implemented on the Fourier spectrum in order to detect the angle of image rotation. After that the searching for the template points is performed. The algorithm has the following steps:

- Apply DFT on the original and received image.
- In order to calculate the angle of the image rotation, apply the Radon Transform on the DFT spectra of original and received image. The difference between the peaks of the Radon transform will give the angle of rotation.
- Rotate the received image for the calculated angle.
- Extract the local peaks of the DFT spectra. The extracted peaks include the template peaks, which are possibly affected by a geometrical transform, and many other peaks, which originally exist in the DFT spectra of the image.
- Search for the template points and calculate the new distance between the template points.
- The ratio between the new and old distance of the template points will correspond to the scaling parameter in DFT domain and the inverse scaling in spatial domain.

In Figure 4.9.a an example of the Radon Transform of the Lena image is presented. In Figure 4.9.b the corresponding graph with the Radon Transform of the Lena image rotated for 30° is presented. By extracting the peaks of the Radon Transform of the original

and rotated image and by subtracting them the angle of the rotation can be calculated. From Figure 4.9 it is obvious that the unknown angle (30°) can be simply determined.

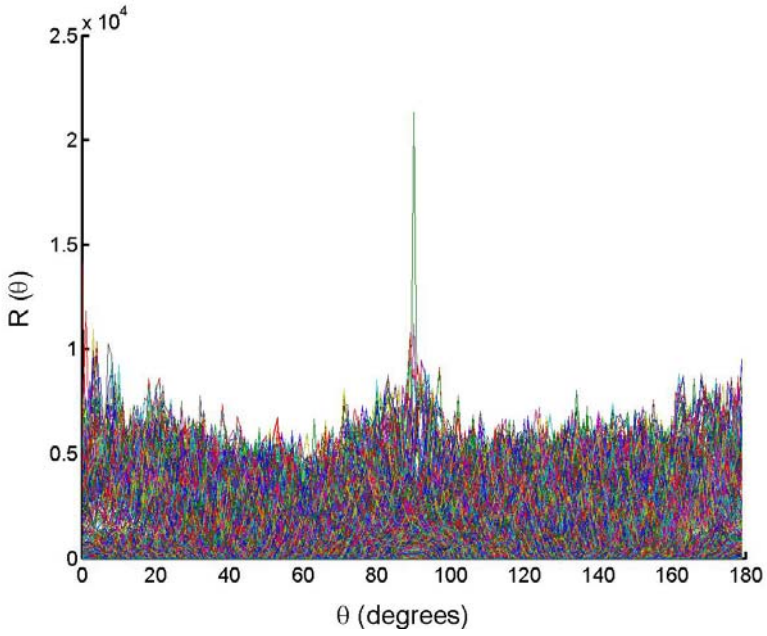

(a)

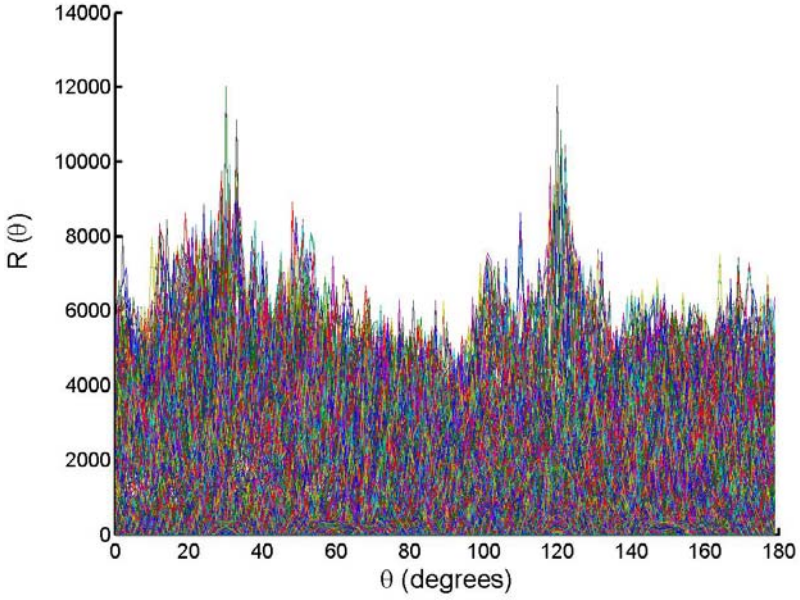

(b)

Figure 4.9: Radon Transform of: (a) Lena image; (b) rotated Lena image for 30°

One of the drawbacks of the template based approaches is its security. Even with the usage of key-dependent template, an attacker can easily predict the template without knowledge about the key and remove it. One example of such an attack is template removal attack [94].

Another synchronization possibility is provided by the approaches based on self-reference watermarks. They do not use any additional template. The watermark itself is arranged in the special spatial structure, which has desired statistical properties. Based on the watermark design and the watermark statistic used for the estimation the parameters of affine transformation, the following types of self-reference watermark can be distinguished:

- self-reference watermark based on 4 times repeated patterns and affine estimation based on autocorrelation function (ACF) [95];
- periodic watermarks with any geometry and affine estimation based on the magnitude watermark spectrum [96, 97];
- self-similar patterns or patterns with a special spatial structure [87, 98, 99].

In [95] the same watermark is four times embedded in the image, which enables to have nine peaks in the ACF that are used to detect the parameters of undergone geometrical transformation. The need of computing the two times DFT and reduced robustness in the case of lossy compression are some problems with this approach. To improve the robustness after lossy compression the algorithms based on magnitude spectrum of periodical watermarks are proposed [97]. The magnitude spectrum of the estimate watermark is computed. Due to the periodicity of the embedded information the magnitude spectrum showed aligned and regularly spaced peaks. If the affine distortion is applied on the watermarked image, the peaks layout will be rescaled, rotated, or shared but alignments will be preserved. Actually it is easy to estimate the affine geometrical distortions from these peaks by fitting the alignments and estimating periods.

4.2.5 Content based approaches

These approaches use the availability of the original image content at the detecting stage. The building of the reference system for watermark embedding is based on the robust image features. The main assumption behind that is that content reference system undergoes the same geometrical distortions as the watermarked image. In [35, 36, 37] the robust features are extracted from the image in order to produce a partitioning of the image in several regions. The watermark is embedded in this region. The content based algorithms are already described in Chapter 3.1.

All discussed techniques have common drawbacks. They are very complicated to perform and they require very high computational costs for developing the searching algorithms. In a case of techniques that are working in invariant domains which use two time Fourier transform and log-polar mapping, the problems caused by interpolation should be also taken into account. Vulnerability to cropping attacks is also common for the most of these techniques. In the next Section we will propose the new synchronization technique that combines a template and content based approach. The main idea of this technique is to extract the robust feature points with SIFT detector and to embed in the neighborhood of every feature point two information independently, which can be later used to detect the parameters of undergone geometrical transformations. To compute the parameters of undergone transformation is very simple and it is enough correctly to detect at least from one feature point neighborhood these two information. The technique is not sensitive to certain percentage of image cropping because it uses the redundant embedding of synchronization information.

4.3 Proposed synchronization technique

In this part the proposed synchronization technique will be described [44]. This technique uses the two dimensional Fourier transform and its log-polar representation.

Before we start with the description of the proposed technique the two dimensional Fourier transform with its properties will be introduced in Subsection 4.3.1. The log-polar representation of the Fourier spectra will be also given in 4.3.1. After that the synchronization technique will be described in details in Subsections 4.3.2 and 4.3.3. In Subsection 4.3.4 the relevant parameters of the proposed technique will be discussed. The proposed technique will be tested in Subsection 4.3.5 and compared with other synchronization techniques in Subsection 4.3.6.

4.3.1 Fourier transform

In this Section, we shall describe the Fourier transform in some detail highlighting those properties, which make it particularly suitable to digital image watermarking.

Let the image be a real valued continuous function $\mathrm{I}(x_1, x_2)$ defined on an integer-valued Cartesian grid $0 < x_1 < N_1,\ 0 < x_2 < N_2$. The Discrete Fourier Transform (DFT) is defined as follows:

$$F(\omega_1, \omega_2) = \frac{1}{N_1 N_2} \sum_{x_1=0}^{N_1-1} \sum_{x_2=0}^{N_2-1} \mathrm{I}(x_1, x_2) e^{-j2\pi x_1 \omega_1 / N_1 - j2\pi x_2 \omega_2 / N_2} \tag{4.9}$$

The inverse transform is:

$$I(x_1, x_2) = \sum_{\omega_1=0}^{N_1-1} \sum_{\omega_2=0}^{N_2-1} F(\omega_1, \omega_2) e^{j2\pi x_1 \omega_1 / N_1 + j2\pi x_2 \omega_2 / N_2} \tag{4.10}$$

The DFT of a real image is generally complex valued. This leads to magnitude and phase representation for the image:

$$A_{\mathrm{mp}}(\omega_1, \omega_2) = \left| F(\omega_1, \omega_2) \right| \tag{4.11}$$

$$\Phi(\omega_1, \omega_2) = \angle F(\omega_1, \omega_2) \tag{4.12}$$

For the real images the Fourier transform has certain symmetries:

$$A_{\mathrm{mp}}(\omega_1,\omega_2) = A_{\mathrm{mp}}{}^{*}(-\omega_1,-\omega_2) \tag{4.13}$$

The symbol $(^{*})$ indicates complex conjugation. For real signals equation (4.13) leads directly to:

$$\left|A_{\mathrm{mp}}(\omega_1,\omega_2)\right| = \left|A_{\mathrm{mp}}(-\omega_1,-\omega_2)\right| \tag{4.14}$$

$$\Phi(\omega_1,\omega_2) = -\Phi(-\omega_1,-\omega_2) \tag{4.15}$$

General Properties of the Fourier Transform

It is very important to study the effect of an arbitrary linear transform on the spectrum of an image. In the case of $N_1 = N_2$ (i.e. square blocks) the kernel of the DFT contains a term of the form:

$$x_1\omega_1 + x_2\omega_2 = \begin{bmatrix} x_1 x_2 \end{bmatrix} \begin{bmatrix} \omega_1 \\ \omega_2 \end{bmatrix} \tag{4.16}$$

If we compute a linear transform on the spatial coordinates:

$$\begin{bmatrix} x_1 \\ x_2 \end{bmatrix} \rightarrow T \begin{bmatrix} x_1 \\ x_2 \end{bmatrix} \tag{4.17}$$

then the value of the DFT will not be changed if:

$$\begin{bmatrix} \omega_1 \\ \omega_2 \end{bmatrix} \rightarrow (T^{-1})^{T} \begin{bmatrix} \omega_1 \\ \omega_2 \end{bmatrix} \tag{4.18}$$

FFT Rotation

Consider a rotation matrix:

$$T = \begin{bmatrix} \cos\theta & -\sin\theta \\ \sin\theta & \cos\theta \end{bmatrix} \tag{4.19}$$

Therefore,

$$(T^{-1})^T = \begin{bmatrix} \cos\theta & -\sin\theta \\ \sin\theta & \cos\theta \end{bmatrix} \tag{4.20}$$

Rotating the image through an angle θ in the spatial domain causes the Fourier representation to be rotated through the same angle.

$$F(\omega_1 \cos\theta - \omega_2 \sin\theta, \omega_1 \sin\theta + \omega_2 \cos\theta) \leftrightarrow I(x_1 \cos\theta - x_2 \sin\theta, x_1 \sin\theta + x_2 \cos\theta) \tag{4.21}$$

Note that the grid is rotated so the value of the image at the new grid points may not be defined. The value of the image at the nearest valid grid point can be estimated by interpolation.

FFT Scale

Consider a scaling matrix:

$$T = \begin{bmatrix} S_{x_1} & 0 \\ 0 & S_{x_2} \end{bmatrix} \tag{4.22}$$

Therefore,

$$(T^{-1})^T = \begin{bmatrix} \frac{1}{S_{x_1}} & 0 \\ 0 & \frac{1}{S_{x_2}} \end{bmatrix} \tag{4.23}$$

Hence, scaling the axes in the spatial domain causes an inverse scaling in the frequency domain.

$$\frac{1}{\rho} F(\frac{\omega_1}{\rho}, \frac{\omega_2}{\rho}) \leftrightarrow I(\rho x_1, \rho x_2) \tag{4.24}$$

FFT Shearing

Consider a shearing matrix:

$$T = \begin{bmatrix} 1 & 0 \\ Sh & 1 \end{bmatrix} \tag{4.25}$$

Therefore,

$$(T^{-1})^T = \begin{bmatrix} 1 & -Sh \\ 0 & 1 \end{bmatrix} \tag{4.26}$$

Therefore, shearing the x_2 coordinates of the spatial coordinates inverse shearing the ω_1 coordinates of the frequency coordinates (and vice versa).

FFT Translation

Shifts in the spatial domain cause a linear shift in the phase component.

$$F(\omega_1, \omega_2) \exp\lfloor - j(t_{x_1}\omega_1 + t_{x_2}\omega_2 \rfloor \leftrightarrow \mathrm{I}(x_1 + t_{x_1}, x_2 + t_{x_2}) \tag{4.27}$$

Note that both $F(\omega_1, \omega_2)$ and its dual $\mathrm{I}(x_1, x_2)$ are periodic functions so it is implicitly assumed that translations cause the image to be “wrapped around". We shall refer to this as a circular translation or a cyclic shift. From property (4.27) of the Fourier transform it is clear that spatial shifts affect only the phase representation of an image. This leads to the well-known result that the magnitude of the Fourier transform is a circular translation invariant.

Log-polar mapping

Consider a point $(x_1, x_2) \in \Re^2$ and define:

$$x_1 = e^{\mu} \cos\theta \tag{4.28a}$$

$$x_2 = e^{\mu} \sin\theta \tag{4.28b}$$

where $\mu \in \Re$ and $0 < \theta < 2\pi$. One can see that for every point (x_1, x_2) there is a point (μ, θ) that uniquely corresponds to it. The new coordinate system has the following properties:

Scaling is converted to a translation.

$$(\rho x_1, \rho x_2) \leftrightarrow (\mu + \log\rho, \theta) \tag{4.29}$$

Rotation is converted to a translation.

$$(x_1 \cos(\delta) - x_2 \sin(\delta), x_1 \sin(\delta) + x_2 \cos(\delta)) \leftrightarrow (\mu, \theta + \delta) \tag{4.30}$$

How does a log polar map look like?

Figure 4.10 shows the effect of a log polar map on the standard Lena image (Figure 10.a). Figure 4.10.b is the log-polar representation of Lena image. Figure 4.10.c is obtained by computing the inverse log-polar mapping. The effect of interpolation can be observed more on the borders of the Figure 4.10.c. Figure 4.10.d presents the difference between the original and reconstructed image. In order to show the difference image better, the intensity values on Figure 4.10.d are rescaled.

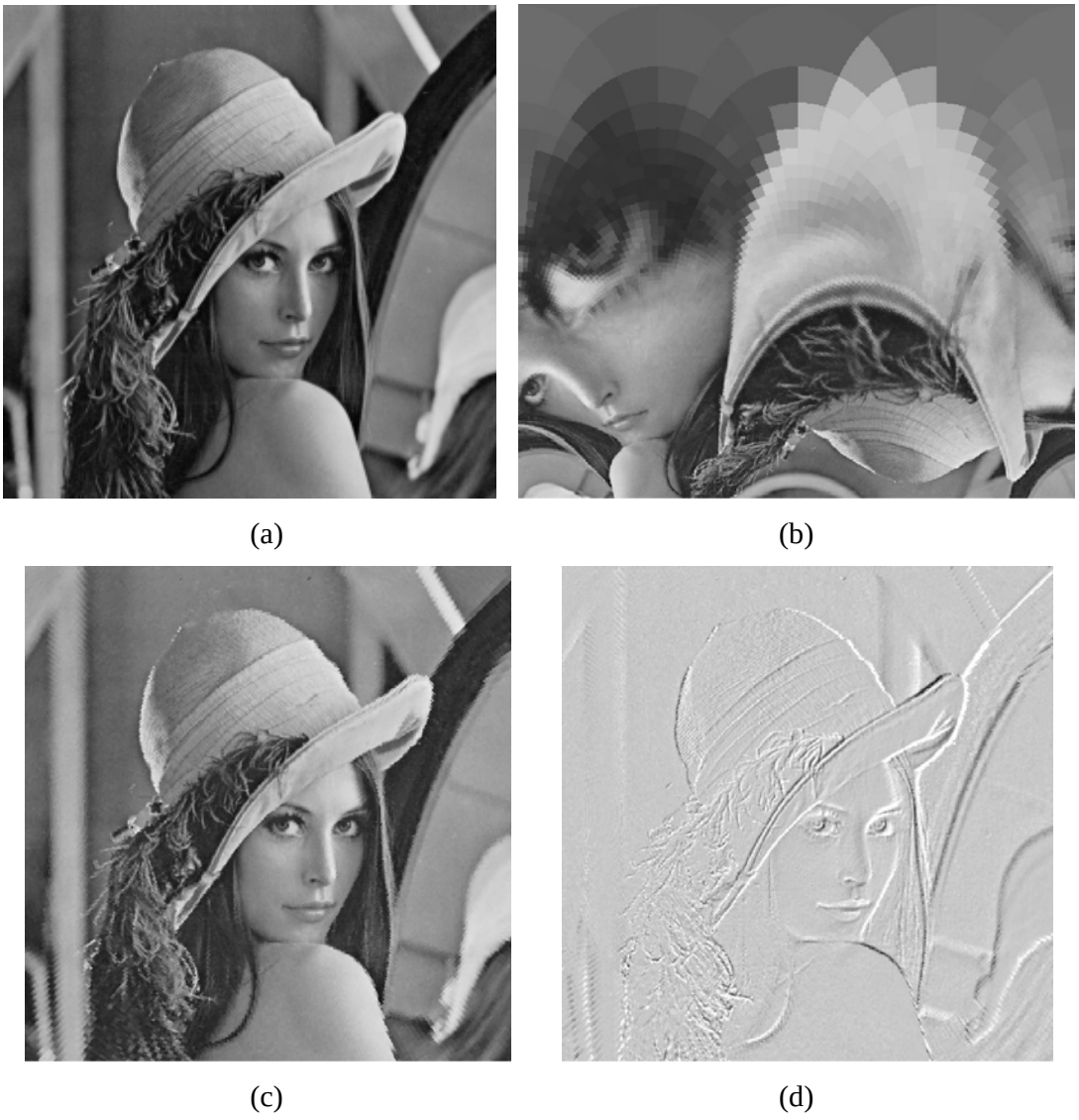

(a) (b)

(c) (d)

Figure 4.10: (a) standard Lena image 512 x 512; (b) log-polar mapping of Lena image 452x512; (c) reconstructed Lena image (inverse log-polar transformed image); (d) the difference between the image (a) and (c) with the rescaled intensity values.

4.3.2 Description of the proposed synchronization technique

In this part the proposed synchronization technique will be described. It combines the template based and content based approach. Firstly, the feature points on original image are extracted using the SIFT detector. In Chapter 3.3 it is shown that the feature points extracted with SIFT detector are robust on filtering, compression and geometrical transformation. Then the 10 feature points with the largest characteristic scale are selected. Around every feature point the circle regions are extracted. The radius of the circle will be equal to the integer value of the characteristic scale multiplied with a constant. This constant will be kept secret. In our case it will be set to one. This circle image region with the feature point in its centre will be firstly zero-padded to the size 256 x 256 and then DFT transformed. The zero padding is performed in order to obtain the desired properties of the Fourier spectra (4.16-4.27). The Cartesian coordinates of the DFT spectra will be transformed to polar. There are two reasons why we have extracted circle region around the feature point rather then the block-based region. Firstly, in the case of geometrical transformation (rotating, scaling) using the circular region the image region most similar to the original one will be extracted. Secondly, the DFT spectra will not strongly depend on the squared region borders.

In the DFT spectra two template point structures will be embedded carrying the information about the reference angle and the information about the characteristic scale. Every template point structure will be placed on the line, which runs through the centre of the polar grid. The position of the lines will be determined by different angles (see Figure 4.11). First line is determined by user defined reference angle. The same reference angle will be used in all regions around the feature points. The second angle, (denoted as “scaling” angle) will be secretly encoded and it will present the information about the characteristic scale of the feature point. This angle will determine the position of the second line where template points will be embedded. Actually, the idea behind it is that when we extract correctly the regular template points in the template extraction procedure, the information about the location of template points will give us the embedded reference and scaling angle.

After the template embedding procedure, the selected image part will be inverse DFT transformed, cropped to the original size and added back to the original image.

If an affine transformation occurs which consists of rotation and scaling the template structures embedded in the image will help us to detect the unknown angle of rotation and scaling parameter. In order to detect the angle of unknown rotation, the rotation property (4.21) of the DFT spectra will be used in our detection scheme. After detecting the rotation parameter, the unknown scaling parameter will be easily calculated using the relationship between the two characteristic scales of the rescaled images (see Chapter 3). This algorithm will be later described in details.

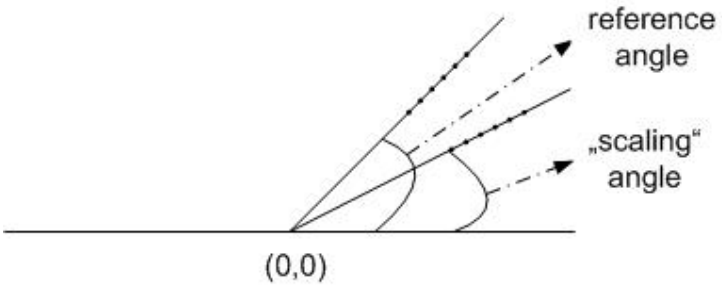

Figure 4.11: In this Figure only the half of the Fourier spectra is presented. Two template point structures are placed on the line, which runs through the centre of the polar grid. First line is determined by user defined reference angle. The second line is determined by angle, (denoted as “scaling” angle) which presents the information about the characteristic scale of the feature point. Template points have a regular structure and they are presented in the Figure with the dots. The same template structure will be also symmetrically embedded in the other half of Fourier spectra, which is not presented in this Figure.

In our practical implementation we have faced few difficulties that are introduced by using the DFT coordinate transformations: Cartesian to polar and polar to Cartesian. Due to interpolation, which occurs in coordinate transformation process some template points will be not detected correctly. To overcome these difficulties the log-polar mapping is used in the following way. The DFT spectra of the image region will be log-polar transformed. Then the position of the template points are calculated firstly using the log-polar coordinates and then transformed in Cartesian. As a consequence of the interpolation process, a few template points will be obtained in Cartesian coordinate system that corresponds to one point in log-polar domain. In the following Subsections the template embedding and extraction procedures will be described.

4.3.2.1 Template embedding algorithm

The embedding algorithm is performed in the following steps:

- Find the feature points on original image using SIFT detector.
- Select the first 10 points with the largest characteristic scale.
- Around every feature point select 10 non-overlapping circle regions, where the radius is equal to the integer value of characteristic scale multiplied with a constant. Set this constant to one. If the point region overlaps with another point region already selected exclude this point region.
- Every selected point region pad with zeros to the size $256 x 256$.
- Apply DFT and select the magnitude spectra.
- Select the reference angle θ_r and encode the characteristic scale:

$$s_e = s_o + c \tag{4.31}$$

  where s_o is original characteristic scale, s_e is encoded value and c is arbitrary selected integer constant, that is kept secret. Integer value of s_e will be referred to "scaling" angle θ_s. The value of the reference angle θ_r will be the same for all feature point regions and $\theta_r > \theta_s$.
- Transform the DFT magnitude spectra in log-polar coordinates.
- The template points in log-polar domain will lie on the line which is determined by θ_r and θ_s. According to the angles θ_r and θ_s calculate the positions of the template points in log-polar coordinates and then transform them to the Cartesian. The template points will be placed in the higher part of the DFT spectra even beyond the spectra of the non zero-padded feature point region (see one example on Figure 4.12).
- Embed the template points in the magnitude spectra of the image region according to the calculated position in Cartesian coordinate system.

$$f_n(x_{1i}, x_{2i}) = f(x_{1i}, x_{2i}) + alfa \tag{4.32}$$

where *alfa* is the template strength and it will be later discussed. $f(x_{1i}, x_{2i})$ are the DFT magnitudes of the selected template points and $f_n(x_{1i}, x_{2i})$ are the new modified magnitudes of the DFT spectra, where $i = 1 \cdots N_t$ and N_t is the total number of template points.

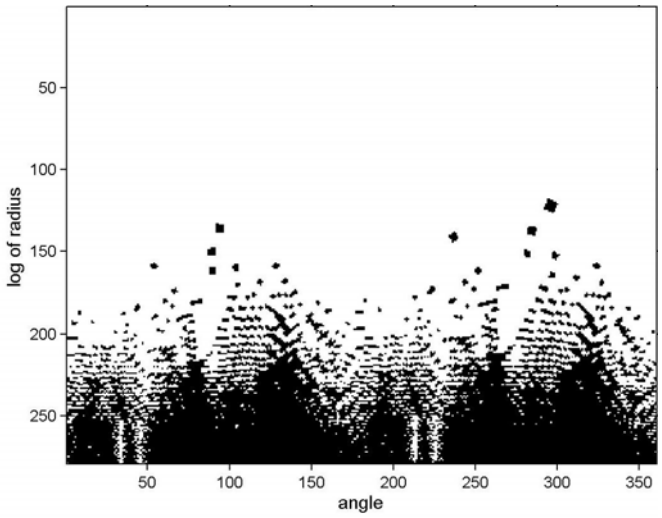

Figure 4.12. One example of embedded template points in log-polar coordinates of Fourier spectra.

- Embed the same template points also in conjugate-complex part of DFT spectra in order to obtain the real image part (see equation (4.14)).
- Apply the inverse DFT transform of the spectra of the image region, crop it to its original size and add to the original image.

4.3.2.2 Template extraction algorithm

In this part the detection algorithm will be performed on received image, which is possibly affine transformed image, which contain the template structure. The template extraction algorithm is described as follows:

- Find the feature points on received image using SIFT detector.
- Select the first 10 points with the largest characteristic scale.
- Around every feature point select 10 non-overlapping circle regions, where the radius is equal to the integer value of characteristic scale multiply with the constant. Set constant to one.
- Every selected point region pad with zeros to the size $256 x 256$.
- Apply DFT and select the magnitude spectra.
- Transform the DFT magnitude spectra in log-polar coordinates.
- From the highest region of log-polar spectra calculate the four angles that present new reference angle θ_{nr}, new scaling angle θ_{ns} and the shifted angles (θ_{nr} and θ_{ns}) for 180 grad coming from the symmetry of the DFT spectra.

The calculation of the reference and scaling angle is performed in the following way:

- Compute the one dimensional mask vector $mask_t$ that represents the template points in the log-polar domain.
- For every angle from the highest part of log polar spectra select an array p_i, $i = 1,\ldots,360$. The array p_i presents actually the column vector in log-polar domain.
- Apply the cross correlation between the mask array $mask_t$ and selected array p_i:

$$c_i = xcorr(mask_t, p_i) \tag{4.33}$$

where the cross correlation function $xcorr$ for two arrays y_1 and y_2 with length N_y and without using the normalization is given by:

$$xcorr(y_1, y_2) = R_{y_1 y_2}(\tau) = \begin{cases} \sum_{i=0}^{N_y - \tau - 1} y_1(i+\tau) y_2^{*}(i), \tau \geq 0 \\ R_{y_2 y_1}(-\tau), \tau < 0 \end{cases} \tag{4.34}$$

where $\tau = 1,\ldots,(2N_y - 1)$.

- Save the maximal value of cross correlation in an array $C = \{c_i\}, i = 1,\ldots,360$.
- Find the 4 maximal values over the entire array C, which represent the reference angle, scaling angle and the shifted angles.
- The reference angle has always higher value then the scaling angle (defined in the template embedding procedure) which implies that $\theta_{nr} > \theta_{ns}$.

When the geometric transformation occurs which consists of rotation, scaling or combination of them, the angle of rotation and scaling parameter can be calculated for every selected region. Using the rotation property of the DFT spectra (equation 4.21) the difference between the new- and old reference angle (θ_{nr} and θ_r, respectively) presents the parameter of image rotation θ_{rot}:

$$\theta_{rot} = \theta_{nr} - \theta_r \tag{4.35}$$

The parameter of image scaling will be computed in a different way. Let s_o be the original characteristic scale and s_e is the encoded image scale. Let θ_{ns} is the new calculated scale angle. Using the rotation property of the DFT spectra (equation 4.21):

$$\theta_{ns} = s_e + \theta_{rot} = s_o + c + \theta_{rot} \tag{4.36}$$

The integer value of the original characteristic scale can be calculated as:

$$s_o = \theta_{ns} - c - \theta_{rot} \tag{4.37}$$

Using the relationship between the two characteristic scales of the rescaled images.

$$s_{cal} = s_a / s_o \tag{4.38}$$

where s_a is the integer value of the characteristic scale of selected feature point. The scaling parameter s_{cal} is computed according to the equation (4.38).

After the calculating the rotation angle θ_{rot} and scaling parameter s_{cal} it is possible to calculate the inverse affine transformation.

4.3.3 Discussion about the relevant parameters of the proposed technique

In this Subsection we will discuss about the relevant parameters of the proposed synchronization technique.

First important parameter in this technique is the strength of the template points (denoted as *alfa* value (see equation (4.32)). The strength of the template points represents the trade off between the invisibility and robustness. In our case the template points are embedded in the higher part of the DFT spectra in diagonal way which introduce in spatial domain a certain percentage of the additional high frequencies. On the other hand the template points will be embedded in affine-invariant part of the image selected around the feature point. These regions are often smoothed or dark regions which does not contain the important information about the image and the human eye is less sensitive to the changes in this part of the image In the Figure 4.13 the selected image parts where the template points were embedded are presented on: 4.13.a couple image; 4.13.b Barbara image and 4.13.c Lena image.

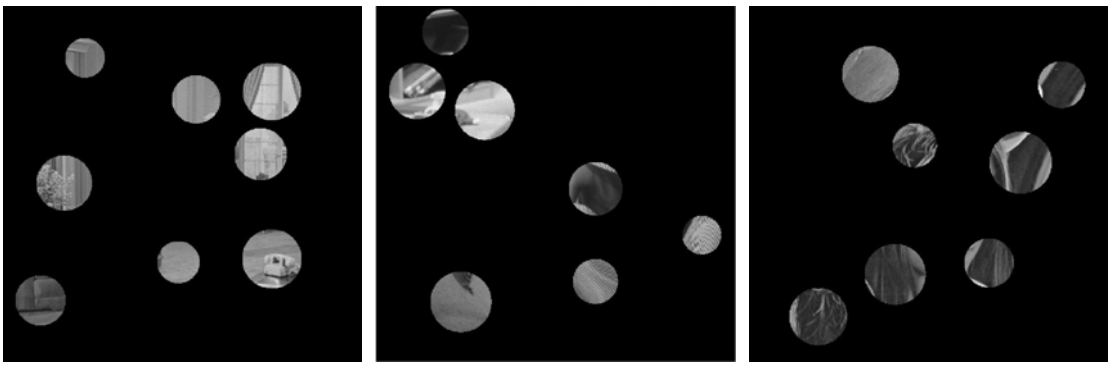

(a) (b) (c)

Figure 4.13: The circular regions selected for template embedding on (a) couple image; (b) Barbara image; (c) Lena image.

The value of the template strength should be carefully selected. Firstly the template points after embedding in DFT magnitude spectra go through the process of the inverse DFT transform, cropping to its original size, and forward transforming in order to detect the template points. As a consequence of the cropping the amplitude of the template points will be reduced. The *alfa* should not be too small because it would be very difficult to distinguish the template points from the neighboring points. If the *alfa* value is to high the visual artefacts will be detectable on image. In our case we have calculated separately *alfa* value for every selected image region:

$$alfa = \frac{m_{DFT_1}}{20} \tag{4.39}$$

where m_{DFT_1} was the maximal value of the DFT_1 spectra. DFT_1 was obtained from the DFT spectra of the image region in that way that the maximal value of the DFT region spectra is set to zero. The equation (4.39) is experimentally obtained as a trade off of invisibility and robustness.

The second parameter, which should be considered, is related to the detection of the template points. In our practical realization we will not observed the entire DFT spectra of the image region in log-polar domain. Only the component of the DFT spectra which magnitude is higher than a threshold will be observed. If the threshold value is to small, more spectral components will be passed through and it will be more difficult to distinguish the template points from other DFT components. If the threshold value is to high there would be no template points. Also abovementioned effect of cropping should be also taken in consideration. The threshold value should be smaller then $m_{DFT_1} / 20$. Also the effects of image scaling (see equation (4.24)) which have the influence on the magnitude of the DFT spectra should be also considered in establishing the threshold value. In our practical realization the threshold value was iteratively selected for every image region. The threshold value was set at the beginning to m_{DFT_1} / p_{r1} and observed how many peaks are obtained. If there is no cross correlation peaks (see equation (4.34)) the threshold value was increased. A procedure stops if the peaks are detected or if the threshold value is approximately around the m_{DFT_1} / p_{r2}. The values for p_{r1} and p_{r2} are experimentally obtained with $p_{r1} = 40$ and

$p_{r2} = 230$. The incrementing step was set to 10. A more intelligent method that adaptively selects the threshold value and spares the computation time should be further developed.

In our experiments the distance between the template points in log-polar map was 3. Also the template structure, which has 10 template points in log-polar representation, is used.

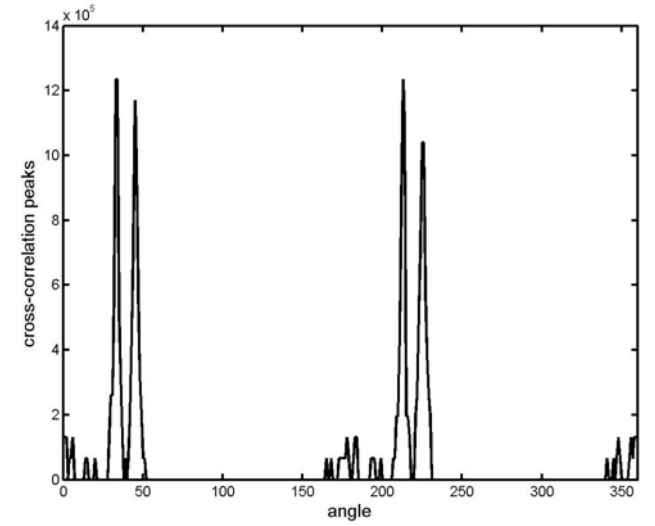

(a)

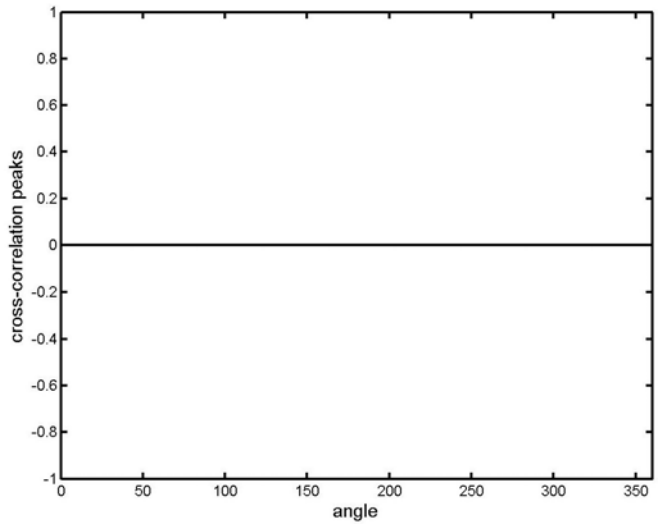

(b)

Figure 4.14: The peaks of cross-correlation function for the region where (a) template points were embedded; (b) no template points were embedded.

In Figure 4.14. a typical representation of cross correlation peaks is given. In this case it was easy to detect the cross correlation peaks that correspond to the scaling and reference angle. In our experiments we were always able to obtain at least one image region from which we could clearly extract the cross correlation peaks. If the image region does not contain the template points, the corresponding cross correlation function gives no peaks, like in the Figure 4.14.b.

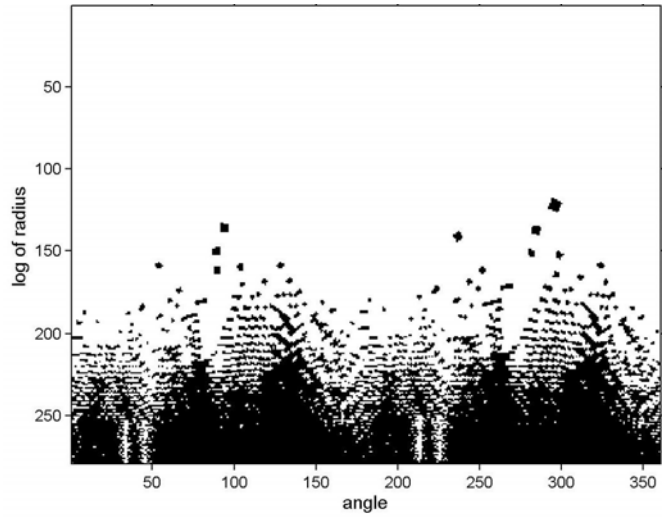

(a)

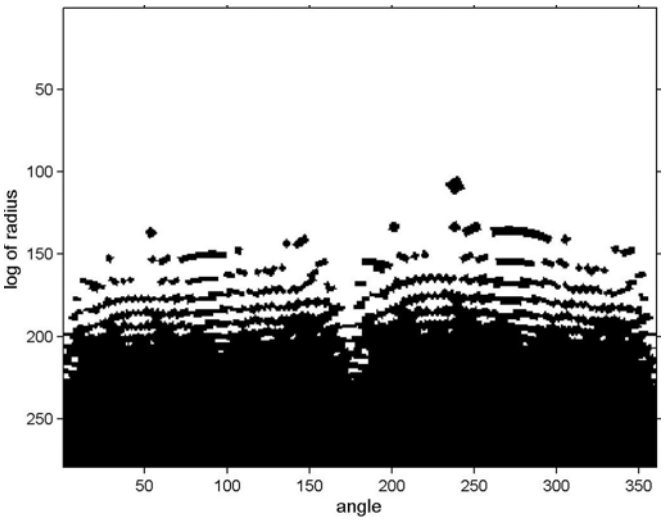

(b)

Figure 4.15: (a) Originally embedded template points in log-polar domain of Fourier spectra. (b) Log-polar representation of the region where template points were not embedded.

In Figure 4.15.a the extracted template points in log-polar domain are presented. Figure 4.15.b presents the log-polar representation of the DFT spectra of the circular image region where the template points were not embedded.

Figures 4.14 and 4.15 are obtained for the Lena image. From the Figure 4.14.a it can be seen that the reference angle was 45°. The value of characteristic scale for that image region was 43.42. From the equation (4.31) $s_o = \text{int}(43.42) = 43$; $c = -10$; and the encoded scaling angle was $s_e = 33^{\circ}$. This encoded scaling angle can be seen on Figure 4.14.a as the first peak of cross-correlation function.

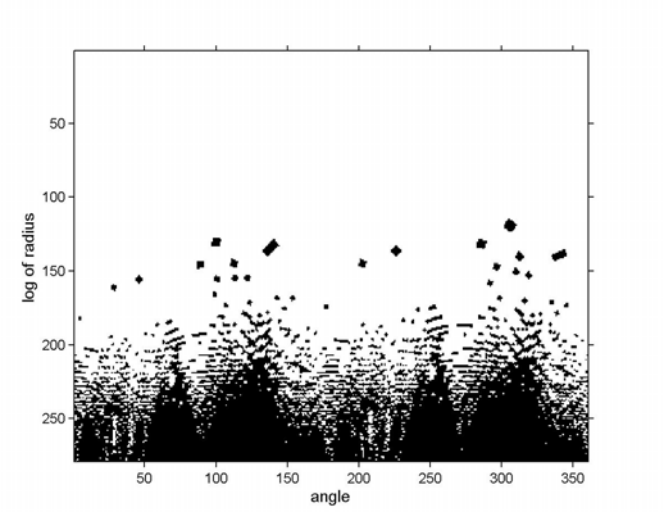

(a)

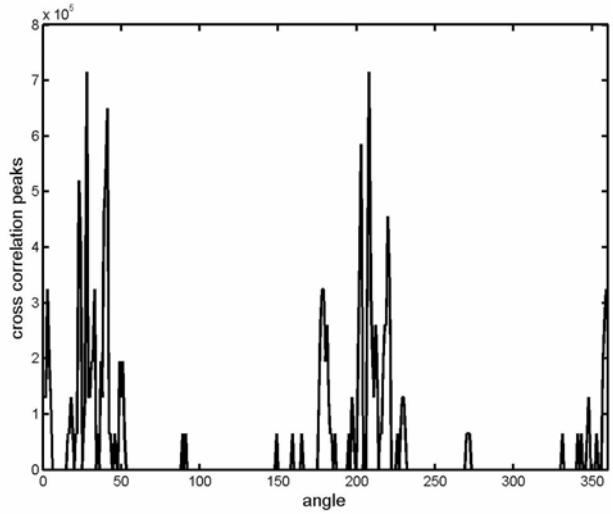

(b)

Figure 4.16: (a) Template peaks extracted after geometrical distortion, which consists of rotation with $\theta = -5^{\circ}$ and scaling $S_{x_1} = S_{x_2} = 1.1$. (b) corresponding cross-correlation peaks.

In order to demonstrate the template extraction procedure we perform on Lena image one distortion which consists of rotation with $\theta = -5^{\circ}$ and scaling $S_{x_1} = S_{x_2} = 1.1$. The characteristic scale of the image region where the template peaks were extracted was 47.32. Figure 4.16.a presents the log-polar DFT representation of the extracted image region. It is obvious that in that region the template points were embedded. The Figure 4.16.b represents the corresponding peaks of cross-correlation.

In the spectral part from 0° till 180° there were two peaks at 28° and 40° that correspond to the new scaling angle θ_{ns} and new reference angle θ_{nr} respectively. The reference angle in the embedding stage was $\theta_r = 45^{\circ}$. From the equation (4.35) $\theta_{rot} = -5^{\circ}$ and equation (4.36) $s_o = 43$. Using the equation (4.38) the calculated scaling parameter is $s_{cal} = 1.093$. In Figure 4.17.a the Lena image with the embedded template is presented. Figure 4.17.b shows the difference between the original and marked image. Here a stronger template is embedded in order to get the better representation. Figure 4.17.c shows the selected circle regions around the feature points containing the template.

(a)

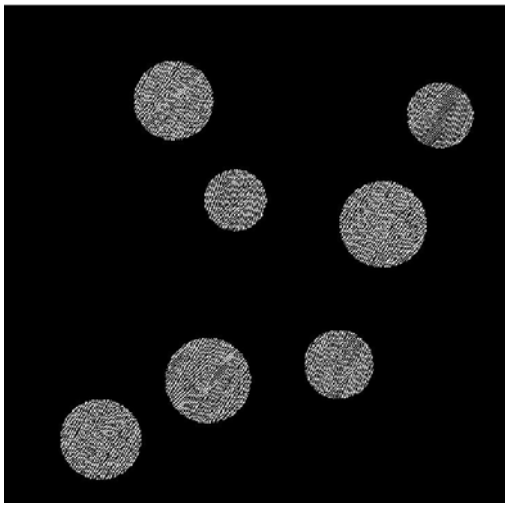

(b)

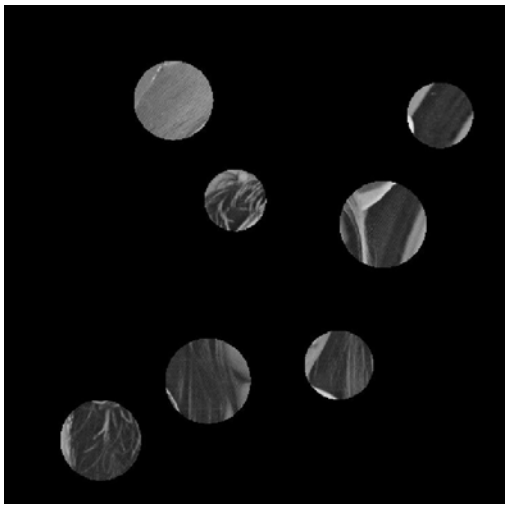

(c)

Figure 4.17: (a) Lena image with embedded template points; (b) difference between the original and marked image; (c) circle regions around the feature points containing the template.

4.3.4. Testing results

The method was tested on the geometrical transformation and image compression. The geometrical attacks are the same as in the Chapter 3: rotations with different angles (rot1- 5º , rot2- 10º, rot3- 15º, rot4- 30º), scaling transform with different scaling operations

(sc1- 80%, sc2- 90%, sc3- 120%, sc4- 150%) or combined geometric attacks (rs1- rotation of 5º, scaling 120%; rs2- rotation of 15º, scaling 90%; rs3- rotation of 10º, scaling 150%; rs4- rotation of 30º, scaling 120%); image cropping with different cropping percentage (cr1- 5%, cr2- 10 %, cr3- 15 %, cr4- 20 %) and compression: JPEG compression with quality factor: 40 (jpg40) and 50 (jpg50); JPEG2000 compression with 0.4 bpp (wc40) and 0.5 bpp (wc50). The experiments are performed on 10 standard images with the size of 512 x 512: *barbara*, *boats*, *cameraman*, *couple*, *einstein*, *elaine*, *f16*, *goldhill*, *house* and *lena* image. In our investigation the "template remove" attack is included [94]. This attack destroys the local peak values in DFT spectra of the analyzed image.

Based on experiments carried out, the following has been concluded:

1. The parameters of rotation and scaling are successfully calculated after all geometrical attacks from at least one image region.
2. In a case of template remove attack the results were also good. That was expected due to the fact that local peaks are destroyed in the DFT spectra of the entire image, but not in the DFT spectra of the local image regions.
3. Compressions (JPEG and JPEG 2000) have no effect on template detection procedure.

The fidelity of the marked images, measured by Peak Signal to Noise Ratio (PSNR) metric (see equation (2.6)) is given in the Table 4.2.

Table 4.2: The calculated PSNR values

	barbara	boats	couple	cameraman	einstein	elaine	f16	goldhill	house	lena
PSNR(dB)	42,15	40	47,65	41,02	42,03	44,33	43,52	45,9	41,84	44,9

4.3.5. Comparison with other techniques and the advantages of the proposed technique

The proposed synchronization technique can be compared with the template based techniques. The main advantages of this technique are:

- Simplicity of calculation of the parameters of affine transformation. It is enough to detect correctly the reference and scaling angle from at least one selected circular image region.

- The technique is not sensitive to image cropping because it uses the redundant embedding of synchronization signals.
- Robustness to template remove attack which destroys the typical template signal embedded in the DFT spectra of the entire image.
- The security of this technique can be increased if the radius of the circular region around the feature point secretly encoded.

4.4 Chapter Summary

In this Chapter firstly an image registration technique is described. This technique can be implemented to recover the watermark synchronization before the watermark detection and it is based on establishing point-by-point correspondence between the original image and image possibly altered by unknown geometrical transformation (received image). It is experimentally demonstrated that this technique effectively estimates the parameters of undergone affine transformation. Next, an overview of the existing watermarking techniques, which consider the problem of synchronisation without access to the original image content, is given. A new synchronization technique which combines the template based and content based approach is proposed in this Chapter. This technique does not require the presence of original or watermarked image to recover the watermark synchronization. The proposed technique is tested under various geometrical distortions which consist of rotation, scaling, cropping or combinations of them. It is shown that this technique can effectively detect the parameters of rotation and scaling. It is experimentally shown that compressions (JPEG and JPEG2000) and cropping have no influence on the extraction the parameters of rotation and scaling, as well.

In the next Chapter firstly, the wavelet transform with its properties will be introduced. Then the watermarking algorithms based on wavelet transform will be considered in more details. It will be shown how the proposed image registration and synchronization technique can be successfully combined with the wavelet watermarking algorithms developed in the next Chapter in order to improve the robustness on geometrical distortions.

Chapter 5

Digital image watermarking in wavelet domain

In this Chapter firstly the Discrete Wavelet Transform will be briefly presented. Next, the basic watermarking algorithms in the wavelet domain will be given. Furthermore, two wavelet watermarking algorithms based on wavelet transform will be proposed.
In the first algorithm the original image is used at the detection stage. The robustness of this algorithm is further improved by using the image registration technique from Section 4.1. The second algorithm belongs to the class of blind techniques, in which the watermark detector is able to detect the watermark without accessing to the original image content. The robustness of this algorithm is additionally improved by using the synchronization technique proposed in Section 4.3. In both algorithms the scale invariant feature points are used as reference locations for the embedding of watermark pattern.

5.1 Discrete wavelet transform

In this Section the basic idea of the Discrete Wavelet Transform (**DWT**) for one-dimensional signals is briefly described [100, 101].

DWT splits an one dimensional signal into two parts, usually the high frequency and the low frequency parts. This splitting is called decomposition. The signal is passed through a series of high pass filters to analyze the high frequencies, and it is passed through a series of low pass filters to analyze the low frequencies. Filters of different cutoff frequencies are used to analyze the signal at different resolutions. Let us suppose that $x[n]$ is the original

signal, spanning a frequency band of 0 to π rad/s. Next, the original signal $x[n]$ is passed through a halfband highpass filter $g[n]$ and through a lowpass filter $h[n]$. Since the signal now has the highest frequency of $\pi/2$ instead of π radians, after the filtering, the half of samples can be eliminated according to the Nyquist's rule. The signal can be therefore subsampled by 2, simply by discarding every second sample. This constitutes *one level of decomposition* and can be mathematically expressed as follows:

$$y_{low}[k] = \sum_n x[n]\, h[2k - n] \tag{5.1}$$

$$y_{high}[k] = \sum_n x[n]\, g[2k - n] \tag{5.2}$$

where $y_{high}[k]$ and $y_{low}[k]$ are the outputs of the highpass and lowpass filters, respectively after subsampling by 2. The above procedure can be repeated in the next decomposition.

The outputs of highpass and lowpass filters are called DWT coefficients and by using them, the original image can be reconstructed. The process of reconstruction is called the Inverse Discrete Wavelet Transform (IDWT).

The above procedure is followed in reverse order for the reconstruction. The signals at every level are upsampled by two, passed through the synthesis filters $g'[n]$ and $h'[n]$ (highpass and lowpass, respectively) and finally added to each other. Therefore, the perfect reconstruction formula becomes (for each layer):

$$x[n] = \sum_k (y_{high}[k]\, g[-n + 2k] + y_{low}[k]\, h[-n + 2k]) \tag{5.3}$$

To ensure the above IDWT and DWT relationship, the following orthogonality condition for filters $H(\omega)$ and $G(\omega)$ must hold:

$$\left|H(\omega)\right|^2 + \left|G(\omega)\right|^2 = 1 \tag{5.4}$$

where

$$H(\omega) = \sum_n h[n] e^{-jn\omega} \tag{5.5}$$

$$G(\omega) = \sum_{n} g[n] e^{-j n \omega} \tag{5.6}$$

A simple example of such $H(\omega)$ and $G(\omega)$ is given by:

$$H(\omega) = \frac{1}{2} + \frac{1}{2} e^{-j\omega} \tag{5.7}$$

$$G(\omega) = \frac{1}{2} - \frac{1}{2} e^{-j\omega} \tag{5.8}$$

which is known as the *Haar wavelet filter*.

For one-dimensional signal, the DWT and IDWT can be also described in the form of two channel tree-structured filter banks. The DWT and IDWT for a two-dimensional image **I**, can be similarly defined by applying the DWT and IDWT for image rows and columns separately $DWT_{\text{columns}}[DWT_{\text{rows}}[\mathbf{I}]]$, what is shown in Figure 5.1.

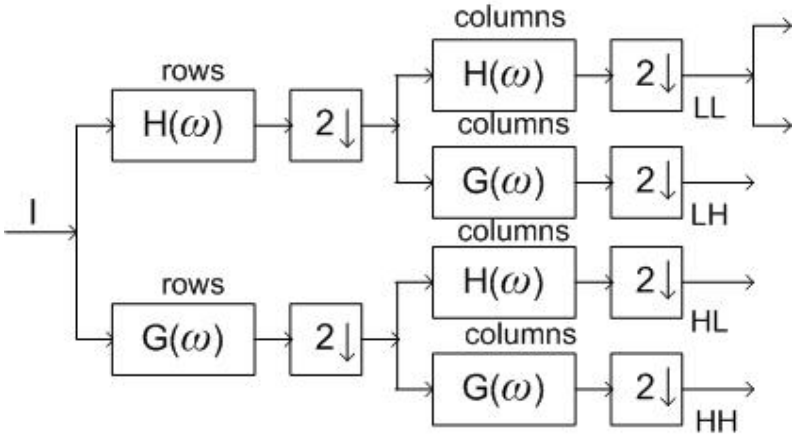

Figure 5.1: One level of decomposition of two-dimensional DWT.

In this way an image can be decomposed into a so-called *pyramidal structure*, as shown in Figure 5.2. In Figure 5.2 various band information are available: the low-low frequency band **LL**, the low-high frequency band **LH**, the high-low frequency band **HL** and the high-high frequency band **HH**.

In the Figure 5.3 Lena image was decomposed into the two levels of DWT decomposition using the Haar wavelet filters.

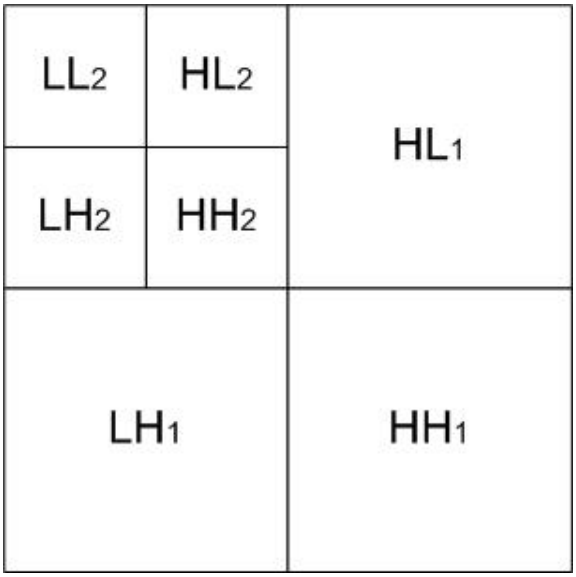

Figure 5.2: The *pyramidal structure*.

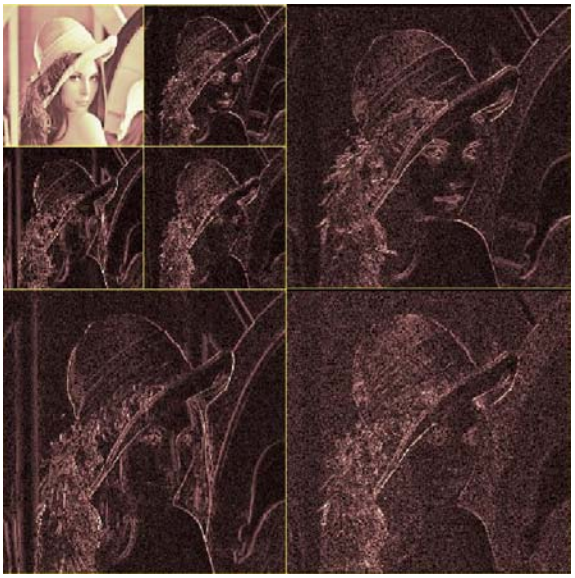

Figure 5.3: Two-level DWT decomposition of Lena image obtained by using the Haar wavelet filter.

5.2 Properties of the wavelet transform

The wavelet transform decomposes an image into three spatial directions (see Figures 5.2 and 5.3), i.e. the horizontal HL, the vertical LH and the diagonal HH. At each level of decomposition the magnitude of the DWT coefficients is larger in the lowest subbands ("approximation" LL subband), and smaller for other subbands ("detail" subbands: HL, LH and HH). The most significant coefficients in a subband are those with large magnitudes. For an arbitrary image the high resolution subbands help in locating the edge and texture patterns.

Watermarking in DWT domain has a number of advantages over other transforms, namely, the Discrete Cosine Transform (**DCT**):

1. Wavelet coded image is a multi-resolution description of image. Hence an image can be shown at different level of resolution and can be sequentially processed from low resolution to high resolution.

2. The DWT is closer to the human visual system than the DCT, since it splits the signal into individual bands, which can be processed independently.

3. The distortions introduced by wavelet domain coding with high compression ratio are less annoying than those introduced at the same bit rate by the DCT. In the JPEG case, block-shaped distortions are clearly visible, since image coding based on the DCT usually operates on independent 8x8 blocks.

4. Watermarking schemes put more watermark energy into the large DWT coefficients, thus affecting mostly regions, like lines and texture on which the human visual system is not sensitive too.

5. DWT has spatial frequency locality, which means if the watermark is embedded into the DWT coefficients it will affect the image locally. Hence a wavelet transform provides both frequency and spatial description for an image.

5.3 HVS Perceptual models based on DWT

The human visual system (**HVS**) is humanistic information processing system, which receives spatially sampled images from the retina of human eye. The retina of our eye splits a visual signal into different components and each component excites the visual cortex over separate channels [102]. The colors and the texture of an object are influenced by its orientation and illumination. Hence the edges are commonly the most significant means of recognition. Most of image compression algorithms try to minimize the edge distortions.

Exploring the properties of the human visual system it is possible to increase the watermark energy in specific transform coefficient, which is less sensitive to the human eye.

There are several HVS models based on wavelet transform that are used in watermarking. One of them is HVS model based on DWT quantization algorithm [103]. Using this model a JND threshold can be calculated. By this, JND threshold [104] is such that changes in the frequency content in the image in the particular frequency band below the threshold are not noticeable. JND can be also defined as the smallest difference between luminances or colors of areas, usually adjacent to each other, that can be easily discerned or is obvious from ordinary observation.

In [105] an example of watermarking algorithm that uses this model is described in details. Other visual models can be found in [106, 107].

Generally, according to the [108] the following conclusions can be drown from understanding the HVS regards to watermarking:

- High frequencies are less visible then low frequencies.
- Studies of visual cortex showed a multi-resolution characteristic of our visual system.
- In order to embed a watermark as strong as possible the watermark should be embedded just below the JND.

5.4 Algorithms Classification

The wavelet watermarking algorithms can be distinguished in terms of:

1. the availability of the reference image for watermark extraction:
   - oblivious (blind),
   - semi-blind,
   - non-oblivious (non-blind),

2. embedding strategy:
   - linear addition of a spread spectrum signal,
   - image fusion (embedding a “logo”),
   - quantisation method,

3. implementation of perceptual models:
   - with visual masking,
   - without visual masking,

In additive watermarking algorithms [105, 109-115, 17-20] the watermark data is a sequence of numbers (usually pseudorandom Gaussian sequence) w of length L, which is embedded, in the selected subset of the signal coefficients f. The general embedding formula has the following form:

$$f' = f + alfa \cdot f \cdot w(k),\ k = 1, \ldots, L \tag{5.9}$$

where $alfa$ is embedding strength and f' are the modified coefficients of the host data. The watermark detection procedure is usually based on correlation.

In watermarking algorithms based on image fusion [116-120] the logo image is used as a watermark instead of a pseudorandom sequence. The logo image is generally smaller than the host image and decorrelated (encrypted) before embedding.

The quantisation schemes [21, 121-124] on the other hand perform non-linear modifications and detect the embedded message by quantizing the received samples to map them to the nearest reconstruction points.

5.5 The non-blind additive watermarking algorithm (NB-T01)

In this Section the non-blind watermarking method proposed in [45, 125] will be described. The watermarking procedure is split into two procedures:

- watermark embedding procedure and
- watermark extraction procedure.

5.5.1 The watermark embedding procedure

At the beginning of embedding procedure a bipolar sequence of bits is transformed into a new sequence $w(1),\ldots,w(L)$ by replacing 0 by -1, where L is the length of the sequence and $w(k)\in\{-1,1\}$ $(k=1,\ldots,L)$. The new sequence is used as the watermark. The original image $\mathbf{I}$ is decomposed into two levels of DWT decomposition. Decomposition is performed using the "Haar" wavelet filters (see equations (5.7) and (5.8)). The Haar wavelet filters are chosen for the DWT decomposition because from our previous research it was concluded that this filter gives the best results among other tested wavelet filters (biothogonal and Daubechies wavelets). The watermark is added to L largest coefficients in all of the detail subbands (HL_i, LH_i, HH_i, $i=1,2$) of the DWT decomposition. HL_1, LH_1, HH_1 represent the high frequency ranges and HL_2, LH_2, HH_2 represent the middle frequency ranges of the image processed. Let $f(m,n)$ denote the set of L largest DWT coefficients at the position (m,n) in any of subband matrices (HL_i, LH_i, HH_i, $i=1,2$). The embedding procedure is performed according to the following formula:

$$f'(m,n) = f(m,n) + alfa \cdot f(m,n) \cdot w(k),\ k = 1,\ldots,L \tag{5.10}$$

where *alfa* is the strength of the watermark, controlling the level of the watermark. $f'(m,n)$ is modified coefficient at the position (m,n) in any of subband matrices. The watermarked image $\mathbf{I}_w$ is obtained by applying the inverse discrete wavelet transform (IDWT). The position vectors of modified coefficients in all subbands are kept secretly and used in extraction procedure as a secret key. The upper part of the Figure 5.4 shows the block diagram of the embedding procedure. The lower part of the Figure 5.4 represents the extraction procedure discussed in the next Section.

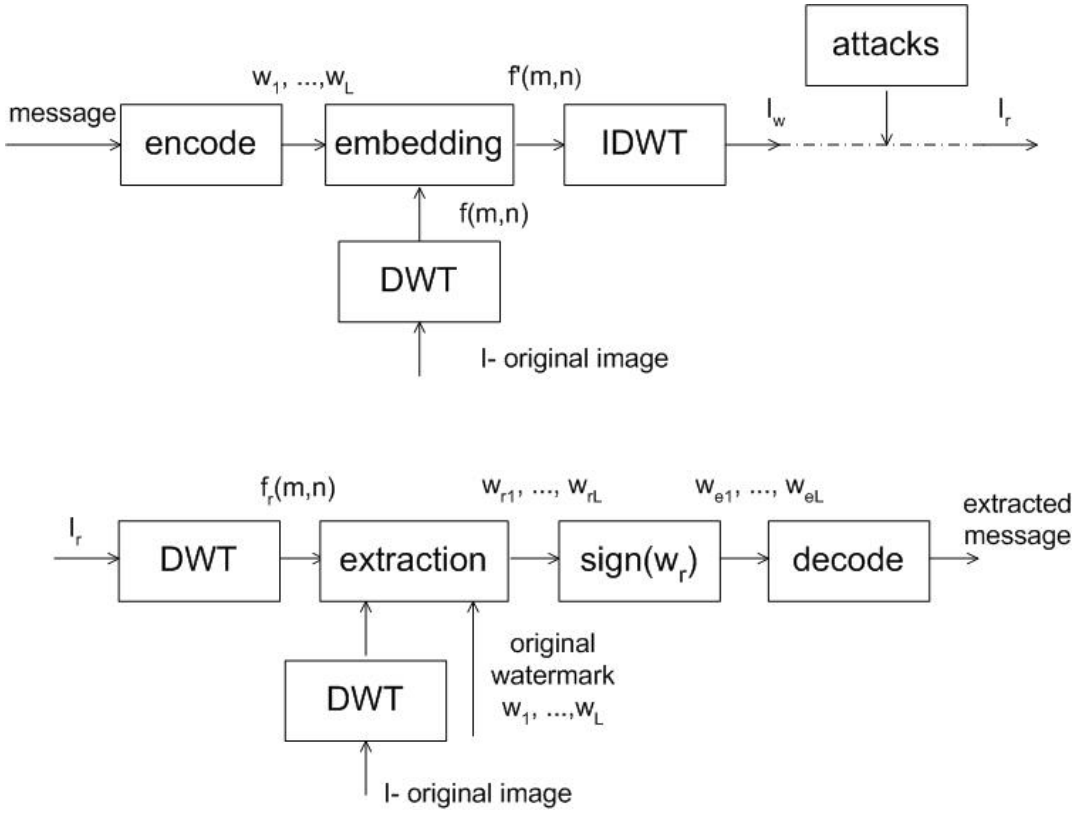

Figure 5.4: Block diagram of the embedding method.

5.5.2 Watermark extraction procedure

In the watermark extraction procedure (see lower part of the Figure 5.4) both the received image $\mathbf{I}_r$ and the original image $\mathbf{I}$ are decomposed into levels of the DWT decomposition. By this the received image $\mathbf{I}_r$ is possibly modified by attacks. It is assumed that the original image $\mathbf{I}$ is available in the extraction procedure i.e. that is used as an input to this procedure.

When images are decomposed using the DWT, the positions of the modified coefficients in the subbands of original and received images are calculated according to the secret key generated in embedding procedure. This set of selected DWT coefficients will be denoted with $f(m,n)$ and $f_r(m,n)$ for original and received image, respectively. (m,n) represents the particular position in the subband. The extraction procedure is described by the following formula:

$$w_r(k) = (f_r(m,n) - f(m,n))/(alfa \cdot f(m,n)) \tag{5.11}$$

where w_r is the extracted watermark. The extracted watermark is further transformed as follows:

$$w_e(k) = \text{sign}(w_r(k)) \tag{5.12}$$

After extraction of the watermark w_e the bit stream is reconstructed by similar replacing as at the beginning (-1 is now replaced by 0).

5.5.3 Algorithm NB-T01 testing

For the purpose of robustness testing the following set of ten standard test images with the size of 512x512 are used: b*arbara*, *boats*, *cameraman*, *couple*, *einstein*, *elaine*, *f16*, *goldhill*, *house* and *lena* image. By this, the message *Universitaet Duisburg* is used as the watermark. This message is firstly converted into ASCII code and than encoded with error

correction code (ECC) in order to improve the robustness. Here the robustness of the algorithm will be tested for the watermark sequence encoded with 3 different ECC and for the watermark sequence that is directly embedded (without using any ECC). The following ECC are used in our investigation in order to determine which ECC performs the best from the robustness point of view:

- (15,7) Bose-Chaudhuri-Hocquenghem (BCH) code,
- (7,4) Hamming code and
- (15,7) Reed Solomon code.

The same watermark is embedded in all detail subbands of the two-level DWT according to the embedding procedure described in Section 5.5.2. The message *Universitaet Duisburg* consists of 21 characters. According to the ASCII rule every character is encoded with 8-bit sequence. More important bits are those from 2,..., 8 and the first bit is used for encoding the special characters. In order to fit our sequence to the codeword of the ECC for Hamming code the 8 bit representation of the particular character will be used. For other ECC as well as for the directly embedded watermark sequence the 7-bit representation will be used. In the Table 5.1 the characteristic of the embedded watermark will be given:

Table 5.1: The characteristic of the embedded watermark

	message length	enc. message length	additional information
no ECC	147 bits	147 bits	7 bits per char.
BCH	147 bits	315 bits	7 bits per char.
Hamming	168 bits	294 bits	8 bits per char.
RS	147 bits	360 bits	7 bits per char.

This means that with the Reed-Solomon coding more than twice of bits have to be embedded into the DWT subband compared to the approach without ECC. This fact must be taken into account when designing the watermarking scheme, due to the possible problem with the capacity of the cover image.

In the testing, several non-geometrical signal processing operation are applied on the watermarked test images: med- median filtering with 3x3 window size; gaus- gaussian filtering with 5x5 window size; wien- wiener filtering with 5x5 window size; trim- trimmead mean filtering with 7x7 window size; sh- sharpening with 3x3 high pass filter; JPEG compressions with different quality factors from 50 to 10 (jpg50, jpg40, jpg 30, jpg25, jpg15, jpg10) and JPEG2000 compressions with different bit-rates from 0.5 to 0.1 bpp (bit per pixel) (wc50, wc40, wc30, wc20 and wc10).

The watermark is extracted separately from every subband in order to compare the robustness of the watermark embedded in that subband. In Figure 5.5 the results for *Lena image* are given. The similar results are obtained for other test images. In all graphs in Figure 5.5 on the *x*-axes different attacks are presented. The results are calculated as the total number of not correctly extracted watermark bits (errors) divided by the total number of watermark bits, expressed in percentage and presented on the y axes of all three graphs. The best results are obtained for the watermark embedded in subbands HL_2 and LH_2 and only results for these subbands are presented. The results for other tested subbands were not good and they were not being further considered. This was expected due to the fact that the common signal procession operations like filtering and compression will be most effective in the high frequencies (level 1 of the DWT decomposition).

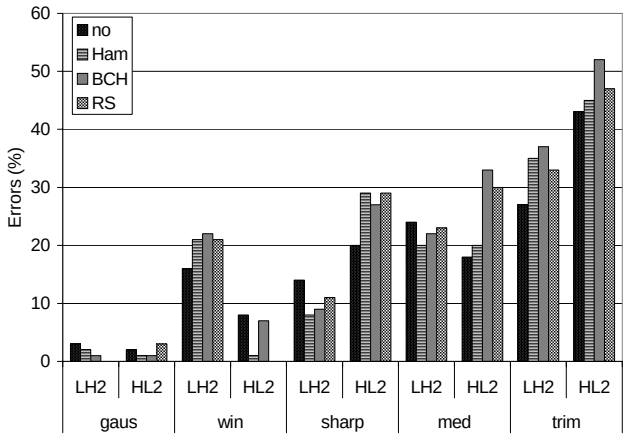

(a)

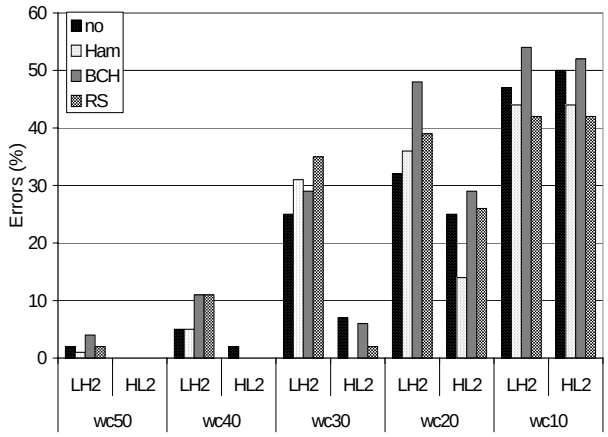

(b)

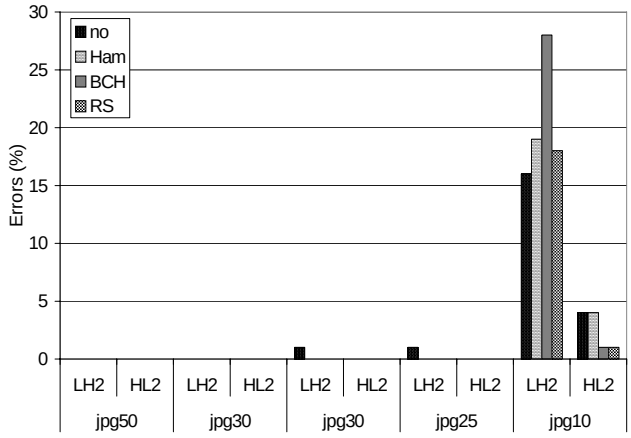

(c)

Figure 5.5 The testing results for (a) different filtering attacks; (b) JPEG2000 compression attacks; (c) JPEG compression attacks.

From Figure 5.5 it can be concluded that for the most attacks the Reed-Solomon code gives less errors than other ECC. It can be also concluded that the results strongly depend on the subband in which the watermark sequence was embedded. In some cases like trimmed mean filtering better results are obtained without using ECC.

5.5.4 Impact of different Reed-Solomon codes

In [46] the importance of the use of ECC and the different lengths of codewords are investigated. By this the (15,7), (15,9), (31,11), (31,15) and (31,19) Reed-Solomon codes are investigated. According to the designation the different message lengths were 360, 300, 465, 310 and 310 bits, respectively. To investigate and evaluate the influence of these five Reed- Solomon codes the encoded watermark sequences were embedded into several test images using the DWT based watermarking method described in Section 5.5.1. It was concluded in [46] after testing the robustness that the (15,7) and (31,11) Reed-Solomon codes are the most effective codes for image watermarking.

5.5.5 Improvement of the algorithm

The robustness of the proposed algorithm can be increased by combining it with the image registration technique described in Section 4.1. The scale invariant feature points can be used as reference locations for calculation of the positions of modified coefficients in the subbands. In this way the robustness against cropping attack or affine attacks that also include cropping can be increased.

5.6 Proposed blind watermarking algorithm (B-T02)

In this Section a new blind watermarking algorithm will be proposed. In the algorithm the original image is decomposed into $l, (l \in \{2,3,4\})$ levels of decomposition using the "Haar" wavelet filters. The watermark is a bipolar pseudorandom sequence $w_o(1),\ldots,w_o(L)$, where L is the length of the sequence. This sequence is encoded with (15,7) Reed-Solomon error correction code in order to improve the robustness. The new sequence is further divided into two equal sequences and each sequence (with length $L/2$) is embedded into subbands LH_l and $\mathrm{HL}_l, (l \in \{2,3,4\})$ of the DWT decomposition. The main improvement of this algorithm comparing with the previous one is that the modified DWT coefficient depends additionally

on the mean value of all DTW coefficients selected for watermark embedding. In this way the stronger watermark is embedded into the image and it is possible to perform the blind watermark detection. This will be discussed in the Section 5.6.2 and experimentally confirmed in the Section 5.6.3.

In order to increase the robustness to cropping attacks, a new position vector of the selected DWT coefficients for embedding is calculated relative to the location of the feature points in the subband. This points will be denoted as reference locations and they are selected as the first three feature points with the largest characteristic scales, extracted with SIFT detector. In the Appendix A (see Tables A.1-A.3.) it is shown that in a case of filtering, compression, and image noise attacks it was possible to extract at least 7 feature points with the largest characteristic scale that correspond to the points on the original image. The non-corresponding points in our comparison had a smaller characteristic scale then the point with the maximal scale. The watermark embedding is performed in the central part of the image. In that way that the image cropping with the certain percentage of the image size will have no influence on watermark detection. Now the embedding procedure will be described in details.

5.6.1 Embedding procedure

The embedding procedure is performed in the following steps:

1. Select the central part of the image for watermark embedding (denoted as image $\mathbf{I}_c$).
2. Decompose the image $\mathbf{I}_c$ into $l, (l \in \{2,3,4\})$ levels of DWT decomposition using the "Haar" wavelet filters.
3. Select subbands LH_l and $\mathrm{HL}_l, (l \in \{2,3,4\})$ for embedding.
4. Generate a pseudorandom bipolar signal w_o of length L.
5. Encode the watermark sequence with the (15,7) Reed-Solomon error correction code to obtain the encoded sequence w_{rs} with length L_{rs}.
6. Divide a new sequence w_{rs} into the two sequences w_1 and w_2 with lengths L_1 and L_2, respectively (L_1 and L_2 should be approximately $L_{rs}/2$).

7. Select L_1 largest coefficients f_{LH_l} from the subband LH_l and L_2 largest coefficients f_{HL_l} from the subband HL_l.
8. Calculate the variable th_{LH_l} and th_{HL_l} as mean values of the coefficients f_{LH_l} and f_{HL_l}:

$$th_{\mathrm{LH}_l} = \mathrm{mean}(f_{\mathrm{LH}_l}) \tag{5.13.a}$$

$$th_{\mathrm{HL}_l} = \mathrm{mean}(f_{\mathrm{HL}_l}) \tag{5.13.b}$$

9. Embed sequence w_1 in subband LH_l and sequence w_2 in subband HL_l according to the following formula:

$$f'_{\mathrm{LH}_l}(m,n) = f_{\mathrm{LH}_l}(m,n) + th_{\mathrm{LH}_l} + f_{\mathrm{LH}_l}(m,n)\cdot alfa \cdot w_1(k),\ k = 1,\ldots,L_1 \tag{5.14.a}$$

$$f'_{\mathrm{HL}_l}(m,n) = f_{\mathrm{HL}_l}(m,n) + th_{\mathrm{HL}_l} + f_{\mathrm{HL}_l}(m,n)\cdot alfa \cdot w_2(k),\ k = 1,\ldots,L_2 \tag{5.14.b}$$

where $f_{\mathrm{LH}_l}(m,n)$ is selected largest coefficient- and $f'_{\mathrm{LH}_l}(m,n)$ is modified coefficient at the position (m,n) in subband matrix LH_l; $f_{\mathrm{HL}_l}(m,n)$ is selected largest coefficient- and $f'_{\mathrm{HL}_l}(m,n)$ is modified coefficient at the position (m,n) in subband matrix HL_l; *alfa* is a strength parameter.

10. Select 3 feature points with the largest characteristic scale, extracted with SIFT detector. In our investigation we have selected only the 3 feature points as a minimal number of feature points that surely survive the different filtering and compression operations. It is of course possible to select more then 3 feature point to compute the redundant position vector, if the memory resources allowed it.
11. Calculate the position of the reference locations in the subbands. For this calculation the position of the selected feature point will be used. If the position of the feature point is (x_1, x_2) on original image, the location of this reference location in the DWT subband will be calculated as $m_p = \mathrm{int}(x_1 / 2^l)$ and $n_p = \mathrm{int}(x_2 / 2^l)$. This simple computation is possible while we are using the "Haar" wavelet filter.

12. The new position vector of the selected coefficients in the subband calculate relative to the position of the reference locations in the subband.
13. Repeat step 11 three times in order to get a redundant position vector.
14. Keep this vector as a secret key.
15. Apply the IDWT transform and add the watermarked part of the image $\mathbf{I}_{\text{cw}}$ to the non-watermarked image part ($\mathbf{I} - \mathbf{I}_{\text{c}}$).

5.6.2 Detection procedure

An important feature of the algorithm presented is that for the purpose of the watermark detection the reference image is not needed. The detection procedure is based on the correlation between the original watermark and the extracted watermark. If the correlation coefficient is greater than a threshold, the watermark was detected in the image. The threshold depends on the probability of false positive. A false positive or false detection occurs when the detector incorrectly concludes that an unwatermarked image contains a given watermark. The probability of false positive is obtained by applying the detection procedure to the unwatermarked image.

The detection procedure is described through the following steps:

1. Decompose the central part of the received image $\mathbf{I}_{\text{cr}}$ into the $l, (l \in \{2,3,4\})$ levels of DWT decomposition using the "Haar" wavelet filters.
2. Extract the feature points with SIFT detector and select first three points with the largest characteristic scale.
3. Calculate the positions of the feature points in the subbands.
4. According to the calculated positions select the coefficients from the subband matrices LH_l and HL_l, f_{LH_l} and f_{HL_l}, respectively.
5. Calculate the mean value of the coefficients f_{LH_l} and f_{HL_l}, which will be used as a thresholds:

$$th_{\text{LH}_l} = \text{mean}(f_{\text{LH}_l}) \tag{5.15.a}$$

$$th_{\mathrm{HL}_l} = \mathrm{mean}(f_{\mathrm{HL}_l}) \tag{5.15.b}$$

6. If the selected coefficient from LH_l or HL_l is greater that the threshold then:

$$\begin{aligned} &if\ f_{\mathrm{LH}_l}(m,n) > th_{\mathrm{LH}_l}\ then\ w_{1e} = 1; \\ &else\ w_{1e} = -1; \end{aligned} \tag{5.16.a}$$

$$\begin{aligned} &if\ f_{\mathrm{HL}_l}(m,n) > th_{\mathrm{HL}_l}\ then\ w_{2e} = 1; \\ &else\ w_{2e} = -1; \end{aligned} \tag{5.16.b}$$

7. Make a new extracted array w_{rse} by gathering the sequences w_{1e} and w_{2e}.
8. The extracted watermark w_e will be obtained by applying the Reed-Solomon ECC decoding on the extracted array w_{rse}.
9. If the correlation coefficient between the extracted watermark and original watermark is greater then a threshold thr then the watermark was detected.

$$\mathrm{corr}(w_o, w_e) > thr \tag{5.17}$$

where thr represents a threshold depending on the false-positive probability. The probability of false positive is obtained by applying the detection procedure to the unwatermarked image $\mathbf{I}$:

$$P_{\mathrm{FA}} = P\{T_{\max} > T\} \tag{5.18}$$

Here T is the correlation coefficient between the extracted watermark and original watermark. $T_{\max}$ is the maximal value of the correlation coefficient between the extracted watermark from the unwatermarked image and original watermark. In our case:

$$thr = T_{\max} \tag{5.19}$$

5.6.3 Algorithm B-T02 Testing

In this Section the results of the blind watermarking algorithm testing are presented. In the testing the pseudorandom bipolar watermark sequence w_o of 80 bits is used. After encoding this sequence with the (15,7) Reed-Solomon ECC, the new sequence w_{rs} contains 180 bits. The sequence w_{rs} is divided into two sequences w_1 and w_2, each having length of 90 bits. The algorithm is tested using the same standard 512 x 512 images (*barbara*, *boats*, *cameraman*, *couple*, *einstein*, *elaine*, *f16*, *goldhill*, *house* and *lena* image). The original image is decomposed in $l, (l \in \{2,3,4\})$ levels of decomposition using "Haar" wavelet filters. The watermark embedding is performed according to the algorithm described in Section 5.6.1. The strength parameter *alfa* is set to 0.4 as trade off between the visibility and robustness requirements.

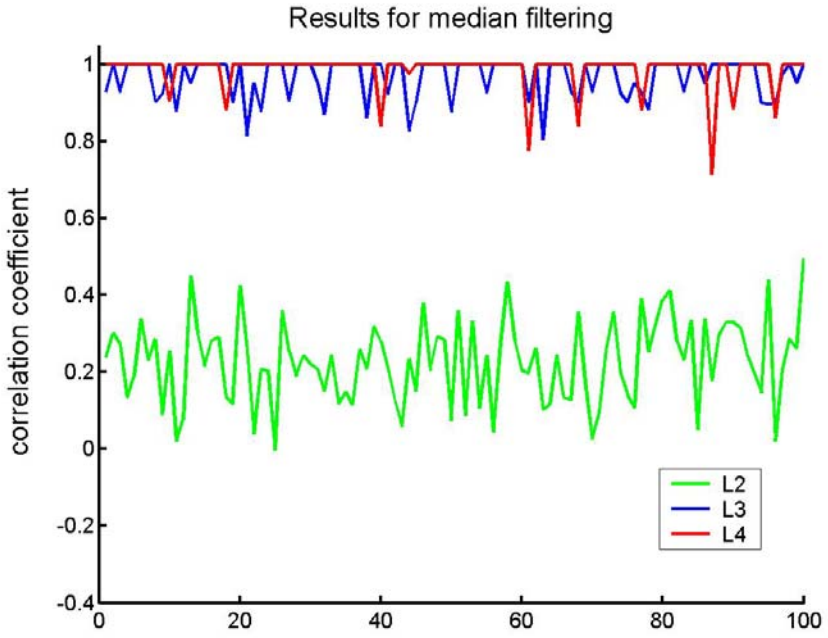

(a)

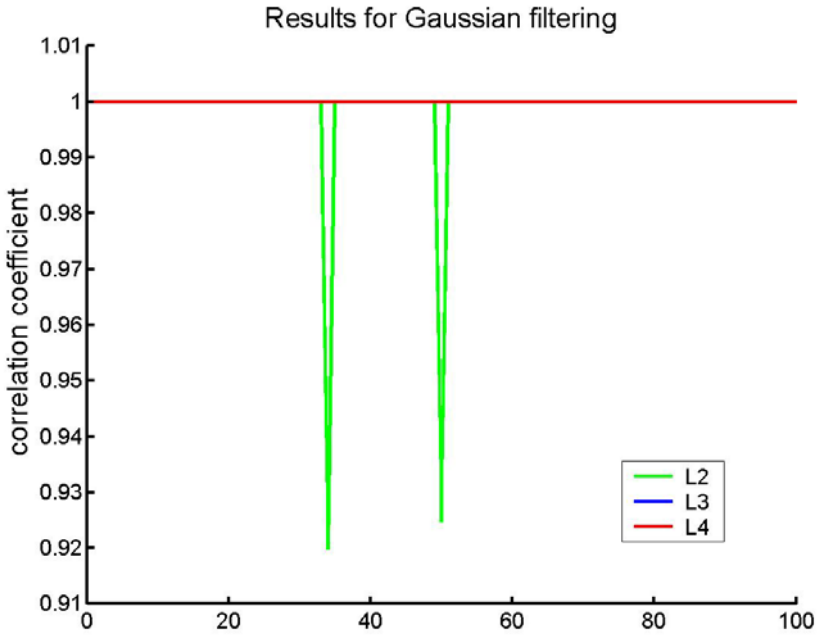
Results for Gaussian filtering
correlation coefficient
1.01
1
0.99
0.98
0.97
0.96
0.95
0.94
0.93
0.92
0.91
0
20
40
60
80
100
L2
L3
L4

(b)

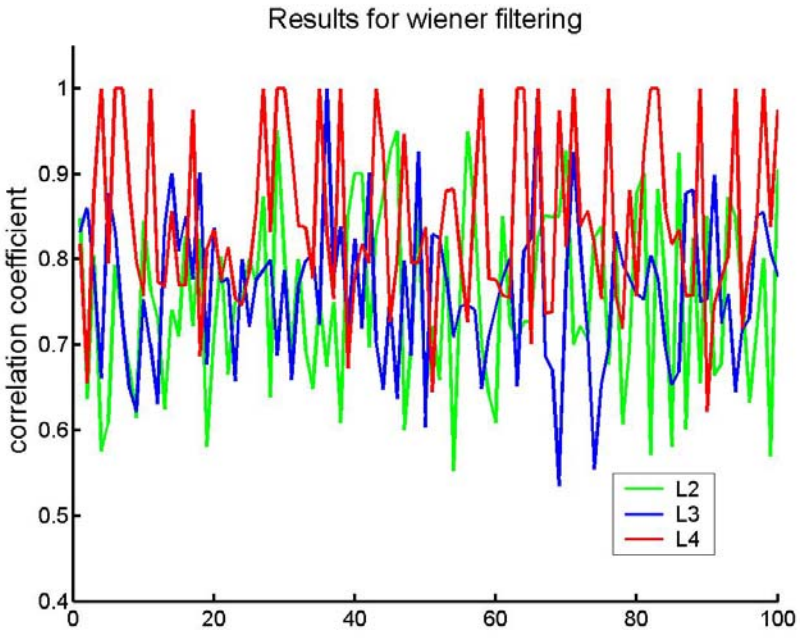
Results for wiener filtering
correlation coefficient
1
0.9
0.8
0.7
0.6
0.5
0.4
0
20
40
60
80
100
L2
L3
L4

(c)

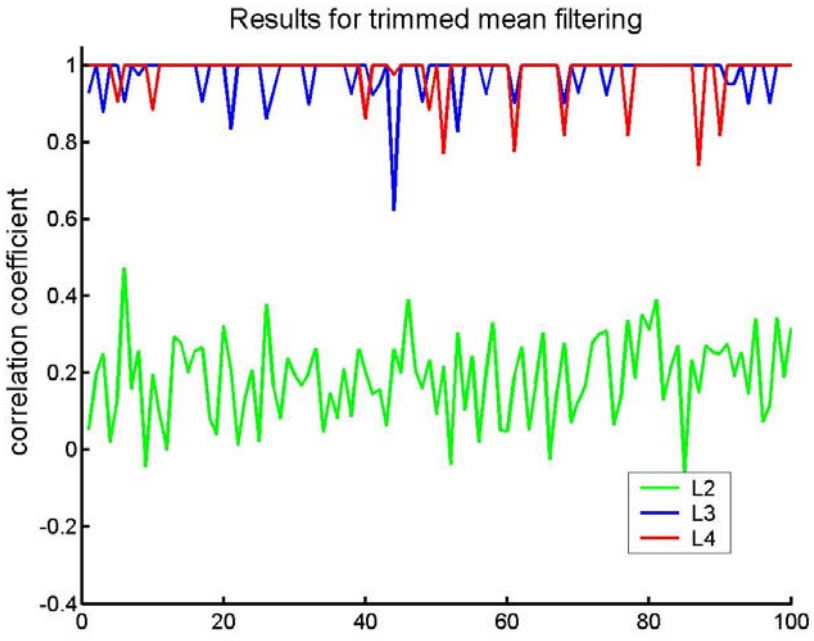
Results for trimmed mean filtering
correlation coefficient
1
0.8
0.6
0.4
0.2
0
-0.2
-0.4
0
20
40
60
80
100
L2
L3
L4

(d)

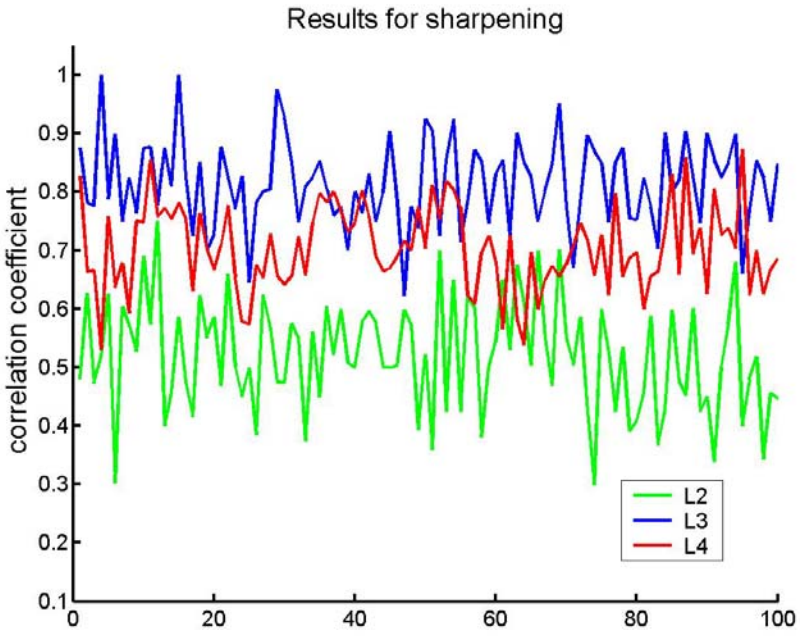
Results for sharpening
correlation coefficient
1
0.9
0.8
0.7
0.6
0.5
0.4
0.3
0.2
0.1
0
20
40
60
80
100
L2
L3
L4

(e)

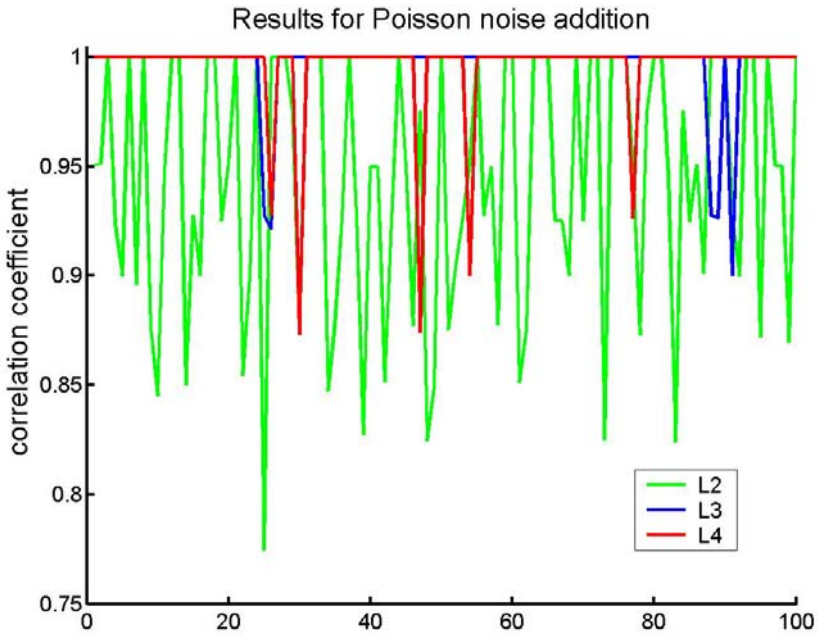
Results for Poisson noise addition
correlation coefficient
1
0.95
0.9
0.85
0.8
0.75
0
20
40
60
80
100
L2
L3
L4

(f)

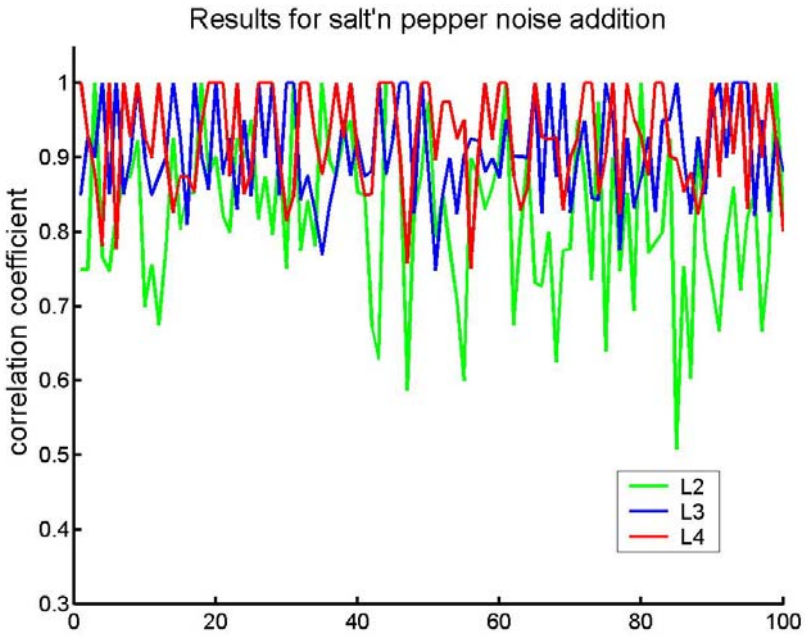
Results for salt'n pepper noise addition
correlation coefficient
1
0.9
0.8
0.7
0.6
0.5
0.4
0.3
0
20
40
60
80
100
L2
L3
L4

(g)

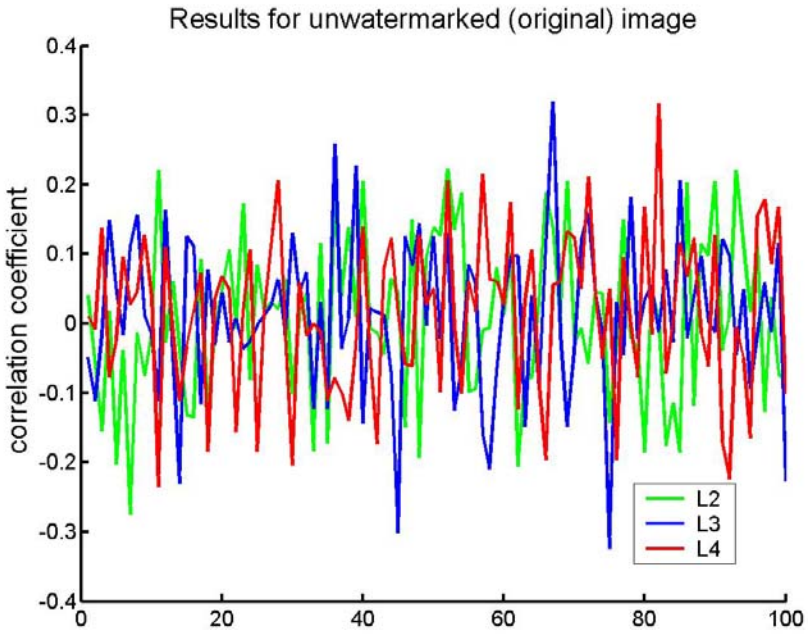
Results for unwatermarked (original) image
correlation coefficient
0.4
0.3
0.2
0.1
0
-0.1
-0.2
-0.3
-0.4
0
20
40
60
80
100
L2
L3
L4

(h)

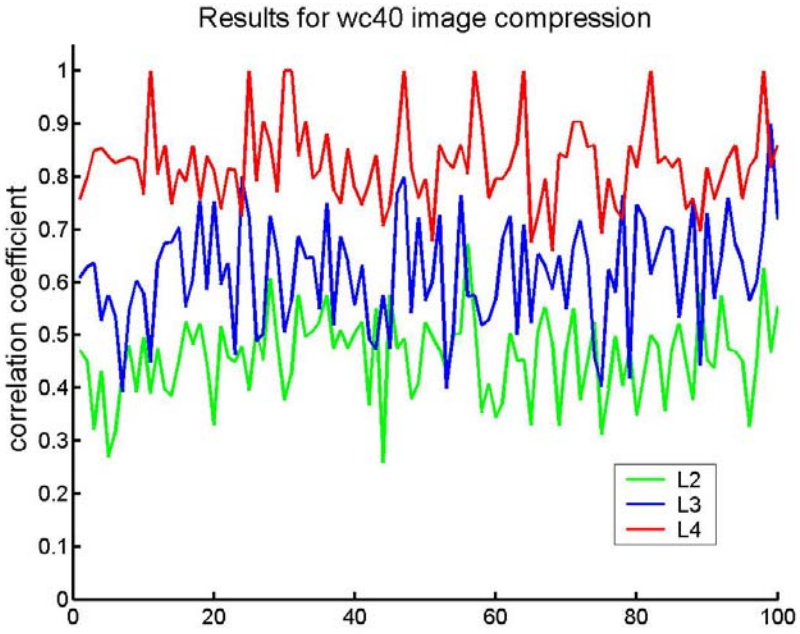
Results for wc40 image compression
correlation coefficient
1
0.9
0.8
0.7
0.6
0.5
0.4
0.3
0.2
0.1
0
0
20
40
60
80
100
L2
L3
L4

(i)

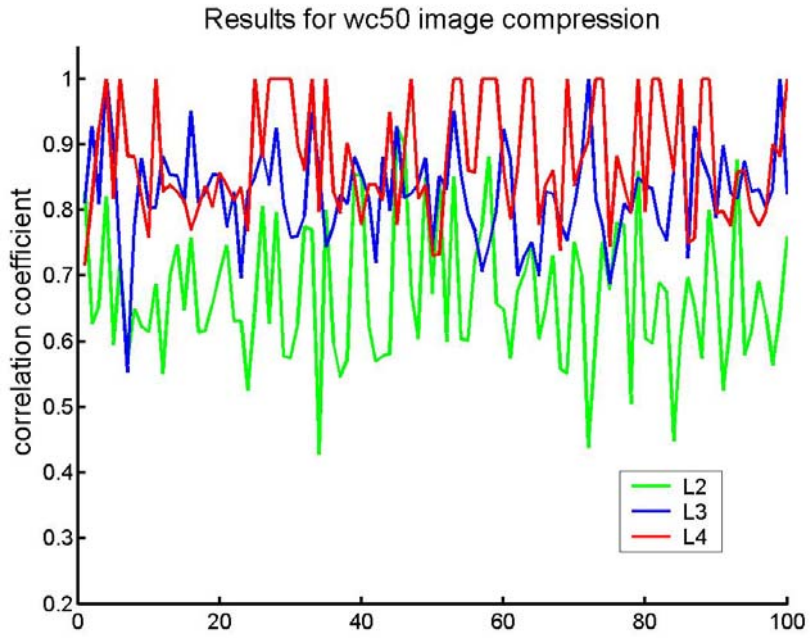
Results for wc50 image compression
correlation coefficient
1
0.9
0.8
0.7
0.6
0.5
0.4
0.3
0.2
0
20
40
60
80
100
L2
L3
L4

(j)

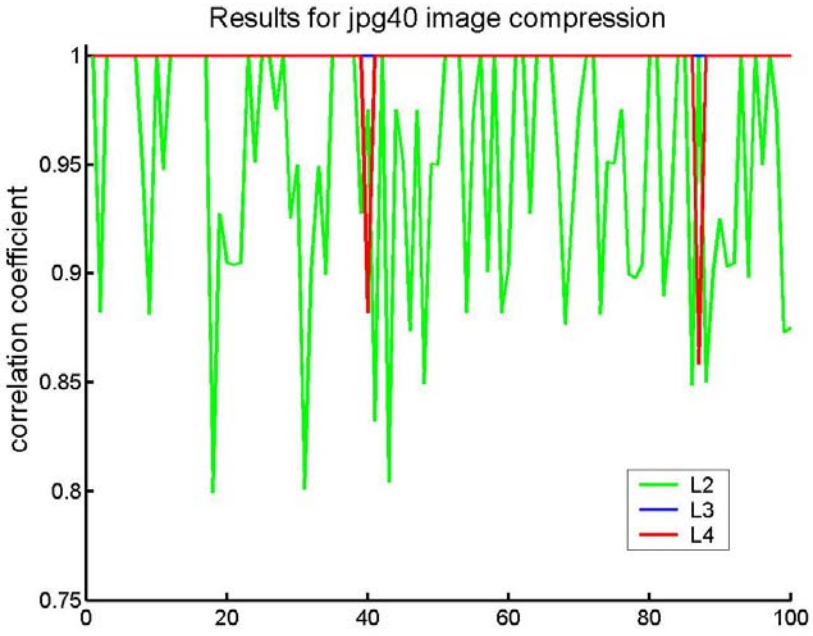
Results for jpg40 image compression
correlation coefficient
1
0.95
0.9
0.85
0.8
0.75
0
20
40
60
80
100
L2
L3
L4

(k)

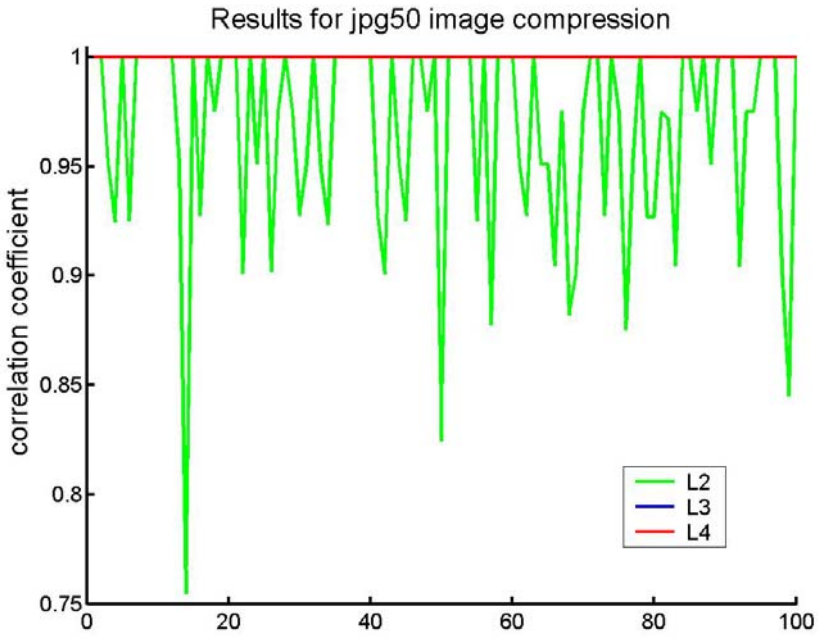

(l)

Figure 5.6: The results of our watermarking algorithm for following attacks: (a) median filtering; (b) gaussian filtering (c) wiener filtering (d) trimmed mean filtering; (e) sharpening; (f) Poisson noise addition; (g) salt'n pepper noise addition (h) watermark extraction from the original image; (i) JPEG2000 compression with 0,4 bit rate; (j) JPEG2000 compression with 0,5 bit rate; (k) JPEG compression with quality factor 40; (l) JPEG compression with quality factor 40. The results of correlation are presented for the watermark embedding into the level 2 (L2), level three (L3) and level four (L4) of DWT decomposition. The method was tested for 100 different random watermark sequences embedded in the *Barbara* image.

The robustness of the algorithm is tested separately for the watermark sequence embedded in the second, third and fourth level of the wavelet decomposition, respectively. In order to investigate the influence of different watermark sequences on the robustness the embedding/detection algorithm has been applied on 100 different watermark sequences for *Barbara* image. The watermark embedded in *Barbara* image was less robust on attacks then watermark embedded in other test images. The same attacks were performed as described in Section 5.5.3: med- median filtering with 3x3 window size; gaus- gaussian filtering with

5x5 window size; wien- wiener filtering with 5x5 window size; trim- trimmed mean filtering with 7x7 window size; sh- sharpening with 3x3 high pass filter; JPEG compressions with quality factors of 50 and 40 (jpg50, jpg40) and JPEG2000 compressions with bitrates 0.5 and 0.4 (wc50, wc40). In Figure 5.6 the results of testing are overviewed presented.

For median filtering attacks (see Figure 5.6.a) the watermark was extracted from levels L3 and L4. For the level L2 the detection was not successful. Gaussian filtering attack (see Figure 5.6.b) has almost no influence on the watermark sequence. Also from the level L2 the watermark sequence was correctly extracted. For wiener filtering attack (see Figure 5.6.c) it was difficult to conclude which level has better performance than others. The watermark was detected in all levels of decomposition. Trimmed mean filtering has similar influence on robustness as median filtering (see Figure 5.6.d). Only sequences that were embedded in the levels L3 and L4 were robust on this attack. The results for sharpening attack (see Figure 5.6.e) shows that the better robustness was obtained if the watermark was embedded in the level L3. In a case of noise addition (Poisson (Figure 5.6.f) and salt'n pepper (Figure 5.6.e)) the watermark was detected in all levels. If the watermark extraction procedure if performed on original image which does not contain the watermark the presence of the watermark cannot be confirmed. The highest absolute value of correlation coefficient was around 0.3. For wc40 attacks the best results are obtained for the level L4. From the Figure 5.6.i it can be observed that watermark was also extracted from the level L3. Weaker results are obtained for L2 level. Similar level comparison applies to wc50 attack (see Figure 5.6.j). Only in this case watermark was detected in the level L2. JPEG compressions with quality factors 40 and 50 have no influence on the watermark embedded in the levels L3 and L4. High values of correlation coefficient are obtained in level L2, too.

After all these experiment it can be concluded that the best trade off between the visibility and robustness is achieved if the watermark is embedded in the level L3.

Figure 5.7.a presents the watermarked Barbara image. The watermark was embedded in the level L3 of wavelet decomposition. In Figure 5.7.b the difference image between the original and watermarked image is given.

In the next test example in all testing images the same watermark sequence was embedded in the third level of DWT decomposition. The PSNR values are calculated, as well as the correlation coefficient between the original and extracted watermark sequence. In Table 5.2 the obtained results are presented.

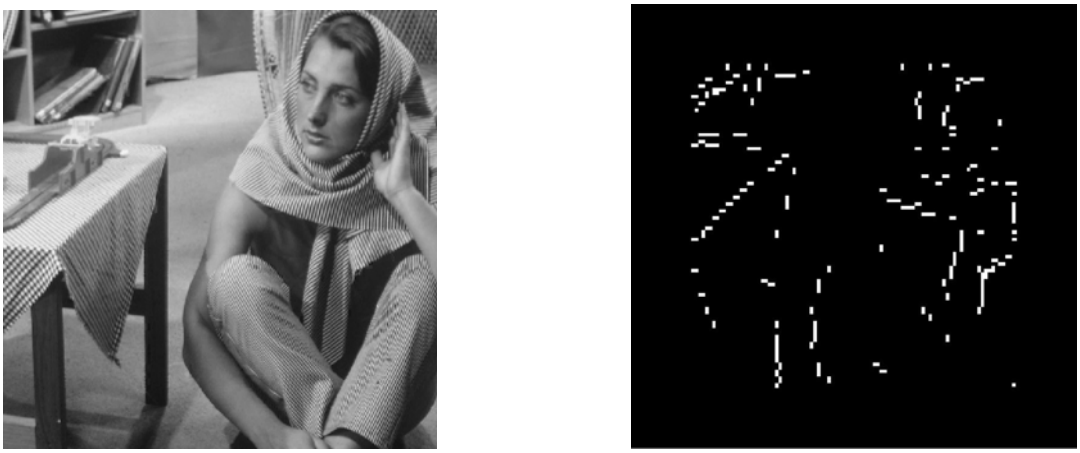

(a) (b)

Figure 5.7: (a) watermarked Barbara image; (b) difference image.

Table5. 2: The results

	barb	boats	cam	couple	Einstein	elaine	f16	goldhill	house	Lena
PSNR(db)	44.46	42.7	38.7	43.1	41.33	40.7	40.7	43.91	41.49	40.18
original	0.1076	0.0852	0.1097	0.0772	0.0772	0.0463	0.0852	0.0463	0.0149	0.0463
pois	0.86	1	1	1	1	1	1	1	1	1
salt	1	1	0.9	0.97	0.82	0.83	1	1	1	0.9
gaus	1	1	1	1	1	1	1	1	1	1
med	0.95	1	0.58	1	0.51	1	1	1	0.7	1
trim	1	1	0.63	1	0.58	1	1	1	0.85	1
win	0.85	1	1	0.88	0.79	1	1	1	0.95	1
sh	0.69	0.75	0.7	0.64	0.53	0.74	0.9	0.68	0.73	0.69
wc50	1	1	1	1	1	1	1	1	1	1
wc40	0.86	1	1	1	1	0.92	1	1	1	1
jpg50	1	1	1	1	1	1	1	1	1	1
jpg40	1	1	1	1	1	1	1	1	1	1

From the Table 5.2 it can be concluded that the watermark sequence was detected after all attacks. The smallest value of correlation coefficient was 0.51. In a case of watermark extraction from the unwatermarked image (original image) the correlation coefficient was less then 0.1. It can be concluded that the watermark does not exist in unwatermarked image.

5.6.4 Robustness on geometrical attacks

The robustness on geometrical attacks is improved by using the syhhronisation technique described in Section 4.3. The embedding procedure consists of the embedding the synchronization signal and watermark embedding. Firstly the synchronization signal is embedded in the original image according to the algorithm from the Section 4.3. Next, the watermark embedding procedure from Section 5.6.1 is performed. If the affine geometrical attacks occur which consists of scaling, rotation, cropping or combination of them, the template extraction algorithm is firstly performed. Then according to the equations (4.35-4.38) the parameters of rotation and scaling are computed. After that the image is inverse affine transformed and proceeded to the watermark detector.

In our experiments the same geometrical attacks are performed on the test images that we have used in our previous experiments: rotations with different angles (rot1- 5º, rot2- 15º, rot3- 30º), scaling transform with different scaling operations (sc1- 70%, sc2- 90%, sc3- 130) or combined geometric attacks (rs1- rotation of 5º, scaling 130%; rs2- rotation of 15º, scaling 90%; rs3- rotation of 10º, scaling 150%); image cropping with different cropping percentage (cr1- 5%, cr2- 10 %, cr3- 15 %, cr4- 20 %).

Based on experiments carried out it can be concluded that the synchronization technique improves the robustness. The watermark was detected after all tested geometrical attacks.

5.7 Chapter Summary

In this Chapter firstly the Discrete Wavelet Transform is presented. Then the important properties of the Wavelet transform, which are used for watermarking, are outlined. Next, the HVS perceptual model based on DWT is described. The classification of the existing watermarking algorithms based on DWT is briefly overviewed.

The first watermarking algorithm developed and presented in this thesis is essentially a classical non-blind additive watermarking algorithm in wavelet domain. Using this algorithm the impact of different error correction codes on the watermark robustness was investigated. From this point of view, it is shown that the Read-Solomon error correction code delivers the best results. Further, it is tested which subband of DWT decomposition shows the best performances for watermark embedding. The robustness of the watermark was tested on different filtering and compression attacks. It was concluded that the best results are obtained if the watermark is embedded in the subbands LH_2 and HL_2. The robustness on geometric attacks of this algorithm is additionally improved by using the image registration technique from the Section 4.1.

The second watermarking algorithm developed in the wavelet domain belongs to a class of blind additive algorithms. The watermark sequence is encoded with Read-Solomon error correction code. The watermark was embedded in the LH and HL subbands of second, third and fourth levels of the DWT decomposition. The best results were obtained for the watermark embedded in the LH and HL subbands of third level of decomposition. The robustness of this algorithm on geometrical attacks is additionally improved by using the proposed synchronization technique from the Section 4.3. In both algorithms the scale invariant feature points are used as reference locations for the embedding of watermark pattern.

In the next Chapter the complex wavelets will be introduced as an extension to the standard wavelet transform. The advantages of the CWT over standard DWT will be outlined. Then the watermarking algorithms based on the CWT will be considered in more detail.

Chapter 6

Digital image watermarking in complex wavelet domain

The *complex wavelet transform* (CWT) is a complex-valued extension to the standard discrete wavelet transform (DWT). The complex wavelets have not been widely used in the watermarking, although they have several desirable features, which can be applied for watermarking. Chapter 6 gives an overview of watermarking algorithms in Complex wavelet domain. In Section 6.2 the Complex Wavelet Transform (CWT) will be briefly described. The literature survey of existing watermarking algorithms is given in Section 6.3. In Section 6.4 the proposed watermark embedding algorithm is described and tested in Section 6.5.

6.1 Introduction

The complex wavelet transform of a signal uses two separate trees of real DWT filters that operate in parallel to generate the real and imaginary parts of a complex filter. That means that the number of coefficients at the output of the Complex wavelet transform is doubled comparing with the number of DWT coefficients. The redundancy of the CWT is then 2:1 for one dimensional signal and 4:1 for two-dimensional signal. This redundancy introduced by the CWT transform itself has an influence on the design of watermarking algorithm. Typically a standard transform watermarking algorithm is based on the addition of a pseudorandom sequence to the host image coefficients in one of the transformation domains like DCT, DFT, DWT, etc. A watermarked image is obtained by taking the inverse

transform. In watermark extraction procedure the CWT transformation is applied on the watermarked image in order to extract the watermark sequence from the transformation coefficients. In absence of attacks it is expected that the extracted watermark is the same as the embedded watermark. Using the CWT transformation this is not the case. Due to the redundancy of 4:1 a certain part of pseudorandom sequence will be lost. Actually a standard watermarking algorithm developed for other transform domains like DWT, DCT, DFT, etc., cannot be directly implemented in CWT domain. This can be also concluded from the survey of the existing watermarking algorithms in open literature, which will be given in Section 6.3.

6.2 Complex wavelet transform and its properties

Wavelet techniques are successfully applied to various problems in signal and image processing. However, the major problem of the commonly decimated discrete wavelet transform is its lack of *shift invariance*, what means that small shifts in the input signal can cause major variations in the distribution of energy between wavelet transform coefficients at different scales. This problem is caused by aliasing due to the subsampling at each wavelet level [101].

The second disadvantage of the DWT is its poor *directional selectivity* for diagonal features. The 2D-DWT decompose image in horizontal (0°), vertical (90°) and diagonal (±45°) directions, HL, LH, HH band respectively. The DWT cannot distinguish between the two opposing diagonal directions (±45°).

Due to difficulty in designing the complex filters satisfying the perfect reconstruction (**PR**) properties, the Complex Wavelets Transform (CWT) has not been used widely in image processing. The dual-tree complex wavelet transform (DT-CWT) [126] is relatively recent enhancement to the discrete wavelet transform (DWT) with the following main properties:

- *nearly shift-invariance*
- *directional selectivity* in two and higher dimensions
- *Perfect reconstruction* using short linear-phase filters

- *Limited redundancy*: 2:1 in 1-D and 4:1 in 2-D
- *Low computation* comparing to other shift-invariant transformations.

In [26] a *dual tree* implementation of the CWT (DT-CWT) is proposed. The DT-CWT uses two trees of *real* filters to generate the real and imaginary parts of an effectively *complex* filter. The approximately shift-invariant property is accomplished with a real DWT by doubling the sampling rate at each level of the tree. Compared with the undecimated wavelet tree, which eliminates downsampling after every level of filtering, the DT-CWT effectively eliminates down-sampling only after the first level of filtering.

In Figure 6.1 the analysis and synthesis filter banks for one dimension are presented. By this, two real wavelet transforms use two different sets of filters, with each satisfying the perfect reconstruction (PR) conditions.

Let H_{0a}, H_{1a} denote the low-pass/high-pass filter pair for the upper filter bank and let H_{0b}, H_{1b} denote the low-pass/high-pass filter pair for the lower filter bank (see Figure 6.1). The corresponding reconstruction filters are: H'_{0a}, H'_{1a} for the upper filter bank and H'_{0b}, H'_{1b} for the lower filter bank. The two real wavelet associated with each two wavelet trees *a* and *b* are denoted as $\psi_{ha}(t)$ and $\psi_{hb}(t)$, respectively. To satisfy the PR condition, the complex wavelet presented as:

$$\psi(t) = \psi_{ha}(t) + j\,\psi_{hb}(t) \tag{6.1}$$

is designed in such a way that the wavelets $\psi_{ha}(t)$ and $\psi_{hb}(t)$ form a Hilbert transform pair [127, 128]:

$$\psi_{hb}(t) = \mathcal{H}\{\psi_{ha}(t)\} \tag{6.2}$$

To invert the transform, the real part and the imaginary part are each inverted separately using the inverse real DWT transform. Through this operation one obtains two real signals. These two real signals are averaged to obtain the final output.

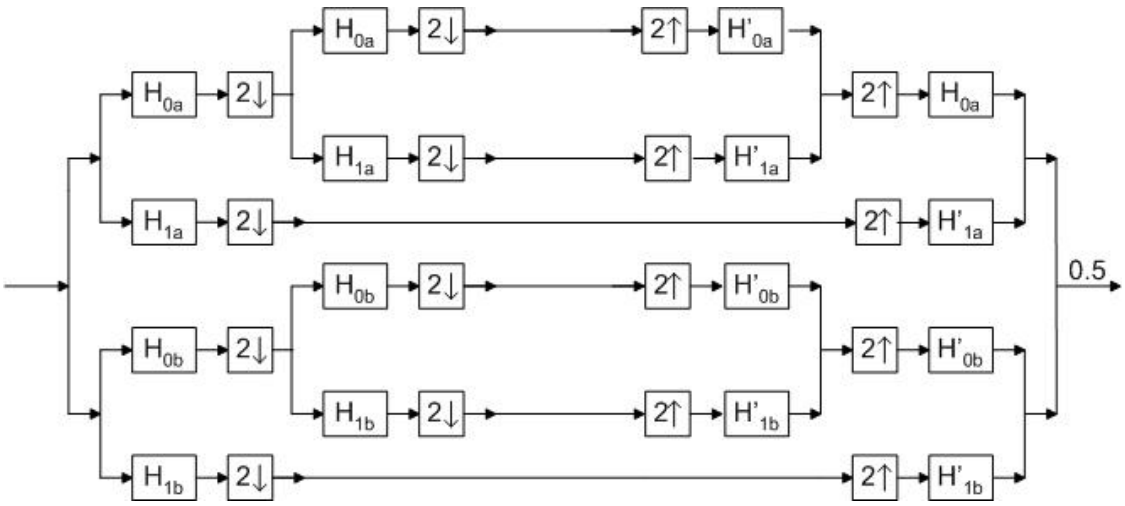

Figure 6.1: Analysis and synthesis filter banks for the dual-tree discrete CWT

Although the DT-CWT uses the two real DWT, the DT-CWT requires the design of new wavelet filters. It requires a pair of filters sets chosen in that way that the corresponding wavelet form an approximate Hilbert transform pair. Using the wavelet filters not satisfying this property, the DT-CWT cannot be nearly shift-invariant transform.

If the wavelet design problem is translating to the filter design problem then it is necessary to design the low-pass filters in both real DWT trees to form an approximate Hilbert transform pair. In [129] it is shown that one low-pass filter should be approximately a half-sample shift of the other:

$$H_{0b}(n) = H_{0a}(n-0.5) \quad \Rightarrow \quad \psi_{hb}(t) = \mathcal{H}\{\psi_{ha}(t)\} \tag{6.3}$$

In the practical realization of DT-CWT this condition is satisfied only approximately.

As aforementioned, the top level filters in two trees operate on the odd and even sample of the input signal, respectively. To get the uniform intervals between the two trees' samples, the subsequent filters in one tree must have delays that are half a sample different. DT-CWT offers both magnitude and phase information. The magnitude of each CWT coefficient is insensitive to small image shifts.

To compute the 2-D DT-CWT of the images, these two trees are applied to the rows and then the columns of the image, as in conventional DWT. Instead of three subbands in one level of DWT decomposition, here are the six oriented subbands obtained per scale. The

orientations of the subbands are: ±15, ±45 and ±75 degrees. The six wavelets associated with the real 2D dual-tree DWT are illustrated in the Figure 6.2 as gray scale images. Note that each of the six wavelets is oriented in a distinct direction.

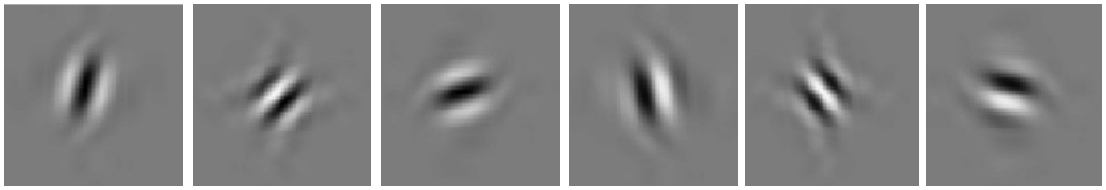

+75 +45 +15 -75 -45 -15

Figure 6.2: 2-D filter impulse responses of DT-CWT.

One example of oriented subbands of CWT decomposition of House image is presented on Figure 6.3.

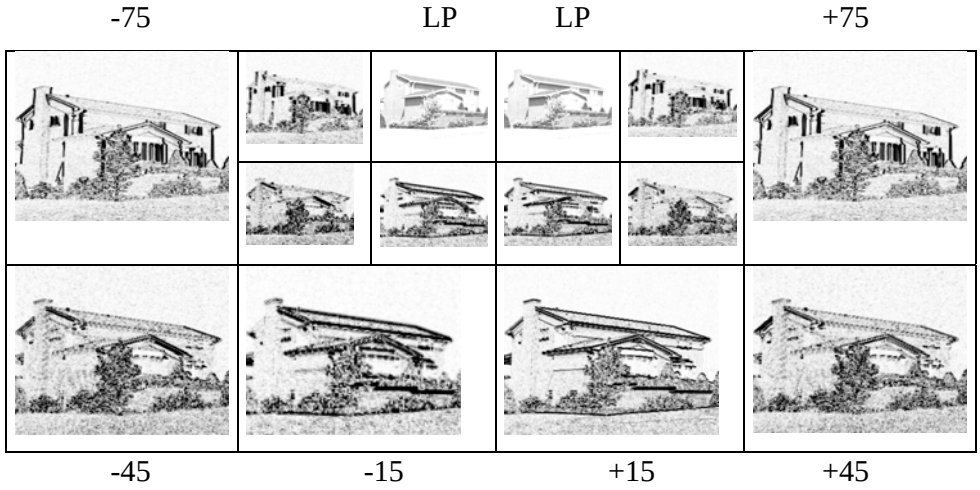

Figure 6.3: Example of the CWT decomposition of House image. Only magnitudes of two levels of decomposition are shown. The orientation of the corresponding filter is shown in corner of each subband. The contrast of the images has been enhanced for illustration purpose. LP corresponds to lowpass CWT coefficients.

The DT-CWT is inherently sensitive to rotation, but the sum of the energies of coefficients across all 6 directional subbands is reasonably invariant to rotation. In [130] the

rotation-invariant texture features using the DT-CWT transform are extracted. This approach is based on the Fourier analysis of the 6 CWT oriented subbands energies. The rotation-invariant features are extracted from the energies of the DT-CWT shift-invariant oriented subbands.

The shift-invariant property [131] by the parallel filter-banks is given in Appendix D.

In our work we have used the Matlab implementation of DT-CWT transform found in [132].

6.3 Watermarking algorithms

In this Section a brief overview of the existing watermark embedding approaches in CWT domain is given:

1. In [22] Loo proposed the following approach. Firstly the CWT coefficients of the original image are computed. A bipolar pseudorandom image, the same size as the original image is used as the watermark. Further the CWT coefficients of the bipolar pseudorandom image, where each pixel has a value of ±1, are determined. The CWT coefficients of the watermark image are than at each coefficient location (m,n) scaled and added to the CWT coefficients of the original image in the following way:

$$f'(m,n) = f(m,n) + G_{cwt}(m,n) \cdot w(m,n) \tag{6.4}$$

$$G_{cwt} = \sqrt{k^2 \cdot \overline{|f|_U^2} + \gamma^2} \tag{6.5}$$

where $f'(m,n)$ and $f(m,n)$ are the modified and the original wavelet coefficient of the host image, respectively; $w(m,n)$ is the CWT coefficient of the watermark; $\overline{|f|_U^2}$ is the average squared magnitude in the 3×3 neighborhood U around (m,n) and k and γ are the level dependent constants designed to make the watermark imperceptible. The embedding process is repeated for each subband and resolution from 1 to 3, where 1 is

the finest resolution. The watermark detection is based on the correlation between the watermark coefficients w and the CWT coefficients of the received image. The watermark capacity was calculated but the robustness of the presented algorithm on the watermarking attacks was not investigated.

2. In [23] a similar approach to [22] is presented. By this at levels 2 and 3 only the embedding procedure is applied. Before embedding the binary watermark data is divided into 6 bit symbols, and each symbol is encoded with (32,6) error correction Hadamard code. The payload is the concatenation of all such codewords. As in the previous algorithm, the robustness on watermarking attacks was not investigated.
3. In [133] the embedding in the spatial domain is performed in the following way. A random image of ±1 of the same size as the host image is generated and the CWT coefficients of both images are computed. The scaling factors (the visual mask) are computed from the host image's CWT coefficients using equation (6.5), independently for each subband. The random image coefficients are modulated by the payload. The modulated coefficients are scaled and then inverse transformed to form a watermark. At the end in order to obtain the marked image, the watermark is added to the host image in the spatial domain. The robustness of this algorithm was tested for three standard images (*Lena, baboon, Pills*) on compression attacks (JPEG, JPEG2000), Additive White Gaussian Noise (AWGN), mean, median and denoising attacks. The presence of the watermark was detected after all tested attacks.
4. In [133] the approach is based on the Chen quantisation based watermarking algorithm [134]. Here the *spread transform*, which is a combination of spread spectrum technique and quantisation based watermarking, is used. The algorithm has the following steps. The host image is divided into 32×32 blocks and the payload is divided into equal-sized portions, with each portion being embedded into separate block. A pseudorandom vector of ±1 (the same size as one block) is generated for each bit of the payload to be embedded. The forward CWT of this vector is computed, and scaled according to local image activity. The scaled coefficients of this vector are frequency partitioned into 3 vectors, with each one reconstructed back into the spatial domain using only one level of CWT coefficients. From this instant the watermarking process takes place in the spatial domain, the CWT domain is only used for adapting the random vector to the image.
5. In [135] an incremental watermarking technique is proposed. A grey-scale image is firstly decomposed into the 1-level DWT and then the low-frequency part LL_1 is

embedded into the image, as a watermark. The original image is decomposed into the 3-level DT-CWT decomposition. The watermark is added to the phase component of the DT-CWT coefficients. At the extracting step, the algorithm incrementally compares the extracted watermark with the original one using correlation from lowest to highest level. The proposed technique through performance evaluation shows that it was more robust in geometric distortions than a conventional CWT-based watermarking. The algorithm was also robust on noise addition and image blurring attacks.

From this brief overview of the existing watermarking algorithms it can be concluded that the watermarking in the CWT domain is still an open problem. In most of this approaches the robustness of the algorithms on different distortions was not enough tested. In the next Session we will propose a new watermarking algorithm and show that this algorithm outperforms the existing watermarking algorithms based on CWT.

6.4 The new watermarking algorithm based on DT - CWT (C - T03)

A new watermarking algorithm based on CWT will be described in the following Sections. The robustness of the algorithm on geometrical attacks will be improved using the image registration technique from the Section 4.1.

6.4.1 Embedding procedure

In this Section a watermarking algorithm based on DT-CWT is presented [42, 43, 47]. The algorithm is performed in spatial domain. By this, the watermark embedding is based on the spread spectrum additive technique. In Figure 6.4 the embedding scheme is presented. The original image $\mathbf{I}$ is firstly CWT transformed into four levels of CWT decomposition. Each level of decomposition with its coefficients f_1, f_2, f_3 and f_4 is separately selected and inverse CWT transformed. The approximation level with

coefficients f_a is also separately inverse CWT transformed. Now the spatial representations of inverse transformed CWT levels 1-4 are obtained: $\mathbf{X}_a$, $\mathbf{X}_1$, $\mathbf{X}_2$, $\mathbf{X}_3$ and $\mathbf{X}_4$. In this algorithm watermark embedding will be performed in the $\mathbf{X}_3$ and $\mathbf{X}_4$ because the watermark embedded in $\mathbf{X}_3$ and $\mathbf{X}_4$ is less sensitive to image compression and filtering then watermark embedded in $\mathbf{X}_1$ and $\mathbf{X}_2$. On the other hand the watermark sequence is obtained in the following way. Firstly, the coefficients of the visual masking model f_{VM3} and f_{VM4} are separately computed from coefficients of the third and fourth level of CWT decomposition f_3 and f_4, respectively, according to the equation (6.5). Then the inverse CWT transform is applied to the coefficients f_{VM3} and f_{VM4} so the spatial representations $\mathbf{X}_{\mathrm{VM3}}$ and $\mathbf{X}_{\mathrm{VM4}}$ are obtained. A bipolar sequence $\mathbf{W}(1),\ldots,\mathbf{W}(L)$, where L is the length of the sequence is used as a watermark. This sequence is modulated with coefficients of $\mathbf{X}_{\mathrm{VM3}}$ and $\mathbf{X}_{\mathrm{VM4}}$ and the new watermark matrices $\mathbf{W}_{\mathrm{VM3}}$ and $\mathbf{W}_{\mathrm{VM4}}$ are computed. Actually the L most significant coefficients of $\mathbf{X}_{\mathrm{VM3}}$ and $\mathbf{X}_{\mathrm{VM4}}$ are modulated (in this case multiplied) with the watermark $\mathbf{W}$. The watermark matrices $\mathbf{W}_{\mathrm{VM3}}$ and $\mathbf{W}_{\mathrm{VM4}}$ are embedded into the spatial representations $\mathbf{X}_3$ and $\mathbf{X}_4$ according to the following equation:

$$\mathbf{X}'_l(x_1,x_2) = \mathbf{X}_l(x_1,x_2) + alfa \cdot \mathbf{W}_{\mathrm{VM}l}(x_1,x_2), \quad l \in \{3,4\} \tag{6.6}$$

where $\mathbf{X}'_l(x_1,x_2)$ is the modified and $\mathbf{X}_l(x_1,x_2)$ is original coefficient at the position (x_1,x_2), $(x_1 = 1...N_1, x_2 = 1...N_2)$ and N_1, N_2 are dimensions of the original image $\mathbf{I}$. Here parameter $alfa$ is the strength parameter, which controls the level of the watermark. The watermarked image $\mathbf{I}_w$ is obtained by addition of all spatial representations.

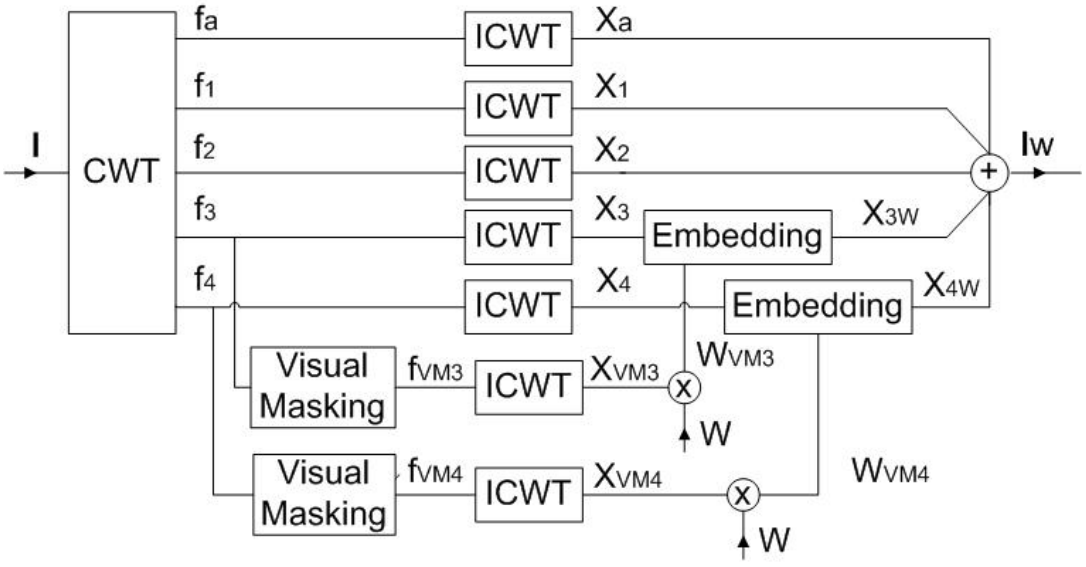

Figure 6.4: Block scheme of the embedding procedure.

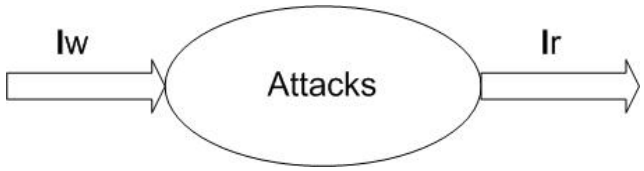

Figure 6.5: Watermarked image $\mathbf{I}_w$ after attacks.

Due to intentional or unintentional alterations of the watermark image (attacks) (see Figure 6.5) in the extraction procedure it will be spoken about received image $\mathbf{I}_r$ instead of watermarked image $\mathbf{I}_w$.

In order to improve the robustness on geometrical attacks the positions of the modified coefficients in $\mathbf{X}_3$ and $\mathbf{X}_4$ are calculated relative to the three feature points with the largest characteristic scale extracted with SIFT detector.

The watermark embedding procedure can be described using the following steps:

1. Decompose the image into the four-level CWT. Every level of CWT decomposition is separately ICWT reconstructed to form the spatial representations: $\mathbf{X}_1$, $\mathbf{X}_2$, $\mathbf{X}_3$, $\mathbf{X}_4$ for detail levels and $\mathbf{X}_a$ for approximation level.
2. Calculate the visual masks $\mathbf{X}_{VM3}$ and $\mathbf{X}_{VM4}$ for the representations $\mathbf{X}_3$ and $\mathbf{X}_4$.
3. Modulate the L largest coefficients from $\mathbf{X}_{VM3}$ and $\mathbf{X}_{VM4}$ with a bipolar watermark sequence $\mathbf{W}$ in order to obtain the watermark matrices $\mathbf{W}_{VM3}$ and $\mathbf{W}_{VM4}$. The position of the significant coefficients will be used in extraction procedure as a secret key.
4. Embed the watermark into the spatial representations $\mathbf{X}_3$ and $\mathbf{X}_4$ according to the equation (6.6).
5. The watermarked image $\mathbf{I}_w$ is obtained by addition of watermarked spatial representations $\mathbf{X}'_3$ and $\mathbf{X}'_4$ to $\mathbf{X}_a$, $\mathbf{X}_1$ and $\mathbf{X}_2$:

$$\mathbf{I}_w = \mathbf{X}_a + \mathbf{X}_1 + \mathbf{X}_2 + \mathbf{X}'_3 + \mathbf{X}'_4 \tag{6.7}$$

6. Apply the SIFT to the original image $\mathbf{I}$ and find the first three points with the largest characteristic scale.
7. Calculate the redundant position vector relative to the selected feature points.

6.4.2 Detection procedure

Detection procedure consists of two stages. If the watermarked image is altered with an affine geometrical distortion, firstly the parameters of affine transformation will be computed using the original and received image (see algorithm from the Section 4.1). After that, the image is inverted and the watermark detection procedure is performed. In the case of cropping attacks or non-geometrical attacks, the watermark detection procedure can be directly implemented to the received image. In the watermark detection procedure (Figure 6.6) the classical non-blind technique is implemented. The received, possibly altered image after attacks $\mathbf{I}_r$ is CWT decomposed into four levels of decomposition. The coefficients of the third and the fourth level of decomposition f_{3r}, f_{4r} are separated and inverse CWT transformed ($\mathbf{X}_{3r}, \mathbf{X}_{4r}$). The same procedure is repeated for the original image $\mathbf{I}$. The spatial representations $\mathbf{X}_3$ and $\mathbf{X}_{3r}$, $\mathbf{X}_4$ and $\mathbf{X}_{4r}$ are now subtracted and the watermark sequences $\mathbf{W}_{e3}$ and $\mathbf{W}_{e4}$ are extracted.

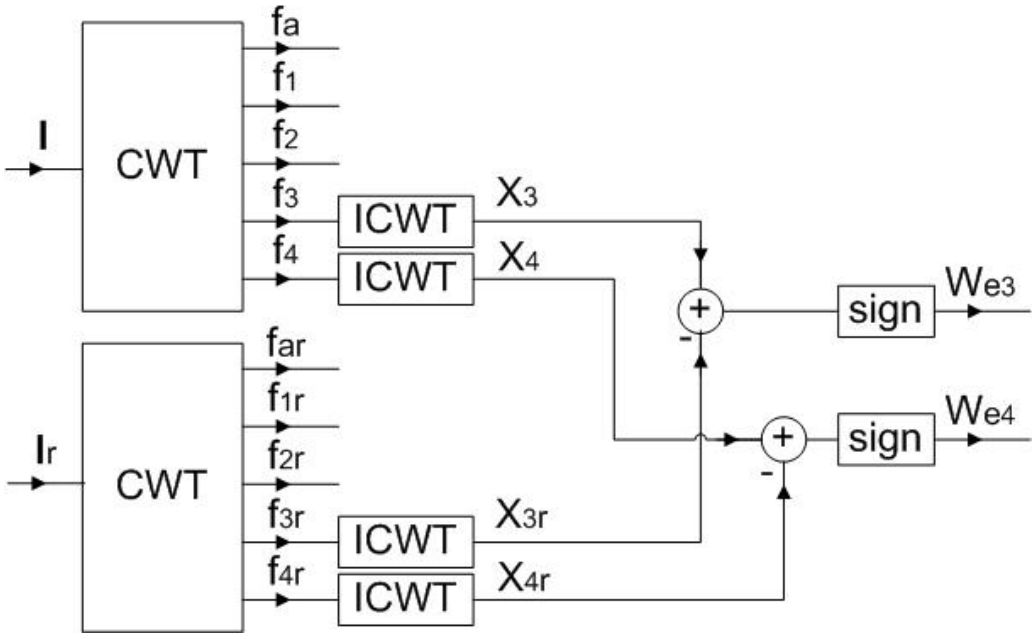

Figure 6.6: Block scheme of the extraction procedure

The detection procedure is given in the following steps:

1. Apply the SIFT detector to the image $\mathbf{I}_r$ and find the first three points with the largest characteristic scale.
2. Calculate the position vector of the modified coefficients relative to the selected feature points.
3. Apply the four-level CWT and ICWT to the image $\mathbf{I}_r$ and $\mathbf{I}$ in order to obtain the spatial representations $\mathbf{X}_{3r}$ and $\mathbf{X}_{4r}$, $\mathbf{X}_3$ and $\mathbf{X}_4$, respectively.
4. Extract the watermark using the following formula:

$$\mathbf{W}_{rl}(k) = (\mathbf{X}_{rl}(x_1, x_2) - \mathbf{X}_l(x_1, x_2))/alfa,\ l \in \{3,4\} \tag{6.8}$$

$$\mathbf{W}_{el}(k) = \text{sign}(\mathbf{W}_{rl}(k)),\ l \in \{3,4\} \tag{6.9}$$

5. Compare the extracted watermark $\mathbf{W}_{el}$ with original watermark $\mathbf{W}$ by applying the correlation:

$$\text{corr}(\mathbf{W}_{el}, \mathbf{W}) \geq \eta(P_{FA}) \tag{6.10}$$

where $\eta(P_{FA})$ represents a threshold depending on the false-positive probability P_{FA}. The probability of false positive will be obtained by running the detector on the unwatermarked image $\mathbf{I}$. The maximal value of the correlation coefficient ($T_{\max}$) between the extracted watermark from the unwatermarked image and original watermark will be used as a threshold:

$$\eta(P_{FA}) = T_{\max} \tag{6.11}$$

6.4.3 Testing results (C-T03)

For the testing purpose 10 tested standard images with the size of 512 x 512 are used: *barbara*, *boats*, *cameraman*, *couple*, *einstein*, *elaine*, *f16*, *goldhill*, *house* and *lena*

image. The watermark sequence is obtained in the following way. The message "Watermark" is firstly converted into the ASCII code. Every letter is converted into an eight bit sequence according to the ASCII rule. By using 8 bits per character for 9 watermark characters a 72-bits watermark message is obtained. The watermark message consists of zeros and ones and for the embedding purpose the sequence is bipolar encoded in that way that 0 is replaced with –1 and 1 with 1.

Before embedding, the watermark message is encoded with a Reed-Solomon (15,7) Error Correction Code (ECC). The Reed-Solomon code uses a codeword length of 15 bits and a message length of 7 bits. The length of the encoded watermark message is 180 bits.
The watermark is embedded according to the embedding rule from Section 6.3.1 (see equation 6.6). The values of constants k and γ used for evaluation of the visual model are listed in Table 6.1, where k_0 is set to 0.9 [133]. We have used the same value of the constants k and γ for third and fourth level of CWT decomposition.

In Table 6.2 the Peak Signal to Noise Ratio (PSNR) values are calculated for every used image and respectively presented. The strength parameter *alfa* is selected for every image differently in such a way that the computed PSNR value is grater than 44 dB. By visually analyzing Lena image (see Figure 6.7), it can be concluded that the watermark is invisibly embedded. The same was valid for other analyzed images. In Figure 6.8 the Lena image is decomposed into the spatial representations $\mathbf{X}_a$, $\mathbf{X}_1$, $\mathbf{X}_2$, $\mathbf{X}_3$, $\mathbf{X}_4$.

Table 6.1: Table of constants used in CWT visual model [133].

	Level 1 ±75 ±15	Level 1 ±45	Level 2 ±75 ±15	Level 2 ±45	Level 3 ±75 ±15	Level 3 ±45
k	$1\cdot k_0$	$0.55\cdot k_0$	$1.05\cdot k_0$	$1.05\cdot k_0$	$1.10\cdot k_0$	$1.35\cdot k_0$
γ	1.5	3.1	0.75	0.9	1.05	1.0

Table 6.2. PSNR values (dB) of the analyzed images:

	barb	boats	cam	couple	einstein	elaine	f16	goldhill	house	lena
PSNR(db)	47.56	47.24	44.2	48.44	47.59	48.9	46.3	48.2	47.87	47.9

original image watermarked image

Figure 6.7: The original and watermarked Lena image

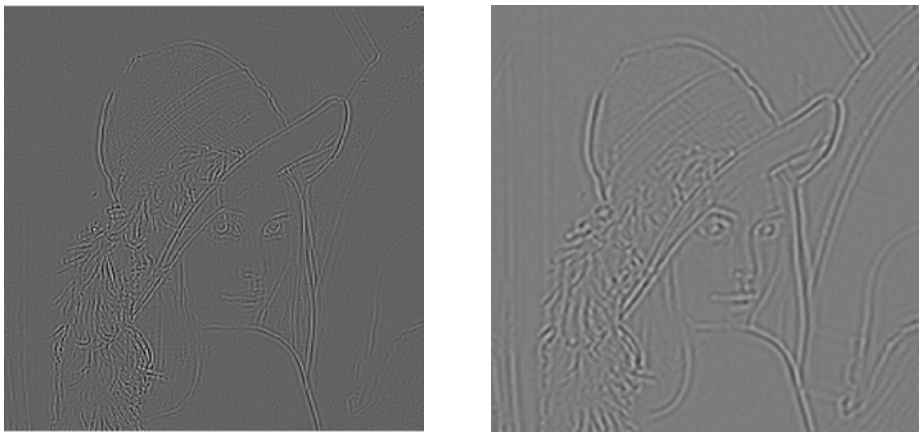

$\mathbf{X}_1$ $\mathbf{X}_2$

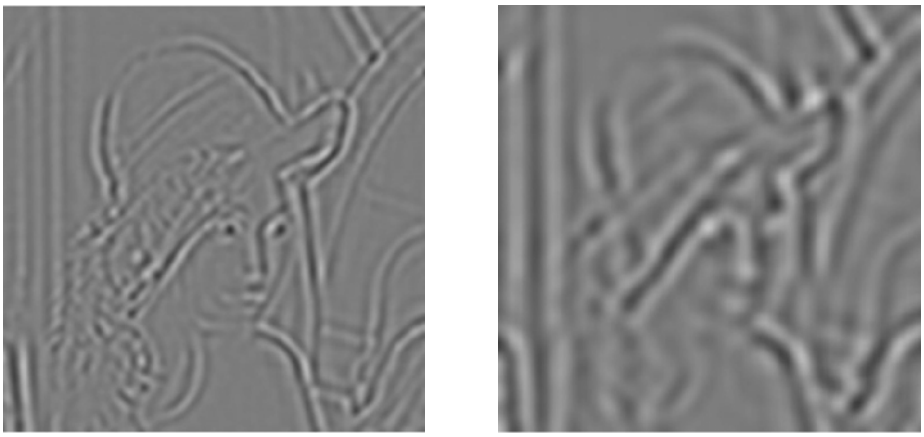

$\mathbf{X}_3$ $\mathbf{X}_4$

$\mathbf{X}_a$

Figure 6.8: Decompositions of Lena image into the spatial representations of approximation CWT level $\mathbf{X}_a$ and detail levels ($\mathbf{X}_1$, $\mathbf{X}_2$, $\mathbf{X}_3$, $\mathbf{X}_4$) are shown. The contrast of the images has been enhanced for illustration purpose.

The robustness of the algorithm is tested separately for the watermark sequence embedded in $\mathbf{X}_3$ and $\mathbf{X}_4$ representations. The same attacks were performed as in Section 5.6.3: med- median filtering; gaus- gaussian filtering; wien- wiener filtering; trim- trimmed mean filtering; sh- sharpening; JPEG compressions with quality factors of 50 and 40 (jpg50, jpg40) and JPEG2000 compressions with bitrates 0.5 and 0.4 (wc50, wc40). After watermark extraction procedure the watermark sequence is decoded with (15,7) Reed-Solomon ECC. This sequence is now compared wit the original watermark sequence by applying the correlation. As a correlation threshold the false-positive probability is computed by running the detector on the unwatermarked image. In our experiments the highest value of the false-positive probability for both $\mathbf{X}_3$ and $\mathbf{X}_4$ representations was 0.2. We used this value as the detection threshold. The results are presented in the Table 6.3.

It can be observed from the table that the watermark was detected in both $\mathbf{X}_3$ and $\mathbf{X}_4$. In all cases the watermark was detected from $\mathbf{X}_4$. The watermark sequence embedded $\mathbf{X}_3$ was robust on all attacks except on median, trimmed mean and wiener filtering. The results for these attacks were different for different images. Generally it cannot be

concluded that for median, trimmed mean and wiener filtering attacks the watermark was detected from the spatial representation $\mathbf{X}_3$.

Comparing the robustness of the proposed algorithm with other algorithms [22, 23, 132, 134], this algorithm shows better performances. It was robust on wider class of filtering attacks, which include wiener, trimmed mean filtering and sharpening. Table 6.4 gives an overview of the comparison of the existing methods. "1" in the Table denotes that the algorithm was robust on specific attack while 0 denotes that algorithm was not robust on specific attack. "n.i." denotes that the robustness was not investigated.

Comparing the proposed algorithm in the CWT domain with the DWT algorithms proposed in the Chapter 5, it can not be concluded that it outperforms the DWT algorithms. Although the CWT has several important improvements with regard to the DWT, the development of the watermarking techniques in the CWT domain, which can fully explore the possible advantages of the CWT, is still an open research problem.

6.4.4 Robustness on geometrical attacks

In order to improve the robustness on cropping attack the watermark was embedded only in the central part of the image. In that way, if the image is cropped till the certain percentage of the image size, the watermark will be still present in the image. The position vector of modified coefficients from the $\mathbf{X}_3$ and $\mathbf{X}_4$ is calculated relative to three scale invariant feature points with the largest characteristic scale. In a case of affine geometrical attack the robustness of the proposed technique can be increased by combining the technique with our image registration technique from Section 4.1. When the parameters of affine transformations are determined, the inverse transformation can be applied to the received image and then the watermark extraction procedure can be performed.

The same geometrical attacks are performed on the test images that we have used in our previous experiments: rotations with different angles (rot1- 5º, rot2- 15º, rot3- 30º), scaling transform with different scaling operations (sc1- 70%, sc2- 90%, sc3- 130) or combined geometric attacks (rs1- rotation of 5º, scaling 130%; rs2- rotation of 15º, scaling 90%; rs3- rotation of 10º, scaling 150%); image cropping with different cropping percentage

(cr1- 5%, cr2- 10 %, cr3- 15 %, cr4- 20 %). The watermark was detected after all tested geometrical attacks in both $\mathbf{X}_3$ and $\mathbf{X}_4$ spatial representations.

Table 6.3: The results for non-geometrical attacks.

		barb	boats	cam	couple	einstein	elaine	f16	goldhill	house	Lena
pois	X3	0.94	1	0.68	1	1	0.92	1	0.84	1	0.91
	X4	1	0.97	1	1	1	1	1	1	1	1
salt	X3	0.8	0.97	0.68	0.88	0.81	0.58	0.78	0.4	0.78	0.8
	X4	0.91	0.75	0.78	1	1	0.89	0.92	0.94	0.86	1
gaus	X3	0.52	1	0.57	0.86	0.94	0.8	0.89	0.69	0.86	0.83
	X4	1	1	1	1	1	1	0.97	1	1	1
med	X3	0.15	0.91	0.56	0.36	0.97	0.5	0.23	0.14	0.16	0.19
	X4	1	1	1	0.95	0.976	1	1	0.95	1	0.92
trim	X3	0.21	0.7	0.51	0.01	0.62	0.45	0.02	0.41	0.08	0.15
	X4	0.92	1	1	0.95	1	1	0.94	0.94	1	0.97
win	X3	0.29	0.86	0.04	0.19	0.84	0.47	0.25	0.16	0.07	0.33
	X4	0.6	0.5	0.75	1	1	0.89	0.43	0.95	0.97	0.78
sh	X3	1	1	0.69	1	1	1	1	0.97	1	1
	X4	1	1	0.97	1	1	1	1	1	1	1
wc50	X3	0.51	1	0.91	1	1	0.89	1	0.8	1	1
	X4	1	1	1	0.94	1	1	1	1	1	1
wc40	X3	0.5	1	0.87	0.92	1	0.89	1	0.64	1	1
	X4	0.91	0.97	1	0.95	1	1	1	1	11	1
jpg50	X3	0.92	1	0.79	1	1	1	1	0.78	1	1
	X4	1	1	1	1	1	1	0.95	1	1	1
jpg40	X3	0.97	1	0.76	1	1	0.89	1	0.75	0.94	1
	X4	1	0.97	1	1	1	1	1	1	1	0.92

Table 6.4: Comparison of the existing watermarking methods based on DT-CWT.

	gaus	med	trim	win	sh	jpg	wc
Loo in [135]	1	1	n.i.	n.i.	n.i.	1	1
Lee in [137]	1	n.i.	n.i.	n.i.	n.i.	n.i.	n.i.
C-T03	1	1	1	1	1	1	1

6.5 Chapter Summary

In this Chapter the drawbacks of the real wavelet transform are reviewed and a dual tree implementation of the complex wavelet transform is introduced. It is outlined how the CWT overcomes the problems with the conventional real wavelet transform. The overview of the existing watermarking algorithms based on CWT is then given. Next, a new watermarking algorithm, based on the CWT, is proposed. This algorithm requires the original image for watermark extraction. In order to improve the robustness, the watermark is encoded with the Read-Solomon error correction code. The scale invariant feature points extracted with SIFT detector are used as reference locations for the embedding and extraction of the watermark. The robustness of the algorithm is tested for different filtering (median, gaussian, wiener, trimmed mean filtering; and sharpening) and compression attacks (JPEG and JPEG2000). The proposed watermarking algorithm shows the robustness on all tested attacks. The robustness of this algorithm on geometrical attacks is further improved by using the image registration technique from the Chapter 4.1. The proposed algorithm is compared with other existing watermarking algorithms based on CWT and it showed better performances.

Chapter 7

Conclusions and Future Research Directions

7.1 Thesis Overview

The work described in this thesis is concerned with the design of robust digital image watermarking algorithms for copyright protection. Various types and application of watermarks were introduced and an overview of existing watermarking algorithms and attacks are given.

In the field of watermarking, the *feature points* can be used as the reference locations for the both the watermark embedding and detection processes. The feature points are detected with feature point detectors and these detectors should extract the feature points that are robust on various distortions (compression, filtering, geometric distortions, etc.).

A new class of scale invariant feature point detectors, which is robust to transformations like rotation, scale and translation, is introduced and later applied for watermarking. A comparison between two scale-invariant feature point detectors:

- SIFT feature point detector and
- Harris-Affine feature point detector,

showed that the SIFT feature point detector gives more robust feature points for the most of the geometrical distortions (e.g. rotation, scaling or combinations of them).

In the case of filtering and compressions (JPEG and JPEG 2000), both detectors showed excellent performances. However, in experiments presented, only the feature points with the largest characteristic scale were observed.

The resistance of watermarking schemes against geometrical distortions is one of the still opened and challenging problems in the field of watermarking. One possibility to recover the watermark synchronization is to implement the *image registration technique* before the watermark detection procedure. An image registration technique, based on establishing point-by-point correspondence between the original image and image possibly altered by unknown geometrical transformation (received image) is demonstrated. The feature points are extracted with the SIFT detector, where as the SIFT descriptors were calculated for every feature point. The correspondences between the points were established by measuring the correlation coefficient between the SIFT descriptors. When the correspondence between two images is determined, the parameters of the undergone geometrical transformation are estimated and an inverse geometrical transformation is calculated and applied to the received image. This technique effectively estimates the parameters of undergone affine transformation.

Another possibility to recover the watermark synchronization is to implement the synchronization technique proposed in Section 4.3. One important feature of this technique is that it does not require the presence of original, or watermarked image. This technique combines the template based and content based approach. The main idea of this technique is to extract the robust feature points with SIFT detector and to embed in the neighborhood of every feature point two information, which can be later used to detect the parameters of undergone geometrical transformations. These two information are embedded robustly using DFT and they represent information about the reference angle and the information about the characteristic scale of the feature point. When the affine transformation, consisted of image rotation, scaling, cropping or combination of them, occurs, it is enough correctly to detect at least from one feature point neighborhood these two information. After that, the parameters of rotation and scaling can be easily calculated. This was demonstrated in experiments presented, and it is shown that compressions (JPEG and JPEG2000) have no influence on the extraction of these two information, as well.

The first watermarking algorithm developed and presented in this thesis is essentially a classical non-blind additive watermarking algorithm in wavelet domain, just like many of the existing algorithms. Using this algorithm the impact of different error correction codes

on the watermark robustness was investigated. From this point of view, it is shown that the Read-Solomon error correction code delivers the best results. The same watermark is embedded in all detail subbands of a two-level DWT. Further, it is tested which subband of DWT decomposition shows the best performances for watermark embedding. The robustness of the watermark was tested on different filtering and compression attacks. It was concluded that the best results are obtained if the watermark is embedded in the subbands LH_2 and HL_2. The robustness on geometric attacks of this algorithm is additionally improved by using the aforementioned image registration technique.

The second watermarking algorithm developed in the wavelet domain belongs to a class of blind additive algorithms. The watermark embedding is performed in the central part of the image. In this way the cropping of the certain percentage of the image size (in our case, we set to 25 %) has no influence on the watermark detection. The watermark sequence is encoded with Read-Solomon error correction code and embedded in the largest coefficients of the LH and HL DWT subbands. In order to increase the robustness on cropping attacks, a new position vector of the modified DWT coefficients is calculated redundantly and relative to the location of the feature points in the subband. In a classical additive approach, the modified DWT coefficient depends on the original DWT coefficient and the watermark. Here this coefficient depends additionally on the mean value of all DTW coefficients selected for watermark embedding. In this way the stronger watermark was embedded into the image which enables later blind watermark detection. In the thesis the robustness of different watermarks on attacks is tested. The watermark was embedded in the LH and HL subbands of second, third and fourth levels of the DWT decomposition. The best results were obtained for the watermark embedded in the LH and HL subbands of third level of decomposition. The robustness of this algorithm on geometrical attacks is additionally improved by using the aforementioned proposed synchronization technique.

The next watermarking algorithm developed is based on the CWT. It is an additive algorithm and it requires the original image for watermark extraction. Here the complex wavelets were introduced as an alternative to conventional real wavelets. They overcome two main drawbacks of real wavelets: a) lack of shift invariance and b) directional selectivity. However, since the CWT is a redundant transform a different watermarking approach is here applied. Firstly, the fourth level of the CWT decomposition is performed and then every level of decomposition is separately inverse transformed to form the spatial representations. In order to improve the robustness, the watermark is encoded with the

Read-Solomon error correction code. The watermark is embedded in the spatial representation of the third and fourth level of decomposition. The scale invariant feature points extracted with SIFT detector are used as reference locations for the embedding of the watermark. The robustness of the algorithm is tested for different filtering (median, gaussian, wiener, trimmed mean filtering; and sharpening) and compression attacks (JPEG and JPEG2000). In all cases the watermark was detected from the spatial representation of the fourth level of the CWT decomposition. The watermark sequence embedded in the spatial representation of the third level of CWT decomposition was robust on all attacks except on median, trimmed mean and wiener filtering. The robustness of this algorithm on geometrical attacks is further improved by using the aforementioned image registration technique. The proposed algorithm showed better performances compared to other existing watermarking algorithms based on the CWT.

7.2 Future Research Directions

In this Section few unresolved issues are summarized, and some possible research directions are addressed.

In Chapter 4 the novel synchronization technique is proposed, which does not require the presence of the original image. This technique calculates the parameters of affine transformation, which include rotation, scaling or combination of them. In the case of an affine transformation, when the scale change is not necessarily the same in every direction, automatically selected characteristic scales do not reflect the real transformation of a feature point. The future work will be related to the development of the technique, which can recover the other parameters of affine transformation like shearing parameter, or scale parameter, which is not the same in every direction.

In Chapter 5, using the non-blind additive algorithm developed in wavelet domain, the impact of different error correction codes was investigated. The use of error correction codes for digital watermarking is still an open problem. It requires design of codes, which are able to take into account many different kinds of attacks. In [136] the enhanced robustness in image watermarking is achieved using block turbo codes. Implementation of

convolution codes, or turbo codes in watermarking algorithms presented in this thesis, should be a part of the future research.

Both watermarking algorithms developed in the wavelet domain and presented in Chapter 5 do not use the perceptual models. The watermarks should be perceptually similar to the cover image if they have to be resistant to copy attacks, or other estimation based attacks. The implementation of different perceptual models should be done as an extension to the proposed watermarking algorithms.

In Chapter 6 the watermarking algorithm in CWT domain is developed. Although the CWT has several important improvements with regard to the DWT, there is still a need to study deeply the watermark embedding techniques in the CWT domain, which can fully explore the possible advantages of the CWT.

Appendices

In this Chapter the results from Section 3.3, as well as the following two important transformations used in this Thesis:

- Radon Transform and
- Fourier-Mellin Transform.

are presented.

In addition, the main features of the shift-invariance of the Complex Wavelets Transform are addressed. Finally, all test images used in this thesis are overviewed presented.

Appendix A Comparaison of Feature Points Detectors: Results

Table A.1: The number of corresponding feature points between the distorted image and original test image. The points are extracted with SIFT detector (column SF) and Harris-Affine detector (column HA).

		jpg40		jpg50		wc40		wc50		med.		gaus		wien.		trim.		salt		poiss	
	n	SF	HA	SF	HA	SF	HA	SF	HA	SF	HA	SF	HA	SF	HA	SF	HA	SF	HA	SF	HA
barbara	10	10	9	10	9	9	8	10	8	8	8	10	10	10	10	10	9	9	8	8	10
	20	19	18	20	19	16	17	17	16	17	14	20	19	19	19	20	17	17	14	16	20
	30	25	25	29	28	24	23	25	24	27	22	28	29	27	29	29	26	25	21	26	28
boats	10	9	9	9	10	8	9	10	9	9	8	9	10	9	10	9	8	7	8	8	9
	20	17	18	18	18	17	18	18	18	17	14	19	20	19	19	18	17	16	15	17	17
	30	27	27	28	27	24	28	28	28	26	21	29	30	27	28	27	25	22	22	26	24
camera-man	10	8	10	9	9	8	9	8	9	9	6	8	10	8	10	8	9	8	8	9	9
	20	18	19	18	19	17	18	17	18	19	12	18	20	17	19	17	17	16	15	19	18
	30	25	28	28	27	23	28	24	28	27	17	22	29	26	27	25	22	22	22	26	23
couple	10	8	10	9	10	8	10	8	10	8	9	10	10	9	10	8	9	7	10	9	8
	20	17	18	17	20	14	19	15	18	16	17	19	20	17	19	16	17	14	15	16	16
	30	25	24	24	29	20	26	18	25	21	23	27	30	25	26	24	24	20	22	23	25
einstein	10	9	10	10	9	9	10	10	9	10	9	10	10	10	9	9	9	8	7	9	9
	20	18	19	18	18	16	19	18	18	19	16	19	20	19	18	18	18	15	15	17	17
	30	28	27	27	28	25	29	27	27	27	23	27	30	28	28	26	27	20	19	24	24
elaine	10	9	10	7	10	7	9	8	9	9	8	9	10	10	10	9	10	9	8	10	9
	20	17	18	16	19	17	17	17	17	17	16	18	20	18	20	17	19	17	16	18	18
	30	25	26	25	27	26	25	26	25	26	21	27	30	27	30	26	29	25	22	27	26
f16	10	10	10	9	9	10	9	10	10	8	10	10	9	10	9	10	9	7	9	10	9
	20	19	19	10	18	18	17	20	20	17	18	20	17	20	18	18	17	16	15	18	18
	30	29	29	29	28	28	27	29	30	26	26	29	26	30	28	29	26	22	24	27	27
goldhill	10	10	10	10	10	9	10	8	10	7	8	10	10	9	10	8	10	8	8	7	10
	20	19	20	20	19	18	19	17	19	16	17	19	20	18	20	18	20	16	16	16	19
	30	27	29	27	28	25	26	24	29	24	26	27	30	28	28	27	28	20	23	24	28
house	10	9	10	9	10	6	10	6	9	8	8	8	10	8	9	9	2	8	10	9	8
	20	11	18	12	19	12	18	10	18	11	17	11	19	13	18	11	4	13	18	17	16
	30	15	27	17	24	17	27	15	27	17	24	17	29	16	28	15	6	18	25	22	25
lena	10	10	10	10	10	9	10	8	10	9	10	10	10	10	10	9	10	9	10	9	10
	20	19	19	19	19	19	18	17	18	18	19	20	20	19	20	19	19	17	16	19	20
	30	28	29	29	29	27	28	25	28	24	25	30	30	28	28	28	29	24	24	27	29

Table A.2: The number of corresponding feature points between the distorted image and original test image. The points are extracted with SIFT detector (column SF) and Harris-Affine detector (column HA).

		rot1		rot2		rot3		rot4		sc1		sc1		sc3		sc4	
	n	SF	HA	SF	HA	SF	HA	SF	HA	SF	HA	SF	HA	SF	HA	SF	HA
barbara	10	5	5	5	1	4	1	3	2	6	2	7	3	8	1	4	3
	20	10	9	8	4	7	3	10	4	14	4	16	8	18	2	14	7
	30	20	13	17	8	15	6	15	7	22	6	23	8	25	3	22	9
boats	10	4	2	4	2	4	3	4	1	7	1	8	2	7	4	4	5
	20	10	4	8	5	8	6	9	4	14	2	16	4	14	6	12	7
	30	17	6	16	9	15	8	15	7	22	5	24	5	23	7	19	10
cameraman	10	5	2	3	2	4	1	6	1	8	1	7	5	8	1	7	4
	20	12	5	12	2	11	4	14	2	14	4	13	5	16	3	14	7
	30	19	7	18	7	18	10	20	6	22	5	10	9	24	5	24	10
couple	10	5	2	6	2	6	1	6	1	5	1	7	4	6	1	2	1
	20	10	7	11	4	10	4	12	1	11	3	13	6	14	3	9	4
	30	16	8	16	8	17	7	15	2	19	5	20	11	20	4	14	5
einstein	10	6	2	6	1	5	1	7	1	6	2	9	2	7	4	5	4
	20	14	7	15	3	15	2	15	5	16	5	17	5	15	8	12	5
	30	21	13	22	5	21	3	22	8	25	11	23	9	24	14	20	10
elaine	10	4	2	4	1	4	1	3	1	3	1	5	3	6	1	5	2
	20	9	5	8	3	7	2	7	2	11	2	15	7	14	2	12	7
	30	15	8	15	4	13	5	13	3	19	3	22	9	22	7	21	9
f16	10	5	6	3	3	2	1	4	2	7	3	8	3	7	1	6	1
	20	13	8	10	5	9	3	10	4	14	5	16	5	14	3	13	4
	30	21	12	16	9	15	5	20	5	19	7	25	8	25	4	19	9
goldhill	10	5	5	4	4	5	1	5	1	5	3	6	3	6	1	5	2
	20	11	6	10	8	14	5	8	6	12	5	16	5	14	3	13	4
	30	17	12	19	10	20	6	15	10	19	7	22	8	21	7	19	7
house	10	7	3	6	1	7	1	5	1	7	3	8	1	4	1	3	2
	20	12	5	13	4	13	4	10	3	14	8	14	2	11	1	6	6
	30	19	10	19	7	19	8	15	4	18	9	20	3	18	2	12	10
lena	10	6	3	5	4	3	3	4	1	6	3	7	2	6	4	4	3
	20	12	7	11	8	10	6	9	4	13	8	15	6	12	10	13	8
	30	21	15	19	16	16	10	17	10	22	16	22	12	18	16	18	16

Table A.3 The number of corresponding feature points between the distorted image and original test image. The points are extracted with SIFT detector (column SF) and Harris-Affine detector (column HA).

		cr1		cr2		cr3		cr4		cr5		rs1		rs2		rs3		rs4	
		SF	HA	SF	HA	SF	HA	SF	HA	SF	HA	SF	HA	SF	HA	SF	HA	SF	HA
barbara	10	9	8	8	8	7	7	6	6	4	2	4	1	5	2	2	2	3	1
	20	19	15	16	14	15	11	12	10	14	6	13	2	12	4	7	5	8	3
	30	27	23	22	20	20	17	17	15	22	11	19	3	15	4	12	8	14	4
boats	10	6	10	5	9	5	8	5	8	5	6	3	2	3	3	2	5	2	1
	20	13	19	12	18	11	18	11	17	10	14	8	4	7	4	7	7	4	2
	30	23	28	20	25	18	24	17	23	16	20	14	7	12	6	14	8	10	3
cameraman	10	9	10	7	7	7	7	7	7	7	7	5	1	4	1	5	1	3	1
	20	19	20	16	16	16	15	16	15	15	15	13	6	10	4	11	3	9	3
	30	25	28	23	24	22	23	22	23	19	23	19	7	17	5	20	5	10	6
couple	10	9	9	5	7	3	5	3	5	3	5	4	1	3	3	2	2	2	2
	20	16	16	11	15	9	11	8	11	8	10	11	4	7	5	7	4	5	3
	30	24	26	16	24	13	20	13	20	12	18	11	6	11	8	12	6	10	6
einstein	10	9	9	9	8	7	8	7	8	7	8	8	2	6	3	5	3	4	1
	20	18	20	18	17	15	17	15	17	14	15	16	5	13	4	12	5	11	2
	30	24	30	23	26	20	26	20	26	17	24	22	7	19	8	17	10	17	4
elaine	10	8	10	6	7	5	4	3	3	3	3	5	1	3	1	4	2	2	2
	20	16	19	14	16	12	12	9	11	8	10	12	1	8	5	10	5	8	4
	30	25	28	22	25	20	21	17	20	16	17	20	5	12	7	15	6	12	6
f16	10	10	8	6	8	5	6	3	4	3	3	5	1	2	1	2	3	1	2
	20	18	16	12	16	11	13	9	11	9	10	9	2	5	1	7	6	4	2
	30	28	28	20	26	18	23	15	21	15	20	15	3	13	2	14	10	8	4
goldhill	10	9	10	8	8	7	6	6	6	6	6	5	3	3	1	4	5	2	4
	20	19	19	15	17	12	14	12	14	11	13	13	3	11	4	13	8	5	4
	30	27	28	20	26	16	23	16	22	15	21	20	5	15	7	17	11	10	6
house	10	7	8	3	6	3	5	2	5	2	5	3	1	6	1	2	2	3	1
	20	18	16	12	13	10	12	8	11	8	10	7	1	8	1	4	5	7	1
	30	24	24	17	21	14	20	12	17	12	15	12	3	12	3	9	8	10	2
lena	10	9	9	6	9	6	8	6	8	5	7	4	4	5	6	3	3	5	3
	20	16	19	15	17	12	15	12	14	11	13	9	11	8	9	9	9	7	5
	30	23	29	21	27	20	25	20	24	19	22	16	17	13	13	16	11	12	10

Appendix B Radon Transform

The Radon Transform represents an image as a collection of projections along various directions. A projection of a two-dimensional function $f(x_1, x_2)$ is a line integral in a certain direction. For example, the line integral of $f(x_1, x_2)$ in the vertical direction is the projection of $f(x_1, x_2)$ onto the x_1-axis; the line integral in the horizontal direction is the projection of $f(x_1, x_2)$ onto the x_2-axis. Projections can be computed along any angle θ. In general, the Radon Transform of $f(x_1, x_2)$ is the line integral of the following expression:

$$R_\theta(x_1') = \int_{-\infty}^{\infty} f(x_1'\cos\theta - x_2'\sin\theta, x_1'\sin\theta + x_2'\cos\theta)dx_2' \tag{B.1}$$

where

$$\begin{bmatrix} x_1' \\ x_2' \end{bmatrix} = \begin{bmatrix} \cos\theta & \sin\theta \\ -\sin\theta & \cos\theta \end{bmatrix} \begin{bmatrix} x_1 \\ x_2 \end{bmatrix} \tag{B.2}$$

Appendix C Fourier-Mellin Transform

The basic translation invariants described in Section 4.3.1 may be converted to rotation and scale invariants using the log-polar map.

Consider a point $(x_1, x_2) \in \Re^2$ and define:

$$x_1 = e^{\mu} \cos\theta \tag{C.1}$$

$$x_2 = e^{\mu} \sin\theta \tag{C.2}$$

where $\mu \in \Re$ and $0 < \theta < 2\pi$. One can see that for every point (x_1, x_2) there is a point (μ, θ) that uniquely corresponds to it. The new coordinate system has the following properties:

Scaling is converted to a translation.

$$(\rho x_1, \rho x_2) \leftrightarrow (\mu + \log\rho, \theta) \tag{C.3}$$

Rotation is converted to a translation.

$$(x_1 \cos(\delta) - x_2 \sin(\delta), x_1 \sin(\delta) + x_2 \cos(\delta)) \leftrightarrow (\mu, \theta + \delta) \tag{C.4}$$

At this stage one can implement a rotation and scale invariant by applying a translation invariant in the log-polar coordinate system. Taking the Fourier transform of a log-polar map is equivalent to computing the Fourier-Mellin transform:

$$F_M(\omega_1, \omega_2) = \int_{-\infty}^{\infty} \int_{0}^{2\pi} f(e^{\mu} \cos\theta, e^{\mu} \sin\theta) \exp\left[i(\omega_1 \mu + \omega_2 \theta)\right] d\mu \, d\theta \tag{C.5}$$

The magnitude of the Fourier-Mellin transform is rotation and scale invariant.

Appendix D Shift Invariance by Parallel Filter Banks

The orthogonal two-channel DWT filter banks with analysis low-pass filter given by the *z*-transform $H_0(z)$, analysis highpass filter $H_1(z)$ and with synthesis filters $G_0(z)$ and $G_1(z)$ is shown in Figure D.1 [131].

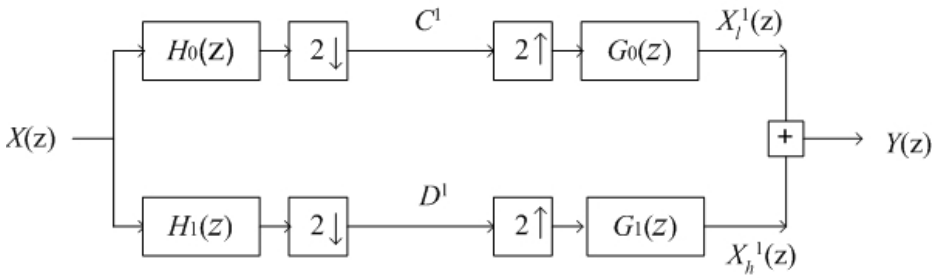

Figure D.1: DWT filter bank.

For an input signal $X(z)$, the analysis part of the filter bank followed by upsampling produces the low-pass (equation (D.1)) and the high-pass (equation (D.2)) coefficients

$$C^1(z^2) = \frac{1}{2}\{X(z)H_0(z) + X(-z)H_0(-z)\} \tag{D.1}$$

$$D^1(z^2) = \frac{1}{2}\{X(z)H_1(z) + X(-z)H_1(-z)\} \tag{D.2}$$

respectively, and decomposes the input signal into a low frequency part $X_l^1(z)$ and a high frequency part $X_h^1(z)$. The output signal $Y(z)$ is the sum of these two components:

$$Y(z) = X_l^1(z) + X_h^1(z) \tag{D.3}$$

where

$$X_l^1(z) = C^1(z^2)G_0(z) = \frac{1}{2}\{X(z)H_0(z)G_0(z) + X(-z)H_0(-z)G_0(z)\} \tag{D.4}$$

$$X_h^1(z) = D^1(z^2)G_1(z) = \frac{1}{2}\{X(z)H_1(z)G_1(z) + X(-z)H_1(-z)G_1(z)\} \tag{D.5}$$

This decomposition is not shift invariant due to the terms in $X(-z)$ of (equation (D.4)) and (equation (D.5)), respectively, which are introduced by the downsampling operators.
If the input signal is shifted, for example $z^{-1}X(z)$, the application of the filter bank results in the decomposition

$$z^{-1}X(z) = \tilde{X}_l^1(z) + \tilde{X}_h^1(z) \tag{D.6}$$

where

$$C^1(z^2) = \frac{1}{2}\{z^{-1}X(z)H_0(z) + (-z^{-1})X(-z)H_0(-z)\} \tag{D.7}$$

and

$$\tilde{X}_l^1(z) = \frac{1}{2}z^{-1}\{X(z)H_0(z)G_0(z) - X(-z)H_0(-z)G_0(z)\} \tag{D.8}$$

and similarly for the high-pass part. From this calculation it can be seen that the shift dependence is caused by the terms containing $X(-z)$, the *aliasing terms*. This filter bank is shift invariant with respect to a double shift since $(-1)^2 = 1$ and

$$z^{-2}X(z) = z^{-2}(X_l^1(z) + X_h^1(z)) \tag{D.9}$$

One possibility to obtain a shift invariant decomposition can be achieved by applying an additional filter bank with shifted analysis filters $z^{-1}H_0(z)$, $z^{-1}H_1(z)$ and

synthesis filters $zG_0(z)$, $zG_1(z)$ and subsequently averaging the lowpass and the highpass channels of both filter banks (Figure D.2).

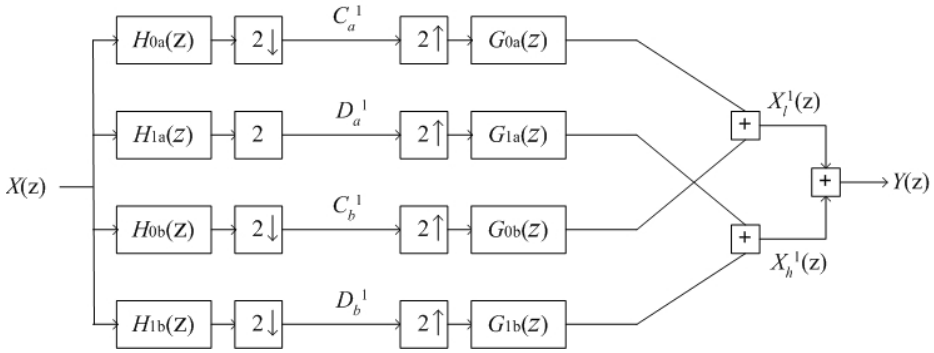

Figure D.2: One level of complex dual tree filter bank.

If we denote the first filter bank by index *a* and the second one by index *b* then this procedure implies the following decomposition:

$$X(z) = X_l^1(z) + X_h^1(z) \tag{D.10}$$

where for the lowpass channels of tree *a* and tree *b* we have

$$\begin{aligned} X_l^1(z) &= \frac{1}{2}\{C_a^1(z^2)G_{0a}(z) + C_b^1(z^2)G_{0b}(z)\} \\ &= \frac{1}{4}\{[X(z)H_0(z) + X(-z)H_0(-z)]G_0(z) + \\ &+ [X(z)z^{-1}H_0(z) + X(-z)(-z^{-1})H_0(-z)]zG_0(z)\} \\ &= \frac{1}{4}\{X(z)[H_0(z)G_0(z) + H_0(z)G_0(z)] + \\ &+ X(-z)[H_0(-z)G_0(z) - H_0(-z)G_0(z)]\} \\ &= \frac{1}{2}X(z)H_0(z)G_0(z) \end{aligned} \tag{D.11}$$

and similarly for the high-pass part. The aliasing term containing $X(-z)$ in $X_l^1(z)$ has vanished and the decomposition becomes indeed shift invariant.

Appendix E Test Images

All test images are grey scale of 512 x512 pixels.

barbara

boats

couple

cameraman

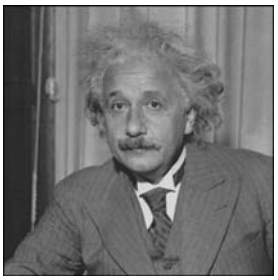

einstein

elaine

f16

goldhill

house

lena

List of Publications

[1] N. Terzija, M. Repges, K. Luck, W. Geisselhardt, "Digital Image Watermarking Using Discrete Wavelet Transform: Performance Comparison of Error Correction Codes", published in Proceedings of the Second IASTED International Conference on Visualization, Imaging and Image Processing, Malaga, Spain, September 2002.

[2] N. Terzija, M. Repges, K. Luck, W. Geisselhardt, "Impact of different Reed-Solomon codes on digital watermarks based on DWT", Multimedia and Security Workshop at ACM Multimedia 2002, Juan-les-Pins, France, December 2002.

[3] N. Terzija, "Digital Image Watermarking in The Wavelet Domain", Technical Report, Faculty of Engineering Sciences, Gerhard-Mercator-Universität Duisburg, December 2002, http://www.fb9dv.uni-duisburg.de/members/ter/trep_1202.pdf

[4] N. Terzija, W. Geisselhardt, "Robust Digital Image Watermarking Method Based On Discrete Fourier Transform", InProceedings of the 5th IASTED International Conference on Signal and Image Processing, Honolulu, Hawaii, August 2003.

[5] N. Terzija, W. Geisselhardt, Digital Image Watermarking Using Complex Wavelet Transform, ACM Multimedia and Security Workshop 2004, Magdeburg, Germany, September 2004.

[6] N. Terzija, W. Geisselhardt, "Robust Digital Image Watermarking Based on Complex Wavelet Transform", In WSEAS Transactions on Communication, Issue 10, Volume 4, pp 1086-1092, October 2005, ISSN 1109-2742.

[7] N. Terzija, W. Geisselhardt, "Robust Digital Image Watermarking Using Feature Point Detectors", In Proceedings of the 9th WSEAS International Multiconference CSCC on Communication, Vouliagmeni Beach, Athens, Greece, July 13-15, 2005.

[8] N. Terzija, W. Geisselhardt, „A Novel synchronisation approach for digital image watermarking based on scale invariant feature point detector", *IEEE International Conference on Image Processing*, (*ICIP 2006*), Atlanta, GA, USA, October 8-11 2006.

References

[1] B. Schneier, Applied cryptography, (2nd Edition), John Wiley, 1996.

[2] I. J. Cox, M. L. Miller, and J. A. Bloom, “Digital Watermarking”, Morgan Kaufmann, 2001.

[3] R. B. Wolfgang, E. J. Delp, “A Watermark For Digital Images”, IEEE International Conference on Image Processing (ICIP'96), 1996.

[4] R. B. Wolfgang, E. J. Delp, “A watermarking technique for digital imagery: further studies”, In International Conference on Imaging, Systems, and Technology, pages 279-287, Las Vegas, NV, USA, 30 June-3 July 1997. IEEE.

[5] A. Z. Tirkel, R. G. Schyndel, C. F. Osborne, “A two dimensional digital watermark“, Digital Image Computing, Te chnology and Applications, pp. 378-383, Brisbane, Australia, 1995.

[6] O. Bruyndonckx, J.-J. Quisquater, B. Macq, “Spatial method for copyright labeling of digital images," in Proc. Workshop on Nonlinear Signal and Image Processing (I. Pitas, ed.), pp. 456-459, June 1995.

[7] I. Pitas, “A method for signature casting on digital images”," in Proc. IEEE Int. Conference on Image Processing, vol. 3, pp. 215{218, 1996.

[8] W. Bender, D. Gruhl, and N. Morimoto, “Techniques for data hiding," in Proc. SPIE, Storage and Retrieval for Image and Video Databases III (W. Niblack and R. C. Jain, eds.), vol. 2420, pp. 164-173, February 1995.

[9] A. Herrigel, J. J. K. Ó Ruanaidh, H. Petersen, S. Pereira, T. Pun, “Secure copyright protection techniques for digital images”, In David Aucsmith ed., Information Hiding, Vol. 1525 of Lecture Notes in Computer Science, pp. 169-190, Springer, Berlin, 1998. (Second International Workshop IH'98, Portland, OR, USA, April 15-17, 1998).

[10] S. Pereira, J. J. K. Ó Ruanaidh, F. Deguillaume, G. Csurka, T. Pun, “Template based recovery of Fourier-based watermarks using log-polar and log-log maps”, In IEEE

Multimedia Systems 99, International Conference on Multimedia Computing and Systems, Vol. 1, pp. 870-874, Florence, Italy, 7-11 June 1999.

[11] J. J. K. Ó Ruanaidh, S. Pereira, "A secure robust digital image watermark", In Electronic Imaging: Processing, Printing and Publishing in Colour, SPIE Proceedings, Zürich, Switzerland, May 1998. (SPIE/IST/Europto Symposium on Advanced Imaging and Network Technologies)

[12] I. J. Cox; J. Kilian, F. T. Leighton, T. Shamoon, "Secure spread spectrum watermarking for multimedia", IEEE Transactions on Image Processing, Volume: 6 Issue: 12, Dec. 1997, pp. 1673 –1687.

[13] A. Piva, M. Barni, f. Bartolini, V. Cappellini, "DCT-based watermark recovering without resorting to the uncorrupted original image", in Proc. ICIP 97, IEEE Int. Conf. Image Processing, Santa Barbara, CA, Oct. 1997, pp. 520-527.

[14] F. M. Boland, J. J. K. Ó Ruanaidh, C. Dautzenberg, "Watermarking digital images for copyright protection", in Proc. IEE Int. Conf. on Image Processing and its Applications, Edinburgh, U.K., July 1995, pp. 326-330.

[15] C.-T. Hsu, J.-L. Wu, „Hidden signatures in images", in Proc. ICIP-96, IEEE Conf. Image Processing, vol. III, Lausanne, Switzerland, Sept. 16-19, 1996, pp. 223-226.

[16] C. Podilchuk, W. Zeng, „Perceptual watermarking of still images", in Proc. 1997 IEEE 1st Workshop Multimedia Signal Processing, Princeton, NJ, June 23-25, 1997, pp. 363-368.

[17] X. Xia, C.G. Boncelet and G.R. Arce, Wavelet transform based watermark for digital images, Optics Express, Vol. 3, No. 12, December 1998.

[18] H.-J. Wang, P.-C. Su, C.-C. J. Kuo, „Wavelet-based digital image watermarking". Optics Express, Vol. 3 pp. 497, December 1998.

[19] W. Zhu, Z. Xiong, Y.-Q. Zhang, "Multiresolution watermarking for images and video: a unified approach", In Proceedings of the IEEE International Conference on Image Processing, ICIP '98, Chicago, IL, USA, October 1998.

[20] N. Kaewkamnerd, K.R. Rao, "Multiresolution based image adaptive watermarking scheme", in EUSIPCO, Tampere, Finland, Sept. 2000.

[21] D. Kundur, D. Hatzinakos, „Digital watermarking using multiresolution wavelet decomposition", In Proceedings of IEEE ICASSP '98, volume 5, pages 2969 - 2972, Seattle, WA, USA, May 1998.

[22] P. Loo, N.G. Kingsbury, Digital watermarking with complex wavelets, Proc IEE Colloquium on Secure Images and Image Authentication, IEE, London, 10 April, 2000.

[23] P Loo, N G Kingsbury, Digital Watermarking using Complex Wavelets, Proc. IEEE Conf. on Image Processing, Vancouver, September 11-13, 2000, paper 3608.

[24] http://www.jpeg.org

[25] A. N. Skodras, C.A. Christopoulos, T. Ibrahimi, "JPEG2000: the upcoming still image compression standard" Proc. Of the 11th Portugese conference on pattern recognition, pp. 359-366, May 2000.

[26] N G Kingsbury, "Image Processing with Complex Wavelets", Phil. Trans. Royal Society London A, 357:2543-2560, September 1999.

[27] J. J. K. O. Ruanaidh, T. Pun, "Rotation, scale and translation invariant spread spectrum digital image watermarking", Signal Processing 66, pp. 303-318, May 1998.

[28] C. Lin, M. Wu, J. A. Bloom, I. Cox, M. Miller, Y. Lui, "Rotation, scale, and translation resilient public watermarking for images", Proceedings of the SPIE, Security and Watermarking of Multimedia Contents 3971, pp. 90-98, 2000.

[29] C.-Y. Lin, "Public watermarking surviving general scaling and cropping: An application for print-and-scan process", Multimedia and Security Workshop at ACM Multimedia 99, (Orlando, FL, USA), Oct 1999.

[30] M. Kutter, F. Jordan, F. Bossen, "Digital signature of colour images using amplitude modulation", in Proc. SPIE Storage and Retrieval for Image and Video Databases, 3022, pp. 518-526, (San Jose, California), 1997.

[31] M. Alghoniemy, A. H. Tewfik, "Progressive quantized projection watermarking scheme", Proc. of the 7th ACM International Multimedia Conference , pp. 295-298, (Orlando, FL), Nov. 1999.

[32] A. Herrigel, J. J. K. O. Ruanaidh, H. Petersen, S. Pereira, T. Pun, "Secure copyright protection techniques for digital images", in In David Aucsmith ed., Information Hiding, L. N. o. C. S. Springer Verlag, ed., 1525, pp. 169-190, (Berlin, 1998. (Second International Workshop IH'98, Portland, OR, USA, April 15-17, 1998)), 1998.

[33] F. Deguillaume, G. Csurka, J. J. K. O. Ruanaidh, T. Pun, "Robust 3d dft video watermarking", Vol. 3657 of SPIE Proceedings, pp. 113-124, Electronic Imaging

'99: Security and Watermarking of Multimedia Contents, (San Jose CA, USA), 23-29 January 1999.

[34] S. Pereira and T. Pun, "An iterative template matching algorithm using the chirp-z transform for digital image watermarking", in Pattern Recognition, 33, 1, pp. 173.175, January 2000.

[35] M. Kutter, S. K. Bhattacharjee, and T. Ebrahimi, "Toward second generation watermarking schemes," in Proc. IEEE Int. Conf. Image Process., vol. 1, 1999, pp. 320–323.

[36] P. Bas, J-M. Chassery, B. Macq, "Geometrically invariant watermarking using feature points", IEEE Trans. on Image Processing, Vol. 11 (2002) 1014-1028.

[37] C.W. Tang, H-M. Hang, "A feature-based robust digital image watermarking scheme", IEEE Trans. on Signal Processing, Vol. 51 (2003) 950-959.

[38] C. Harris, M. Stephen, "A combined corner and edge detector", in 4th Alvey Vision Conf., pages 147-151, 1988.

[39] D. Marr, Vision. San Francisco, CA: Freeman, 1982, pp. 54–61.

[40] K. Mikolajczyk, C. Schmid, "Scale and Affine invariant interest point detectors", In International Journal of Computer Vision 1(60): 63-86, 2004.

[41] D. Lowe, "Distinctive image features from scale invariant keypoints", In International Journal of Computer Vision 2(60): 91-110, 2004.

[42] N. Terzija, W. Geisselhardt, "Robust Digital Image Watermarking Based on Complex Wavelet Transform", In WSEAS Transactions on Communication, Issue 10, Volume 4, pp 1086-1092, October 2005, ISSN 1109-2742.

[43] N. Terzija, W. Geisselhardt, "Robust Digital Image Watermarking Using Feature Point Detectors", In Proceedings of the 9th WSEAS International Multiconference CSCC on Communication, Vouliagmeni Beach, Athens, Greece, July 13-15, 2005.

[44] N. Terzija, W. Geisselhardt, „A Novel synchronisation approach for digital image watermarking based on scale invariant feature point detector", IEEE International Conference on Image Processing, (ICIP 2006), Atlanta, GA, USA, October 8-11 2006.

[45] N. Terzija, M. Repges, K. Luck, W. Geisselhardt, "Digital Image Watermarking Using Discrete Wavelet Transform: Performance Comparison of Error Correction Codes", published in Proceedings of the Second IASTED International Conference on Visualization, Imaging and Image Processing, Malaga, Spain, September 2002.

[46] N. Terzija, M. Repges, K. Luck, W. Geisselhardt, “Impact of different Reed-Solomon codes on digital watermarks based on DWT”, Multimedia and Security Workshop at ACM Multimedia 2002, Juan-les-Pins, France, December 2002.

[47] N. Terzija, W. Geisselhardt, Digital Image Watermarking Using Complex Wavelet Transform, ACM Multimedia and Security Workshop 2004, Magdeburg, Germany, September 2004.

[48] Cox, I. J.; Miller, M. L.; McKellips, A. L.; “Watermarking as communications with side information”, Proceedings of the IEEE , Volume: 87 Issue: 7 , July 1999, pp. 1127 –1141

[49] M. Costa, “Writing on dirty paper ”, IEEE Transactions on Information Theory, Volume: 29 Issue: 3 , May 1983, pp. 439 –441.

[50] F. Hartung, B. Girod, “Digital Watermarking of MPEG-2 Coded Video in the Bitstream domain,”, Proceedings of the IEEE International Conference on Acoustics, Speech and Signal Processing, Vol. 4, Munich, Germany, Apr. 1997, pp. 2621-2624.

[51] A. Z. Tirkel, C. F. Osborne, R. G. van Schyndel, “Image watermarking- a spread spectrum application," in *Proc. IEEE Int. Symposium on Spread Spectrum Techniques and Applications*, vol. 2, pp. 785-789, 1996

[52] C. Berrou, A. Glavieux, “Near optimum error correcting coding and decoding: turbo-codes”, IEEE Transactions on Communications , Volume: 44 Issue: 10, Oct. 1996 Page(s): 1261 –1271.

[53] J. J. Eggers, J. K. Su, B. Girod, "Robustness of a Blind Image Watermarking Scheme," in Proceedings of IEEE International Conference on Image Processing (ICIP 2000), Vancouver, Canada, September 2000.

[54] S. Katzenbeisser, F.A.P Petitcolas, “Information Hiding Techniques for Steganography and Digital Watermarking”, Artech House, Boston – London 2000.

[55] A. B. Watson, ”DCT Quantization Matrices Optimized for Individual Images”, Human Vision, Visual Processing, and Digital Display IV, SPIE-1913:202, 1993.

[56] S. Voloshynovskiy, S. Pereira, V. Iquise, T. Pun, “Attack modelling: Towards a second generation benchmark”, Signal Processing, 81, 6, pp. 1177-1214, June 2001. Special Issue: Information Theoretic Issues in Digital Watermarking, 2001. V. Cappellini, M. Barni, F. Bartolini, Eds.

[57] Langelaar, R. Langedijk, J. Biemond, “Removing Watermarks by Nonlinear Filtering”, Proc. European Signal Processing, Rhodes, Greece, Sept. 1998

[58] J. Su, B. Girod, “Power-Spectrum Condition for Energy-Efficient Watermarking”, ICIP, 1999.

[59] F. A. P. Petitcolas, R. J. Anderson, M. G. Kuhn. “Attacks on copyright marking systems”, in David Aucsmith (Ed), Information Hiding, Second International Workshop, IH’98, Portland, Oregon, U.S.A., April 15-17, 1998, Proceedings, LNCS 1525, Springer-Verlag, ISBN 3-540-65386-4, pp. 219-239.

[60] F. A. P. Petitcolas, “Watermarking schemes evaluation“. I.E.E.E. Signal Processing, vol. 17, no. 5, pp. 58–64, September 2000.

[61] M. Kutter, S. Voloshynovskiy, A. Herrigel, “The watermark Copy Attack”, Security and Watermarking of Multimedia Contents, II, SPIE-3971: 371-280, 2000.

[62] S. Craver, N. Memon, B. Yeo, and M. Yeung, “Can invisible watermarks resolve rightful ownerships," in Technical Report RC 20509. 1997, IBM Research Institute.

[63] http://www.cl.cam.ac.uk/~fapp2/watermarking/stirmark/

[64] http://watermarking.unige.ch/Checkmark/

[65] www.certimark.org

[66] H. T. Sencar, N. Memon, “Watermarking and ownership problem: a revisit”, in Proceedings of the 5th ACM workshop on Digital rights management, Alexandria, VA, USA, 2005, pp. 93-101.

[67] S. Craver N. Memon B. Yeo and M. Yeung, “Resolving rightful ownership with invisible watermarking techniques: Limitation, attacks, and implications," IEEE Journal on Selected Areas in Communications, vol. 16, no. 4, pp.573-586, 1998.

[68] L. Qiao and K. Nahrstedt, “Watermarking methods for mpeg encoded video: Towards resolving rightful ownership," in Proc. of ICMCS, 1998, vol. 9, pp. 194-210.

[69] W. Zeng and B. Liu, “On resolving rightful ownerships of digital images by invisible watermarks," in Proc. of ICIP. 1997, pp. 552-555

[70] A. Adelsbach, B. Ptzmann, and A. R. Sadeghi, “Proving ownership of digital content," in Proc. of IHW'99, Lecture Notes in Computer Science. 2000, vol. 1768, pp. 126-141, Springer-Verlag.

[71] S. Katzenbeisser and H. Veith, “Securing symmetric watermarking schemes against protocol attacks," in Proc. of SPIE: Security and Watermarking of Multimedia Contents, 2002, vol. 4675, pp. 260-268.

[72] A. Adelsbach, S. Katzenbeisser, and H. Veith, “Watermarking schemes provably secure against copy and ambiguity attacks," in Proc. of ACM CCS-10 Workshop on Digital Rights Management, 2003.

[73] J. P. Antoine, P. Vandergheynst, R. Murenzi, “Two-dimensional directional wavelets in image processing”, Int. J. Imaging Sys. and Tech., 7:152-165, 1996.

[74] F. Aurenhammer, R. Klein, "Voronoi Diagrams", Ch. 5 in Handbook of Computational Geometry (Ed. J.-R. Sack and J. Urrutia), Amsterdam, Netherlands: North-Holland, pp. 201-290, 2000.

[75] M. Alghoniemy, A. H. Tewfik, “Geometric distortion correction through image normalization,” in Proc. IEEE Int. Conf. Multimedia Expo., vol. 3, 2000, pp. 1291–1294.

[76] M. Tone, N. Hamada, “Affine Invariant Digital image watermarking using feature points”, International Workshop on Nonlinear Circuit and Signal Processing, Hawaii, USA, Mar. 2005.

[77] T. Lindeberg. “Feature detection with automatic scale selection”, International Journal of Computer Vision, 30(2):79-116, 1998.

[78] K. Mikolajczyk, C. Schmid, ”Indexing based on scale invariant interest points”, In Proceedings of the 8th International Conference on Computer Vision, Vancouver, Canada, pages 525-531, 2001.

[79] K. Mikolajczyk, C. Schmid, “A performance evaluation of local descriptors”, In Proceedings of the Conference on Computer Vision and Pattern Recognition, Madison, Wisconsin, USA, June 2003.

[80] C. Schmid, R. Mohr, and C. Bauckhage, “Evaluation of interest point detectors”, International Journal of Computer Vision, 37(2):151-172, 2000.

[81] H.-Y. Lee, I. K. Kang, H.-K. Lee, Y.-H. Suh, “Evaluation of Feature Extracrion Techniques for Robust Watermarking”, IWDW 2005, LNCS 3710, pp. 418-431, 2005.

[82] http://www.robots.ox.ac.uk/~vgg/research/affine/

[83] J. Lichtenauer, I. Setyawan, T. Kalker, R. Lagendijk, “Exhaustive geometrical search and false positive watermark detection probability”, in SPIE Electronic

Imaging 2002, Security and Watermarking of Multimedia Contents V, (Santa Clara), January 2003.

[84] J. L. T. Kalker, G. Depovere, “Modelling the false-alarm and missed detection rate for electronic watermarks”, in Workshop on Information Hiding, S. L. N. on Computer Science, ed., pp. 329-343,(Portland, OR), 15-17 April 1998.

[85] M. L. Miller, J. A. Bloom, “Computing the probability of false watermark detection”, in Information Hiding, pp. 146-158, 1999.

[86] A. Tefas, I. Pitas, “Multi-bit image watermarking robust to geometric distortions”, in IEEE-ICIP'2000, (Vancouver, Canada), 2000.

[87] V. Solachidis, I. Pitas, “Circularly symmetric watermark embedding in 2-d dft domain”, ICASSP'99 6, pp. 3469-3472, (Phoenix, Arizona),15-19 March 1999.

[88] M. Maes, T. Kalker, J. Linnartz, J. Talstra, G. Depovere, J. Haitsma, “Digital watermarking for dvd video copy protection”, IEEE Signal Processing Magazine 17(5), pp. 47-57, 2000.

[89] D. Delannay and B. Macq, “Generalized 2-d cyclic patterns for secret watermark generation”, in ICIP 2000 - IEEE Signal Processing Society - International Conference on Image Processing, 2, pp. 77-79, (Vancouver, Canada), September 10-13 2000.

[90] F. Hartung, J. Su, B. Girod, “Spread-spectrum watermarking: Malicious attacks and counterattacks”, in Security and Watermarking of multimedia contents, SPIE, 3657, (San-Jose CA, USA), January 1999.

[91] S. Pereira, J. J. K. O. Ruanaidh, F. Deguillaume, G. Csurka, T. Pun, “Template based recovery of Fourier-based watermarks using logpolar and log-log maps”, In IEEE Multimedia Systems 99, International Conference on Multimedia Computing and Systems 1, pp. 870-874, (Florence, Italy), 7-11 June 1999.

[92] S. Pereira, T. Pun, “Fast robust template matching for affine resistant image watermarking”, In International Workshop on Information Hiding, Vol. LNCS 1768 of Lecture Notes in Computer Science, pp. 200-210, Springer Verlag, Dresden, Germany, 29 September -1 October 1999.

[93] N. Terzija, W. Geisselhardt, “Robust Digital Image Watermarking Method Based On Discrete Fourier Transform”, InProceedings of the 5th IASTED International Conference on Signal and Image Processing, Honolulu, Hawaii, August 2003.

[94] A. Herrigel, S. Voloshynovskiy, Y. Rytsar, "The Watermark Template Attack", In W. Wong and E. J. Delp eds., SPIE Photonics West, Electronic Imaging 2001, Security and Watermarking of Multimedia Contents III, No. paper 4314-46, San Jose, CA, USA, January 2001.

[95] M. Kutter, "Watermarking resisting to translation, rotation and scaling", Proc. of SPIE, Multimedia Systems and Applications 3528, (Boston, MA, USA), November 1-6 1998.

[96] S. Voloshynovskiy, F. Deguillaume, T. Pun, "Content adaptive watermarking based on a stochastic multiresolution image modeling", In Tenth European Signal Processing Conference (EUSIPCO'2000), (Tampere, Finland), September 5-8 2000.

[97] F. Deguillaume, S. Voloshynovskiy, T. Pun, "A method for the estimation and recovering from general affine transforms in digital watermarking applications, in SPIE Electronic Imaging 2002, Security and Watermarking of Multimedia Contents IV, (San Jose), February 2002.

[98] S. Tsekeridou, I. Pitas, "Embedding Self-Similar Watermarks in the Wavelet Domain", IEEE Int. Conference Acoustic, Systems and Signal Processing (ICASSP'00), vol. IV, pp. 1967-1970, Istanbul, Turkey, 5-9 June 2000.

[99] S. Tsekeridou, N. Nikoladis, N. Sidiropoulos, I. Pitas, " Copyright Protection of Still Images Using Self-Similar Chaotic Watermarks", IEEE Conf. on Image Processing (ICIP'00), vol. 1, pp. 411-414, Vancouver, Canada, 10-13 September 2000.

[100] I. Daubechies, Ten Lectures on Wavelets, SIAM, Philadelphia, 1992.

[101] G. Strang, T. Nguyen, Wavelets and Filter Banks, Wellesley-Cambridge Press, 1996.

[102] A. K. Jain, Fundamentals of digital image processing, Prentice-Hall, NJ; 1985.

[103] A.B. Watson, "Visibility of wavelet quantisation noise", IEEE Transaction on Image Processing, vol. 6, pp. 1164-1175, August 1997.

[104] A. S. Lewis, G. Knowles, "Image Compression using the 2-D wavelet transform", IEEE Transaction on Image Processing, vol. 1, pp. 244-250, April 1992.

[105] M. Barni, F. Bartolini, V. Cappellini, A. Piva , "A DWT based technique for spatio-frequency masking of digital signatures", Ping Wah Wong, editor, Proceedings o the 11th SPIE Annual Symposium, Electronic Imaging '99, Security and Watermarking of Multimedia Contents, volume 3657, San Jose, CA, USA, January 1999.

[106] S. Voloshynovskiy, A. Herrigel, N. Baumgärtner, T. Pun, "A stochastic approach to content adaptive digital image watermarking", In International Workshop on

Information Hiding, Vol. LNCS 1768 of Lecture Notes in Computer Science, pp. 212-236, Springer Verlag, Dresden, Germany, 29.09-1.10. 1999.

[107] S. Voloshynovskiy, F. Deguillaume, T. Pun, “Content adaptive watermarking based on a stochastic multiresolution image modeling“, In Tenth European Signal Processing Conference (EUSIPCO'2000), Tampere, Finland, September 5-8 2000.

[108] M. Kutter, Digital image watermarking: Hiding information in images, PhD thesis, EPFL, Lausanne, Switzerland, 1999.

[109] M. Corvi, G. Nicchiotti. “Wavelet-based image watermarking for copyright protection”, In Scandinavian Conference on Image Analysis SCIA '97, Lappeenranta, Finland, June 1997.

[110] R. Dugad, K. Ratakonda, N. Ahuja, A new wavelet-based scheme for watermarking images, Proceedings of the IEEE International Conference on Image Processing, ICIP 1998, Chicago, IL, USA, October 1998.

[111] J. R. Kim, Y.S. Moon, A robust wavelet-based digital watermarking using level-adaptive thresholding. In Proceedings of the 6th IEEE International Conference on Image Processing, ICIP ’99, page 202, Kobe, Japan, October 1999.

[112] C.-S. Lu, S.-K. Huang, C.-J. Sze, H.-Y. M. Liao, “Cocktail Watermarking for Digital Image Protection”,. IEEE Transactions on Multimedia 2(4): 209-224 (2000).

[113] C.-S. Lu, S.-K. Huang, C.-J. Sze, H.-Y. M. Liao, „A new watermarking technique for multimedia protection“, CRC Press, 2000.

[114] Christine I Podilchuk and Wenjun Zeng, "Image Adaptive Watermarking Using Visual Models," IEEE Journal on Selected Areas in Communications , pp. 525-539, May 1998.

[115] N. Kaewkamnerd, K.R. Rao, “Wavelet based image adaptive watermarking scheme” in IEE Electronics Letters, vol.36, pp.312-313, 17 Feb.2000.

[116] G. Voyatzis, I. Pitas, “Digital Image Watermarking using Mixing Systems”, in Computer Graphics, Elsevier, vol. 22, no. 4,pp. 405-416, August 1998.

[117] M. S. Raval, P. P. Rege, “Discrete wavelet transform based multiple watermarking scheme”, Conference on Convergent Technologies for Asia-Pacific Region, TENCON 2003, vol. 3, pp. 935 – 938, 15-17 Oct. 2003.

[118] D. Kundur, D. Hatzinakos, “Towards Robust Logo Watermarking using Multiresolution Image Fusion," IEEE Transactions on Multimedia, vol. 6, no. 1, pp. 185-198, February 2004.

[119] P. Tao, A. Eskicioglu, “A Robust Multiple Watermarking Scheme in the Discrete Wavelet Transform Domain”, in Symposium on Internet Multimedia Management Systems V, Philadelphia, PA.,2004.

[120] E. Ganic, A. Eskicioglu, “Robust digital watermarking: Robust DWT-SVD domain image watermarking: embedding data in all frequencies”, Proceedings of the 2004 multimedia and security workshop on Multimedia and Security, pp. 166 –174, September 2004.

[121] C. H. Chu and A. W. Wiltz, "Luminance channel modulated watermarking of digital images," in Proc. SPIE Wavelet Applications Conference, pp. 437-445, Orlando, USA, April 1999.

[122] Hsu Chiou-Ting, Wu Ja-Ling. Multiresolution watermarking for digital images. IEEE Trans. Circuits and Systems- II: Analog and Digital Signal Processing, 45(8): 1097-1101, 1998.

[123] Y. Zhao, P. Campisi, D. Kundur, “Dual Domain Watermarking for Authentication and Compression of Cultural Heritage Images”, in IEEE Transactions on Image Processing, vol. 13, no. 3, pp. 430-448, March 2004.

[124] E. Koch, J. Zhao, “Towards robust and hidden image copyright labeling“, In Proceedings of the IEEE International Workshop on Nonlinear Signal and Image Processing, pages 452 - 455, Halkidiki, Marmaras, Greece, June 1995.

[125] N. Terzija, “Digital Image Watermarking in The Wavelet Domain”, Technical Report, Faculty of Engineering Sciences, Gerhard-Mercator-Universität Duisburg, December 2002, http://www.fb9dv.uni-duisburg.de/members/ter/trep_1202.pdf

[126] I. W. Selesnick, R. G. Baraniuk, N.G. Kingsbury, “The Dual-Tree Complex Wavelet Transform”, IEEE Signal Processing Magazine, November 2005.

[127] I. W. Selesnick, “The double density DWT,” in Wavelets in Signal and Image Analysis: From Theory to Practice, A. Petrosian and F. G. Meyer, Eds. Norwell, MA: Kluwer, 2001.

[128] I. W. Selesnick, “The double-density dual-tree discrete wavelet transform,” IEEE Trans. Signal Processing, vol. 52, no. 5, pp. 1304–1314, May 2004.

[129] I. W. Selesnick, “Hilbert transform pairs of wavelet bases,” IEEE Signal Processing Letters, vol. 8, no. 6, pp. 170–173, June 2001.

[130] P. R. Hill, D. R. Bull, C. N. Canagarajah, Rotationally invariant texture features using the dual-tree complex wavelet transform, Proceedings of Intern. Conf. of Image Processing, September 2000

[131] J. Neumann, G. Steidl, "Dual-tree complex wavelet transform in the frequency domain and an application to signal classification", In International Journal of Wavelets, Multiresolution and Information Processing; Vol. 3, No. 1, March 2005.

[132] http://taco.poly.edu/WaveletSoftware/dt2D.html

[133] P. Loo, Digital Watermarking Using Complex Wavelets, PhD thesis, University of Cambridge, Mar. 2002.

[134] B. Chen, G. Wornell, Quantization Index Modulation: A Class of Provably Good Methods for Digital Watermarking and Information Embedding, IEEE Trans. on Information Theory, 47(4):1423-1443, May 2001.

[135] J.-J. Lee, W. Kim, N.-Y. Lee, G.-Y. Kim, "A New Incremental Watermarking Based on Dual-Tree Complex Wavelet Transform", The Journal of Supercomputing, Volume 33 , Issue 1, pp. 133-140, July 2005.

[136] C. Rey, K. Amis, J.-L. Dugelay, R. Pyndiah. A. Picart, " Enhanced robustness in image watermarking using block turbo codes", *Proceedings of SPIE, Electronic Imaging, Security and Watermarking of Multimedia Contents* , January 2003, San-Jose, CA